Control and Operation of Power Distribution System for Optimal Accommodation of PV Generation

Mr.Yashodhan Prakash Agalgaonkar

Thesis submitted for the degree of
Doctor of Philosophy

Imperial College London
Control and Power Research Group
Department of Electrical and Electronic Engineering

March 2014

I hereby declare that all the work in this thesis is my own. The work of others has been properly acknowledged.

Mr. Yashodhan P. Agalgaonkar.
20 March 2014

Abstract

The renewable policies in various countries are driving significant growth of grid connected renewable generation sources such as the Photovoltaics (PVs). Typically a PV generation is integrated into power systems at the low and the medium voltage distribution level. The uptake of an intermittent power from the PVs is challenging the power system operation and control. The network voltage control is one of the major challenges during the operation of the distribution connected PVs. The active power injection from a PV plant causes variable voltage rise. This forces the existing voltage control devices such as on-load tap-changer (OLTC) and voltage regulator (VR) to operate continuously. The consequence is the reduction of the operating life of the voltage control mechanism. Also, the conventional non-coordinated reactive power control results in the operation of the VR at its control limit (VR *runaway* condition). This research focuses on the distribution voltage control in the presence of PV generation and helps to establish detailed insights into the various associated challenges.

Firstly, the typical grid integrated PV topologies are discussed. The existing power system operational practices are presented and their limitations are identified. A voltage control methodology to tackle challenges such as over-voltage, excessive tap counts and VR *runaway* is presented. These challenges are alleviated through the coordinated reactive power control. The reactive power coordination is achieved through the deterministic distribution optimal power flow solved through the interior point technique. The irradiance and the load forecasting errors are another set of challenges from the distribution network operators' perspective. The stochastic optimal voltage control strategy is proposed to tackle the element of randomness associated with the forecast errors. The stochastic operational risks such as an over-voltage and a VR *runaway* are defined through a chance constrained optimization problem. The simulation study is performed using a realistic 95-bus UK generic distribution network model and a practically measured irradiance to demonstrate the effectiveness of the proposed control strategies. The thesis makes an effort to offer an insight into the operational challenges and propose strategies to achieve a seamless integration of the PVs into the power systems.

Acknowledgements

The research presented in this thesis has been carried out under the supervision of Prof. Bikash C. Pal at the Control and Power research group, Department of Electrical and Electronic Engineering. I wish to thank Prof. Pal for his guidance during the course of this research. I would also like to thank him for all the encouragement and support. This work has been supported by a joint UK-India initiative in solar energy through a project Stability and Performance of Photovoltaic (STAPP) funded by Research Councils UK (RCUK) Energy Programme in UK (contract no:EP/H040331/1) and by Department of Science and Technology (DST) in India. I would like to thank the RCUK for funding this research. I would also like to gratefully acknowledge Dr. R. A. Jabr from American University of Beirut, Lebanon for his valuable suggestions during all stages of this research.

Thanks to Dr. Ravindra Singh from ABB Power Technologies, USA who helped me in many ways. I would like to thank Dr.Tom Betts from Loughborough University, UK for the solar irradiance data. Thanks to all my colleagues at the research lab who created a friendly environment : Dr.Linash Kunjumuhammed, Dr.Dumisani Simfukwe, Arif, Stefanie, Abhinav, Ankur, Georgios and Sara. Finally I wish to express my deepest gratitude towards my mother Sandhya and my father Prakash. I would like to thank my wife Sharayu for her support and understanding during my Ph.D study. I am also thankful to my siblings. I take an opportunity to express my respect towards my grandparents who will always remain my source of inspiration.

Dedicated to my parents

Contents

List of Figures

List of Tables

List of abbreviations

abc-reference frame	Three phase reference frame
AIM	Anti-islanding methods
CCO	Chance constrained optimization
CDF	Cumulative distribution function
dq-reference frame	Direct and quadrature axis reference frame
LDC	Line drop compensation
LV	Low voltage
$LVRT$	Low voltage ride through
$MPPT$	Maximum power point tracking
MV	Medium voltage
$OLTC$	On-load tap changers
PDF	Probability density function
$pf(P)$	Power factor against active power setting
PV	Photovoltaic generation
$Q(U)$	Reactive power against voltage setting
RPS	Renewable portfolio standards
$SCADA$	Supervisory control and data acquisition
$SISB$	Single solar infinite bus system
STC	Standard test condition
TTE	Tap tail expectation
VR	Voltage regulator

Chapter 1

Introduction

Many countries across the world have adopted renewable portfolio standards (RPS). This is proving to be a growth impetus for the renewable energy sources such as the photovoltaics (PVs). The proportion of the photovoltaic (PV) generation into the existing power system generation mix has significantly increased in recent times. The aim of this chapter is to take an overview of the status and the prospective growth of the grid connected PV generation sources across the world. The associated generic power system integration challenges are also discussed. The contribution of this research work and the detailed organization of the thesis are presented.

1.1 Global PV generation scenario

The cumulative global capacity of PV generation is expected to grow up to 200GWp by the year 2017. The cumulative global installed capacity is approximately 137GW, till the end of 2013. PV plants are integrated both at the transmission level and the distribution level from the power system integration point of view. PV plants having capacity greater than 100MWp are shown in Table 1.1 [2]. It can be observed from Table 1.1 that there are only 15 power plants having the capacity greater than 100MWp. The capacity of the largest PV plant to date is 250MW. Europe's cumulative installed capacity is approximately 80GW till the end 2013. The trend in the cumulative global capacity from 2007 to 2013 is indicated in Fig. 1.1. The country-wise cumulative capacity and the future growth trends of the PV generation

Table 1.1: PV plants greater than 100MW capacity

Country	Name of PV plant	Capacity
USA	Agua Caliente,Yuma	289 MWp
India	Charanka Park, Patan	214MW
USA	Mesquite Solar, Arlington	207MWp
China	Golmud	200MWp
USA	Copper Mountain Solar, Boulder City	192MWp
Germany	Meuro	166MWp
Germany	Neuhardenberg	145MWp
USA	Campo Verde	139MW
Germany	Templin	128MWp
USA	California Valley Solar Ranch	130MWp
USA	Arlington Valley	125MW
France	Toul-Rosires	115MWp
Ukraine	Perovo	106MWp
China	Jiayuguan	100MWp
China	Xitieshan	100MWp

are briefly discussed next.

Europe

The renewable directive is the European union (EU) policy which sets the target for its member states on the levels of renewable capacity installation. This has led to the growth in the PV generation in most of the EU countries [3]. It is expected that in EU by 2020, 4% of the total electricity demand will be supplied by the PV generation. The country-wise installation percentage within Europe at the end of year 2013 is shown in Fig.1.2. The growth of the PV generation in Europe is mainly led by Germany. For the last few years, in Germany there is significant and consistent growth in the PV generation installations. The provision of the feed in tariffs in the German renewable energy act has attracted private investment. The German grid integration targets are more ambitious than the EU renewable directives. Germany is aiming to supply 35% of the gross electricity consumption through the renewable generation sources by 2020. PV generation in Germany represents significant share of the total renewable portfolio with the cumulative generation capacity of 33.4GW at the end of the first quarter of the

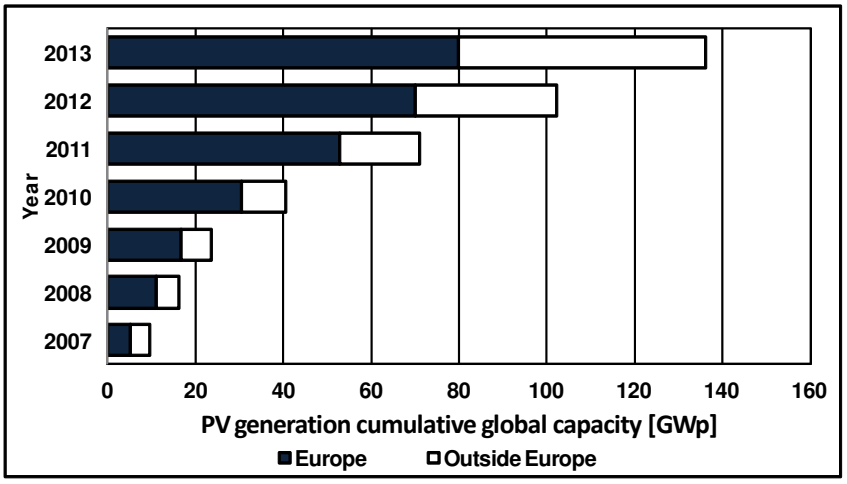

Figure 1.1: Cumulative global capacity[GWp] during 2007-2013

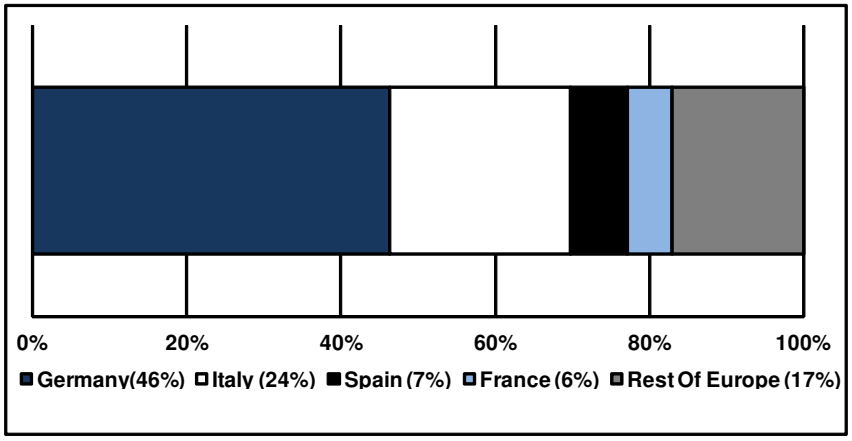

Figure 1.2: Country-wise cumulative capacity percentage in Europe

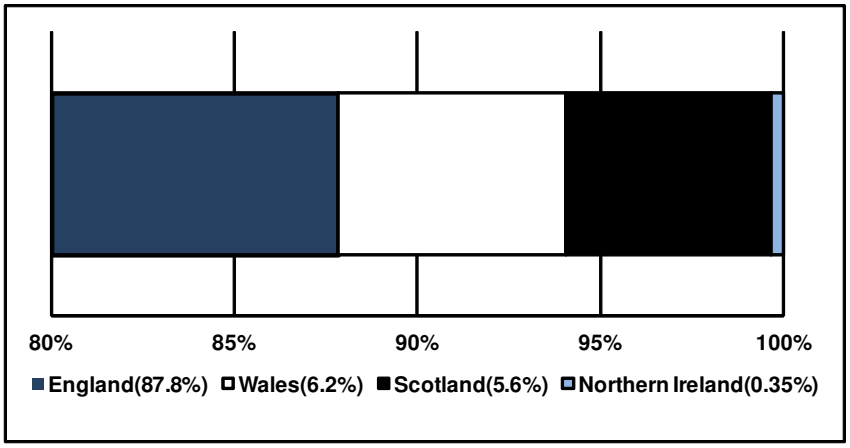

Figure 1.3: Region-wise cumulative capacity percentage in UK

year 2013. On a sunny summer day in 2012 the PV supplied 40% of the German electricity demand during the peak irradiance hours. From the power system point of view 95% of the PV generation is integrated at the low voltage(LV) and the medium voltage (MV) distribution grids [4]. Similar to Germany, the Italian power system also has a significant injection from intermittent PV generation sources. The total PV generation capacity in Italy has grown from merely 87MW in 2007 to a substantial 17GWp by the end of 2013 [5]. The majority of the systems in Italy are also connected at the LV and the MV distribution level. Spain has 5.1GW of PV generation installation accounting for the third largest in Europe. Approximately 80% of the PV generation in Spain is integrated at the LV and the MV distribution levels. Other than these three EU countries, France has a total PV generation of 4.028 GW [6].

The remaining EU countries have approximately 12GW of PV generation cumulative capacity installed. The United Kingdom has approximately 1.8GW of PV generation installed. The region-wise installation percentage within the United Kingdom is shown in Fig.1.3. It can be observed that the maximum installation is in England [7] [8]. The other major EU countries are Belgium (2.6GW), Czech Republic (2GW) and Greece (1.5GW). The remaining EU countries have less than 1GW of PV generation capacity [6]. The great majority of PV capacity in Europe is installed at the LV and the MV distribution levels (approximately 94%) [9].

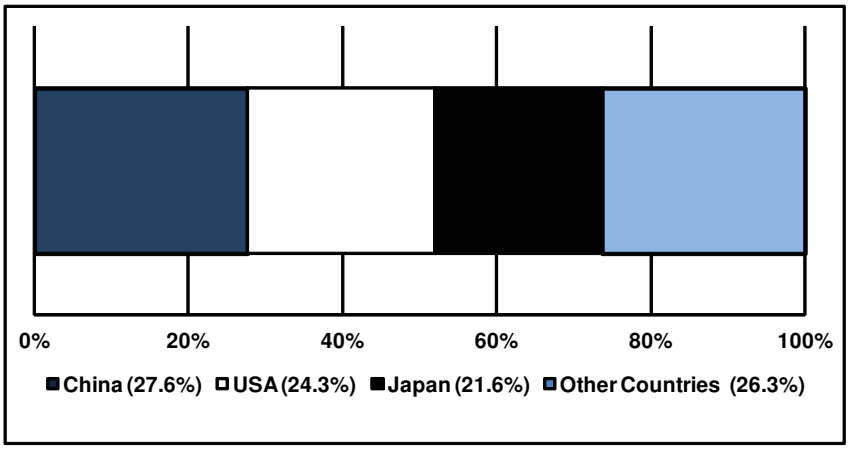

Figure 1.4: Country-wise cumulative capacity percentage outside Europe

China

The country-wise cumulative capacity percentage *outside Europe* is indicated in Fig1.4. China at the end of 2012 had an approximate cumulative installed capacity of 8.3GW. The approximate cumulative capacity added by China in 2013 alone is 11.3GW displaying strong growth of PV generation. As per the proposal drafted by the Chinese bureau of energy forecasts approximately 8GW of the PV distributed generation is planned. The national people's congress has recommended a target in the range 20-30GW by 2020 [10].

United States

Sixteen states in United States have implemented renewable portfolio standards (RPS) which have special considerations for the PV generation. RPS in the USA is also known as a renewable electricity standard (RES). RPS or RES makes it mandatory for the suppliers to purchase a certain amount of the electricity generated from nonconventional sources. The suppliers do have an option to generate the renewable electricity instead of purchasing it. The cumulative installed capacity in the USA at the end of 2013 is approximately 12GW. The most important province is California having the largest installed capacity. The state-wise PV Cumulative capacity in the USA is shown in Fig.1.5. The grid connected PV generation in the USA is categorized as the distributed PV systems and the centralized PV systems.

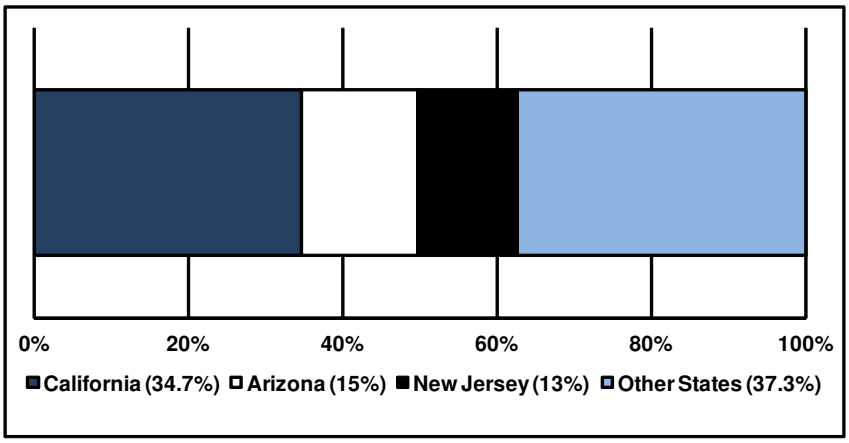

Figure 1.5: Region-wise cumulative capacity percentage in USA

The distributed PV systems comprise the PV installed on residential rooftops and commercial installations etc. These systems are widely referred to as the distributed generation (DG). These DG systems are mostly connected on the customer side of the electricity meter. The centralized PV systems are usually utility scale. The distributed PV systems are approximately 60% of the installed PV capacity in USA [11] [12]. The total 20 GW of the PV plants are under the development in USA. It is projected that the PV generation contribution might grow to 10% of USA's power requirement by 2025. It is a forecast that by the end of 2025, the PV installed capacity in the USA will be 50GW. The major growth is expected to happen in California, Arizona and Nevada [13].

Japan

The Japanese government is targeting a PV installation capacity of 28GW by 2020. The aim is to supply 10% of the domestic energy demand through PV generation by 2050. The renewable energy law enacted in 2011 proposes the feed in tariffs in order to achieve these objectives. The feed in tariff program proposed under the above law began in July 2012. The Ministry of Economy, Trade and Industry is also giving a subsidy for the PV generation growth. This has led to 1.7GW of grid connected PV generation installation in 2012. The cumulative installed capacity till the end of 2013 is approximately 13.5GW [14] [15].

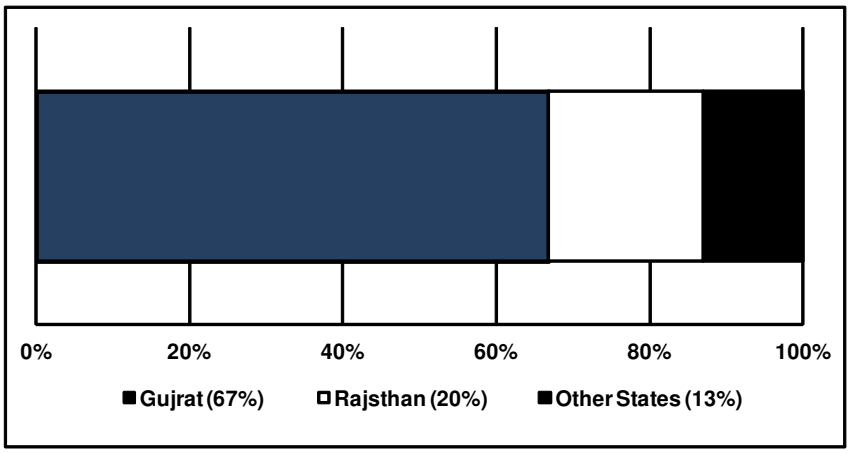

Figure 1.6: Region-wise cumulative capacity percentage in India

Australia

The renewable energy (electricity) act 2000 of the Australian government tries to stimulate the growth of electricity generation from renewable energy sources. An extended renewable energy target was adopted in 2009 which aims at 20% of the electricity supply from the renewable sources. This has spurred the growth of PV generation in Australia. The cumulative installed capacity in Australia is 2.4GW at the end of 2012 [16].

India

The Government of India has developed the national solar mission for the growth of grid connected PV. The cumulative installation capacity targets are subdivided into three timelines. The first stage target of 1.1GW solar installation has been achieved by 2013. The states of Gujrat and Rajsthan of India have higher solar energy potential than other provinces. These are the provinces where the maximum capacity is integrated into the power systems as shown in Fig.1.6. The second phase of the target is 10GW of PV generation installation by 2017. And the third phase of the project aims to integrate 20GW of the PV generation into the grid by the end of 2022 [17] [18].

These are the specifics of the countries having a significant PV generation

cumulative installed capacity. Some of the regions of Africa and the Middle East have a great potential for PV generation sources due to the favorable weather conditions. At the moment, the cumulative installed capacity in these regions is approximately 0.6GW [6].

The power system operators in many countries have faced different challenges while ensuring the uptake from the intermittent PV generation. Some of the generic challenges are discussed in the next section.

1.2 Grid integration challenges

The dependance on irradiance, temperature and other weather conditions is one of the features of the grid connected PV. Due to this feature PV generation is an intermittent energy source. The variability and the uncertainty associated with PV generation is absent in traditional synchronous generation based on thermal, hydro or nuclear power plants. From the power system operation and control point of view, the power output from synchronous machines is deterministic in nature. The existing transmission and the power delivery infrastructure is also designed considering these traditional deterministic generation sources. Hence, the uptake of power from an intermittent PV generation gives rise to several operational challenges. Following are the major operational challenges.

1.2.1 Generation operation and control

Conventional centralised power system generation is usually through megawatt capacity synchronous machines. These power plants typically have a range between 200MW to 2000MW. Their controls are designed considering the centralized operation of a power system. The integration of a distributed PV generation affects the generation operation and control in the following ways.

- **Operating reserves :**

  The operating reserve is the generation capacity utilized to maintain the balance between power generation and load consumption. The load in a power system is not constant at any time. The synchronous generators in

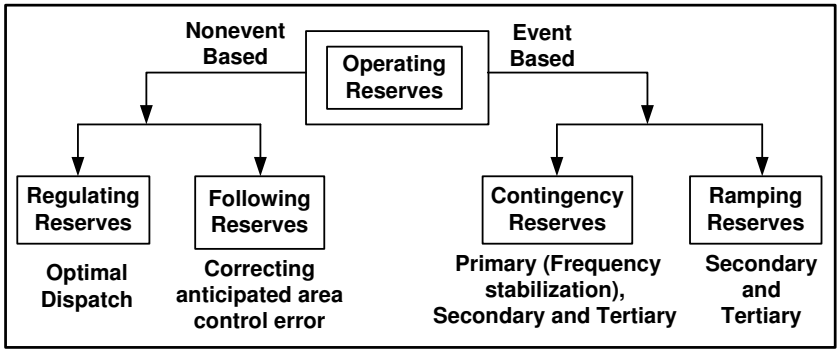

Figure 1.7: Power System operating reserves

a power system produce the power to maintain the load-generation balance at all times. The load change in a power system is a continuous process and it happens from the shorter (minute-to-minute) to the longer (day-to-day) time scale. The power system operator uses various mechanisms to meet this ever varying load. At the same time operators ensure an optimal operation of a power system. The daily generator scheduling through a unit commitment and load-following through an economic dispatch are two such mechanisms. The fast minute-to-minute changes in the load are met by the centralized control center, through the variation of the power generation set points, of some of the power plants. The generation scheduling in the different time frames depends upon the load forecasts. The load forecasts also suffer from errors. Along with this load variability and the forecast errors there are contingencies in the power systems. Typical contingencies are generator faults, line trippings etc. Also, there has to be a generation reserve capacity allocated in order to recover the power balance after such contingency events. Accordingly the operating reserve requirements are characterized as shown in Fig.1.7. The normal operation needs the *non event based reserves* scheduling and the contingent operation needs control of the *event based reserves* to ensure the power balance. The *regulating reserves* and the *following reserves* schedule the generators to correct relatively longer timescale power imbalance. The *contingency reserves* are utilized in an instantaneous contingent event. The contingency reserves are also widely referred to as the *spinning reserves*. The

ramping reserves are used for a severe but a non instantaneous events.

The PV power output is intermittent and randomly varying as it depends on an irradiance value and a temperature value. Clouds and other weather conditions also influence a PV generation power output. Further, PV generation forecast cannot be accurately giving rise to uncertainty. The overall variability and the forecast inaccuracy of the combined load and PV generation is usually higher than the variability and the forecast errors of just the load. This variability in a PV power production disturbs the load-generation balance on the different time scales. Other generation is needed to ensure the balance. The large integration of PV generation can affect the utility controls and increase the need of different operating reserves at different time scales [36] [37].

- 50.2 **Hz Challenge :**

  This is a practical challenge due to the PV inverters envisaged in the European power systems. As explained earlier Europe has 80GW of PV. The PV inverters in Europe are supposed to cut off from a grid in an over frequency event. The cut off frequency setting is country specific. In Germany, distribution integrated PV is disconnected from a power systems if the grid frequency is above 50.2Hz. In the scenario when such an over frequency event will happen, approximately 30GW of PV generation will be shutdown. This in turn might cause an under-frequency event and a blackout [4] [38].

- **Load peak shaving :**

  The power system utilities may wish to reduce the load power peak during the daily operation. This is widely referred to as the *load peak shaving*. Typically the load demand is higher in the evening and less in the afternoon. The PV generation intensifies the scenario for a power system having such a typical load behavior. PV generation by nature is diurnal. In the evening PV power output is zero, conversely the load demand is higher. When the load demand is lower (afternoon) at this time PV generation is available. Thus from a network operator's point of view PV is not operational when utility really needs it. Hence utility's aim of peak shaving can not be achieved through

a PV plant [39]. PV systems need to be equipped with energy storage to alleviate this challenge which involves additional costs [40].

1.2.2 Transmission operation and control

- **Impact on stability :**

  The centralized large capacity PV farms as shown in Table.1.1 will have an impact on the system stability due to sudden change in the multi megawatt PV active power. The multiple intermittent PV generations connected in the distribution grid can also collectively impact the transient stability, the voltage stability and the small signal stability. Some of the recent studies conclude that the centralized large capacity PV have a severe impact on the stability as compared to the collection of the distribution connected PV systems. Till now, the number of such centralized multi megawatt PV plants has been limited. But depending on the case specific power system scenario, a PV generation can have an adverse impact on the transient stability, the voltage stability and the small signal stability [41] [42].

- **Response to voltage sag :**

  A PV inverter is supposed to disconnect from the system when it experience a voltage dip [43]. However load remains connected to the system. So it is equivalent to an effective increase in a load demand for an utility due to loss of the PV generations. This might make the problem of voltage sag even more severe and this may further lead to a black out. PV inverters should have a fault ride through (FRT) capability to avoid this. FRT feature is discussed in detail in next chapter.

1.2.3 Distribution operation and control

- **PV antiislanding :**

  During a fault in a power system, the faulty part of the system is disconnected. In this scenario, PV may continue to feed the load as an island. In this situation a load may be subjected to an unprescribed voltage and frequency. In addition

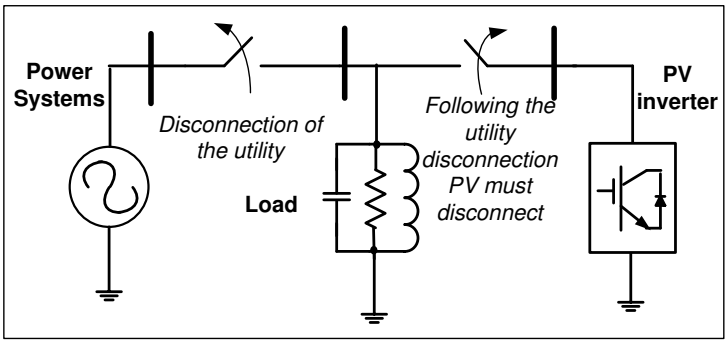

Figure 1.8: PV inverter antiislanding

to this, an out-of-phase connection may occur during an auto reclosing trial. This out of phase connection may damage a PV and a load. The PV acting as an island will keep a power network energized causing a safety hazard to utility personnel. Hence such an islanded operation of the PV has to be avoided [39].

- **Voltage unbalance and flicker :**

  Single phase PV units installed in a low voltage distribution system may lead to an unbalance. The voltage changes due to the injection of an intermittent PV active power might cause problems such as light flicker. The clouds leading to the fluctuations in solar irradiance and hence a PV output power may affect the power quality of the system. This may further necessitate the introduction of fast acting reactive power compensating equipments such as static var compensators.

- **Steady state voltage control :**

  The introduction of a PV as a distributed generation(DG) may interfere with the operation of a transformer tap changer and hence a load may experience an unprescribed voltage. Consider a radial distribution feeder as shown in Fig.1.9. A transformer secondary bus voltage which is set by a tap changer at the beginning of a feeder is based on the line drop compensation. Introduction of a PV immediately down stream to the tap changer will reduce the utility transformer load current. Now in order to have the line drop compensation, an appropriate feeder demand is not measured. Hence the line drop compensation

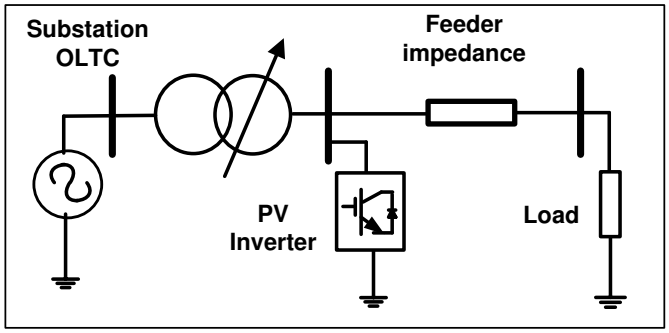

Figure 1.9: PV as a DG connected near substation transformer.

Table 1.2: PV grid integration challenges global overview

Country	**Existing challenges**	**Future challenges**
USA	Steady state voltage support (Overvoltage, VR runaway, Distribution feeder operation), Anti-islanding.	Voltage stability, Frequency stability, Small signal stability
Europe	Frequency stability, Steady state voltage support, Antisilanding, Voltage stability	Small signal stability

will set a smaller voltage than required at the beginning of the feeder. This necessitates appropriate placement of the PV generator in the distribution system. There will usually be an intermittent over voltage due to a PV placed in a distribution system. The PV power output may lead to voltage changes which will result in excessive operations of the tap changers. This will cause an increase in the wear and tear and hence a decrease in the life of transformer tap changers. PV generation also interferes with the voltage regulators in the system and voltage regulator *runaway* is a major challenge for the distribution network operators.

The discussion above highlights the generic grid integration challenges when a PV generation is integrated into the power systems. Table1.2 summarizes the global overview of the PV grid integration challenges.

1.3 Research objectives

As discussed above PV generation presents many grid integration challenges from the generation, transmission and distribution perspectives. However, major growth of PVs is mainly in the distribution networks as discussed in Section 1.1. This research focuses on distribution connected PV generation systems and the main objective is to specifically study distribution system steady state voltage control in the presence of PV generation. The detailed research objectives are as follows :

1. The research objective, here, is to develop an optimal voltage regulation strategy considering the *PV inverter reactive power support capabilities*. This is due to following reasons :

    - PV active power injection is causing intermittent overvoltage on distribution feeders. Present day approaches to mitigate this are through active power curtailment of PV generator [44] [45].
    - The active power curtailment is not the most effective method to regulate the voltage. Firstly, it leads to a suboptimal clean energy capture. Secondly, it may not consider feeder operational performance.

2. As discussed in Section 1.2, one of the major steady state voltage control challenges is the impact of PV generation on voltage control mechanisms such as on-load tap changers (OLTCs) and voltage regulators (VRs). The increase in number of tap operations and VR runaway are major challenges reported in the literature [46] [47] [48]. This research work aims at analysing these challenges in detail.

3. Another research objective is also to use the previous analysis in order to develop a voltage control strategy which mitigates adverse impacts on OLTCs and VRs.

4. Most of the distribution voltage control strategies reported in the literature are based on the load and generation forecasts and a simulation based set-point calculation [49]. These strategies usually neglect forecast errors. This research

work aims at developing a stochastic voltage regulation strategy considering PV generation forecast errors [50] [51].

1.4 Contributions of the thesis

The contribution of the thesis in terms of the outcomes and the research dissemination is as follows.

1.4.1 Research outcomes

- The detailed impact of PV generation on the voltage control devices is not reported in the literature. The challenges such an *over voltage*, *increased tap counts* and Voltage Regulator (VR) *runaway* are analyzed in detail in this research work. A detailed insight is developed into the interaction between the PV generator control settings and the VR control settings while achieving a steady state voltage control. The *distribution reactive power dispatch* is proposed to calculate the optimum reactive power set points of devices in order to alleviate *steady state voltage control challenges*.

- The steady state voltage control challenges are aggravated by the PV and load *forecast errors*. The overvoltage, increased tap counts and VR *runaway* need to be alleviated in the presence of the forecasting errors. An appropriate *stochastic operational strategy* is developed to address this. The *stochastic indices* to model the VR *runaway* phenomenon are developed. The *Chance constraint optimization (CCO)* based technique is proposed to alleviate the challenges. A sample selection based solution strategy to solve this CCO problem is developed.

1.4.2 Research dissemination

1. **Paper 1 :** Y. P. Agalgaonkar, B. C. Pal, and R. Singh, "Impact of Photo Voltaic generation control on Multi machine Small signal stability," International Federation of Automatic Control Conference, 8th Power Plant

and Power System Control Symposium, IFAC-PPPSC 2012, Toulouse, France, Sept. 2011.

Abstract:

The modeling and analysis of the impact of Solar Photovoltaic (PV) on the small signal stability of power system are explored. The analysis provides explanations of the impact of the closed-loop control on the power system stability. Two system models, Single Solar Infinite Bus (SSIB) system and solar connected multi- machine system are considered. In model of PV, module variable are algebraic that is, they change instantaneously and the modeled dynamics are those of the power converter controller. The discussion considers maximum power point tracking, dc link voltage and current controller. In case of SSIB sensitivity to different weather conditions such as irradiance, temperature is studied. Also sensitivity to different power system conditions such as voltage variation, reactive power support from solar is studied. In multi-machine case impact of different active and reactive power injection levels is analyzed. The observations and conclusions obtained from eigenvalue, participation factor analysis suggest that even though the PV generation system dynamic do not participate into low frequency oscillation modes, its control can influence small signal damping depending based on its location in the system.

2. **Paper 2 :** Y. P. Agalgaonkar, B. C. Pal, and R. A. Jabr, "Distribution voltage control considering the impact of PV generation on tap changers and autonomous regulators," IEEE Trans. Power Systems, vol. 29, no. 01, pp. 182192, Jan. 2014.

   Abstract:

   The uptake of variable megawatts from photovoltaics (PV) challenges distribution system operation. The primary problem is significant voltage rise in the feeder that forces existing voltage control devices such as on-load tap-changers and line voltage regulators to operate continuously. The consequence is the deterioration of the operating life of the voltage control mechanism. Also, conventional non-coordinated reactive power control can result in the

operation of the line regulator at its control limit (runaway condition). This paper proposes an optimal reactive power coordination strategy based on the load and irradiance forecast. The objective is to minimize the number of tap operations so as not to reduce the operating life of the tap control mechanism and avoid runaway. The proposed objective is achieved by coordinating various reactive power control options in the distribution network while satisfying constraints such as maximum power point tracking of PV and voltage limits of the feeder. The option of voltage support from PV plant is also considered. The problem is formulated as constrained optimization and solved through the interior point technique. The effectiveness of the approach is demonstrated in a realistic distribution network model.

3. **Paper 3 :** Y. P. Agalgaonkar, B. C. Pal, and R. A. Jabr, "Stochastic Distribution System Operation Considering Voltage Regulation Risks in the Presence of PV Generation," manuscript under review IEEE Trans. on Power Systems, (TPWRS-00169-2014, Revise and resubmit).

   Abstract :

   Variable over voltage, excessive tap counts and voltage regulator (VR) runaway condition are major operational challenges in distribution network while accommodating generation from Photovoltaics (PVs). The conventional approach to achieve voltage control based on off-line simulation for voltage set point calculation does not consider forecast errors. In this work, a stochastic optimal voltage control strategy is proposed while considering load and irradiance forecast errors. Stochastic operational risks such as overvoltage and VR runaway are defined through a chance constrained optimization (CCO) problem. This classical formulation to mitigate runaway is further improved by introducing a stochastic index called the Tap Tail Expectation. Operational objectives such as power losses and excessive tap count minimization are considered in the formulation. A sampling approach is proposed to solve the CCO. Along with other voltage control devices, the PV inverter voltage support features are coordinated. The simulation study is performed using a realistic distribution system model and practically measured irradiance to

demonstrate the effectiveness of the proposed technique.

1.5 Organization of the thesis

The major focus of the thesis is on the *steady voltage control* challenges faced by the distribution network operators in the presence of PV generation. Following this introduction and literature review, the remaining chapters of the thesis are organized as follows.

Chapter 2 provides a brief overview of various PV grid integration standards utilized by the different power system operators. These grid integration standards are used in order to tackle some of the challenges discussed till now. The limitations of some of the standards are identified.

Chapter 3 discusses the detailed components and a topology of a grid connected PV generation. A model suitable for a power system study is developed. The simulation results of the modeling are presented. The results of this chapter are presented in *Paper 1* mentioned in the research dissemination section.

Chapter 4 introduces *steady state voltage control* challenges in the presence of PV generation in detail. The detailed assessment of the impact of PV generation on voltage control devices such as *on-load tap-changers* and *voltage regulators* is carried out. The details of the deterministic optimal reactive power coordination strategy which mitigates an over-voltage and achieves a seamless operation of the voltage control devices is presented. The simulation results of this distribution voltage control strategy are presented. Some of the results of this chapter are published in *Paper 2*.

In **Chapter 5** a voltage regulation technique based on the Chance Constraint optimization (CCO) is presented which takes into account the PV generation and load forecasting errors. The simulation results of this stochastic operational strategy

are presented. The results of this chapter are reported in *Paper 3* which is under review.

Finally, **Chapter 6** summarizes the research outcomes in this work with a brief overview of the future research directions.

Chapter 2

PV Grid integration standards

The capacity of a PV plant determines the voltage level at which it should be integrated. The PV generation is getting integrated mostly at the low voltage (LV) and the medium voltage (MV) distribution level as discussed in Chapter 1. The grid integration standards are evolving in various countries in order to achieve a seamless integration. The PV plants need to comply with the various technical requirements prescribed in a grid integration standard. The set of technical requirements depend upon the voltage level at which the PV plant is getting integrated. The power system operators in different countries have developed the country specific guidelines in the integration standards. The major LV and MV standards reviewed here are as follows.

- IEC61727-Photovoltaic systems characteristics of the utility interface
- IEEE1547-Standard for interconnecting distributed resources with electric power systems
- VDEARN4105-Technical requirements for the connection to and parallel operation with LV distribution networks (Germany)
- BDEW-Technical Guideline for generating plants connected to the MV network (Germany)
- G83-Recommendations for the connection of type tested small-scale embedded generators (up to 16A per phase) in parallel with low voltage distribution systems (UK)

- G59-Recommendations for the connection of generating plants to the distribution systems of licensed distribution network operators (UK)

The aim of reviewing the guidelines is to study the network operators expectations from the PV inverters. The existing standards try to address some of the grid integration challenges. The technical requirements in the standards can be categorized into three broad areas, the protection setpoints, the power quality limits and the grid support functions. This is discussed in upcoming sections in detail.

2.1 Protection settings

There are two kinds of PV generation protection settings. There are the PV plant settings, which protect a PV generator itself from abnormal operating conditions. The other kind of protection settings mitigate the impact of a PV plant on a utility network during abnormal power system conditions. The grid integration standards mostly specify the requirements which mitigate the impact on a utility network. Typical PV generation protection settings are shown in Fig.2.1. The relay settings are discussed as follows.

2.1.1 Over/under voltage and over/under frequency

The abnormal utility situations such as faults etc. result in frequency and/or voltage excursions at the point of common coupling (PCC). The PV grid integration standards define the permissible PCC voltage variation range and the permissible grid frequency variation range under which, the PV generation should continue to operate. The normal operation zone defined by the standard IEC61727 is shown in Fig.2.2. The standard recommends that a PV generation should continue to operate normally if a PCC voltage variation is between -15% to +10% from the nominal value. Similarly, a PV plant should not be disconnected from a grid if a grid frequency variation is ±2% from the nominal value. There should be a PV plant disconnection if either of these bands of the PCC voltage or the frequency is violated. The standard further also prescribes the time interval within which disconnection of the PV plant should occur if the grid frequency or the PCC voltage violation

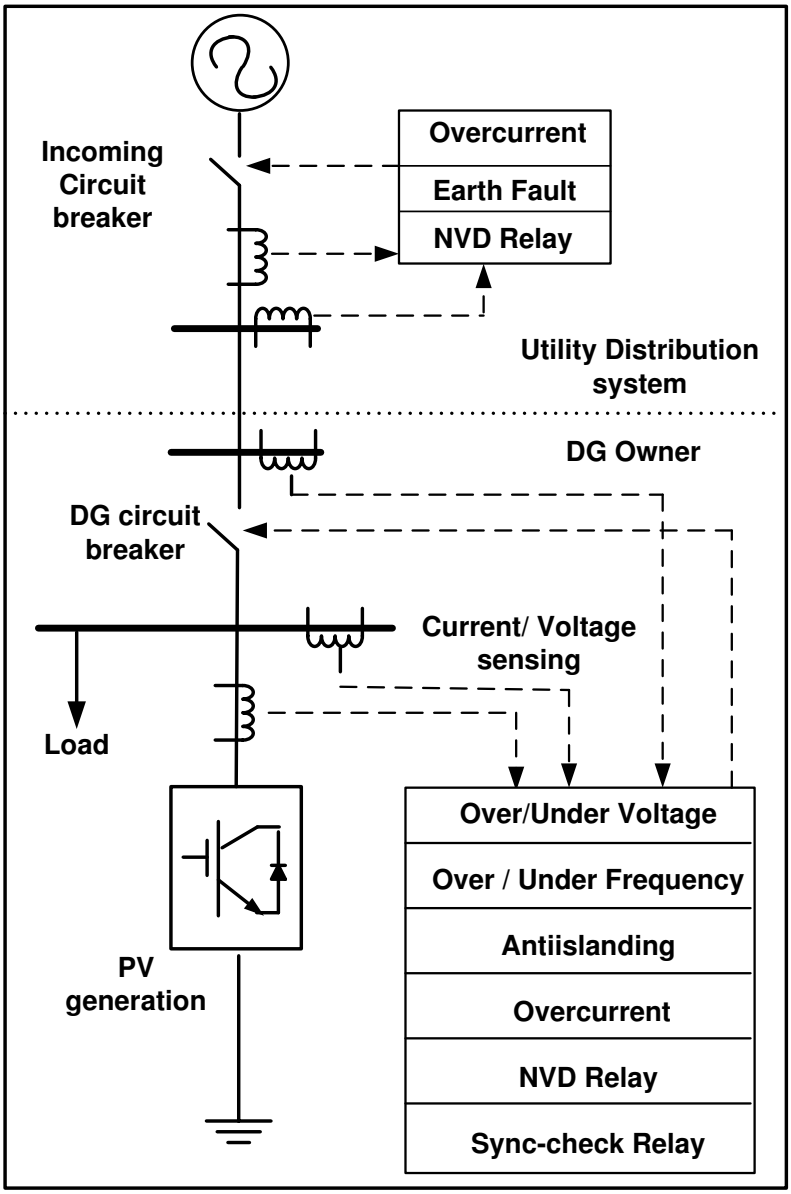

Figure 2.1: Typical PV generator protection

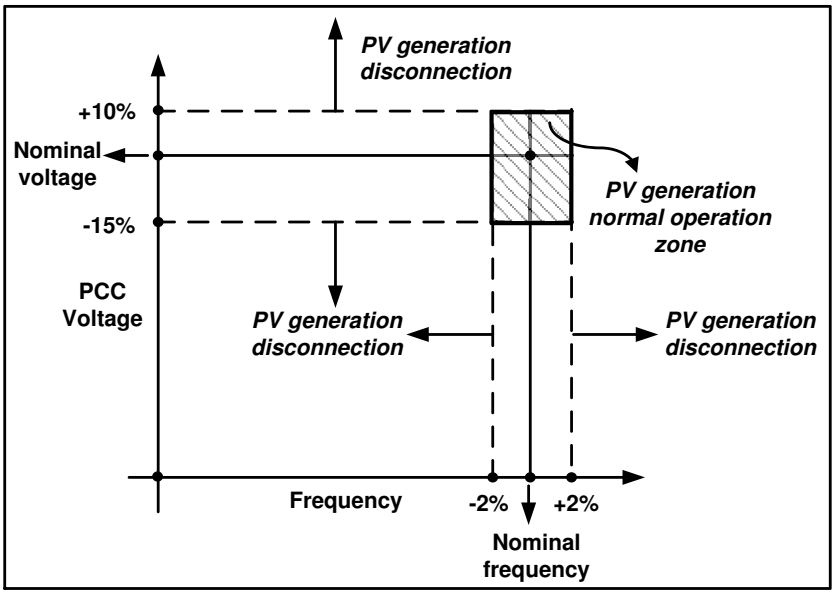

Figure 2.2: IEC61727 : Permissible PCC voltage and frequency variation

is detected. The recommended time delay for the disconnection, if the frequency band is violated, is 0.2 sec. The recommended time interval for the disconnection if the voltage band is violated depends upon the magnitude of the PCC voltage. The recommended disconnection should occur within 2 sec if the PCC voltage magnitude is less than 85% of the nominal. The recommended disconnection time is within 0.1 sec if the PCC voltage magnitude is severely less i.e below 50% of the nominal. Similarly for the severe overvoltage above 135% of the nominal the recommended disconnection time is within 0.05 sec. The disconnection should occur within 2 sec if an overvoltage is between 110% to 135% of the nominal. The standard also defines the reconnection time after a normalcy is achieved following the disconnection. The minimum delay of 3 mins is recommended before reconnecting the PV plant after the PCC voltage and the grid frequency return to the normal operation zone. IEC61727 standard is applicable to a PV generation getting integrated at the LV distribution system. The prescribed PV generation response to the PCC voltage (V_{PCC}) and the grid frequency (f_{grid}) variation in German standards VDEARN4105 and UK Energy networks association(ENA) standard G83 is summarized in Table 2.1. The grid frequency and the voltage variations which are smaller than the disconnection time

Table 2.1: VDEARN4105 and G83 V_{PCC} and f_{grid} variation response

	VDEARN4105	**G83**
Normal operation	$V_{PCC} - 20\% + 10\%$, $f_{grid} - 5\% + 3\%$	$V_{PCC} - 20\% + 19\%$, $f_{grid} - 6\% + 4\%$
Under Voltage	Disconnect in 0.1 sec $V_{PCC} < 80\%$	Disconnect in 2.5sec if $V_{PCC} \leq 87\%$, in 0.5sec if $V_{PCC} \leq 20\%$
Over Voltage	Disconnect in 0.1sec $V_{PCC} > 110\%$	Disconnect in 1sec if $V_{PCC} \geq 114\%$, in 0.5sec if $V_{PCC} \geq 119\%$
Under frequency	Disconnect in 0.1sec	Disconnect in 0.5sec if $f_{grid} \leq 94\%$, in 20sec if $f_{grid} < 95\%$
Over frequency	Disconnect in 0.1 sec	Disconnect in 0.5sec if $f_{grid} \geq 104\%$, in 90sec if $f_{grid} > 103\%$
Remark	LV connected systems	LV connected systems per phase current $\leq 16A$

should be ignored. As soon as a return to the normal voltage and frequency band is achieved there is a delay recommended in most of the standards. The reconnection delay recommended in VDEARN4105 and G83 is 5 sec and 20 sec respectively, after return to normalcy. VDEARN4105 and G83 both define the requirements for the LV connected PV plant [52] [53]. G83 standard specifically deals with the small scale embedded generators (up to 16A per phase current). The generic European directive EN50438 proposes the country-wise settings. There are different sets of grid codes for the MV connected power plant. These requirements are shown in Table. 2.2. BDEW is the specific grid code in Germany for the MV connected PV plants. The PV plants whose output is more than 16A per phase need to comply with G59 standard [43] [54] [55]. IEEE 1547 is the generic guideline applicable for any PV plant less than 10MVA capacity.

2.1.2 Anti-islanding

The challenge of islanding is introduced in Chapter 1. Utilities wish to avoid the islanded operation of the PV generation when an utility supply is disconnected. The

Table 2.2: BDEW, IEEE1547 and G59 V_{PCC} and f_{grid} variation response

	BDEW	**IEEE1547**	**G59**
Normal operation	$V_{PCC} - 20\% + 15\%$, $f_{grid} - 5\% + 3\%$	$V_{PCC} - 12\% + 10\%$, $f_{grid} - 5\% + 3\%$	$V_{PCC} - 20\% + 10\%$, $f_{grid} - 6\% + 4\%$
Under Voltage	Disconnect in 1 sec $V_{PCC} < 80\%$ Disconnect in 0.3 sec $V_{PCC} < 45\%$	Disconnect in 2sec if $V_{PCC} < 88\%$, in 0.16sec if $V_{PCC} < 50\%$	Disconnect in 2.5sec if $V_{PCC} \leq 80\%$
Over Voltage	Disconnect in 0.1sec $V_{PCC} > 115\%$	Disconnect in 1sec if $V_{PCC} > 110\%$, in 0.16sec if $V_{PCC} > 120\%$	Disconnect in 1sec if $V_{PCC} \geq 110\%$
Under frequency	Disconnect in 0.1sec	Disconnect in 0.16sec	Disconnect in 0.5sec if $f_{grid} \leq 94\%$
Over frequency	Disconnect in 0.1 sec	Disconnect in 0.16sec	Disconnect in 0.5sec if $f_{grid} \geq 104\%$
Remark	MV connected systems	PV systems $\leq 10MVA$ capacity	PV systems per phase current $> 16A$

grid integration standards clearly recommend that PV generation should disconnect from the grid as soon as the loss of utility supply and an islanded operation of the PV generation is detected. There are several anti-islanding techniques which can be incorporated to address this challenge.

Anti-islanding methods (AIM) may be categorized basically in two ways. A method which detects an islanding remotely using techniques such as a power line carrier communication and a SCADA are called the *remote AIM*. Other types of techniques which detect an islanding by incorporating an anti islanding algorithm in the PV power converter are called the *local AIM*. The local detection techniques operate according to information and data analyzed by the PV control system. Thus the PV output is usually monitored. Though a remote AIM may have some advantages due to simplicity mostly a local AIM is implemented. A local AIM can be implemented using two different principles. The first technique is known as the *passive AIM*. A passive AIM uses local voltage, current, frequency or harmonics measured at the PV point of common coupling (PCC). A second technique is known as the *active AIM*. An active AIM uses an active signal(disturbance) injected at

the PCC from the PV to drive an operating point of the system towards the frequency/voltage trip limits [56] [57]. Passive and active AIM are widely used techniques. Main passive AIMs described here are under or over voltage, under or over frequency. Usually at the PV PCC, ±10% voltage variation or ±1% frequency variation is permissible. Whenever there is a fault in the power system, that portion of the network is disconnected. But the PV and the load are still connected to the bus at the PCC. There is an active and a reactive power mismatch between the PV generation and the load in most of the cases. This power mismatch varies the PCC voltage or the frequency outside the permissible limits when the utility is disconnected. This is detected by the PV control and it disconnects itself from the PCC. Such passive methods are cost effective. These methods are used when there is a significant mismatch in active and reactive powers of the load and the PV. But if an active and reactive power mismatch after disconnection of the utility grid is not such that it will vary voltage and frequency outside prescribed limits, these detection techniques fail. Another passive antiislanding method is phase jump detection (PJD). The phase of a PV inverter current is instantaneously synchronized at zero crossing with a phase of the PCC voltage with the use of phase lock loop (PLL). When there is islanding the phase difference will be considerable. This can be detected by the PV inverter and it can be disconnected from the PCC. However when the load power factor is unity then this method fails. The above two methods have the disadvantage that under ceratin situations such as a small active or a reactive power mismatch and unity load power factor, they fail. The effectiveness and failure of passive AIM is quantified using the non detection zone (NDZ) [58].

As far as NDZ is concerned an active AIM method is superior to a passive method. One of the techniques is Sandia frequency shift (SFS). The SFS method introduces a positive feedback in the frequency control in order to make an island frequency unstable. This positive feedback will have no effect when PV is connected to a grid (as the frequency of a system is controlled by the utility). The SFS method causes the frequency to shift out of the frequency set point when an utility is disconnected. Thus the island is detected. The Sandia voltage shift (SVS) is another active anti-islanding method similar to SFS. The SVS method uses a positive

feedback on the voltage amplitude rather than frequency. There are other active methods as well, such as the impedance measurement, the slip mode frequency shift etc. All the methods have relative advantages and disadvantages against each other [59].

2.1.3 Other settings

The protection settings displayed in Fig.2.1 vary significantly based on the network voltage at which a PV is integrated and network operators settings. The detailed settings at different voltage levels are discussed in G59 and IEEE 1547. Other than the above discussed relays check-synchronism, over current and neutral voltage displacement (NVD) relay are utilized. Their installation depends upon the country specific grid code and the network operators' requirements. The classical overcurrent protection is utilized to detect the excessive current contribution to the faults. The application of the NVD relay is specifically for the PV integrated at the HV level. The detection of the earth faults on the HV side of the network can be achieved by the NVD relay. The network operators carry out a scenario specific evaluation about need of a NVD relay. G59 standard makes it mandatory to have an under/over voltage, an under/over frequency and an anti-islanding protection [60] [61].

2.2 Power quality limits

The impact on the power quality due to an introduction of PV generation is mitigated by prescribing limits in the grid codes. The standards prescribe the limits on the harmonic distortion, the unbalance and the voltage flicker to mitigate the possible adverse impact due to PV generation.

Harmonics

The connection of a PV generation may inject harmonics into a power system. The current harmonic limits defined in Table.2.3 should not be exceeded. Even harmonics limit is 25% of the odd harmonic limits [43]. The current total harmonic distortion (THD) limit is 5% and the voltage THD limit is 2.5%. In the UK, standards G83 and

Table 2.3: IEEE1547 and IEC61727 current harmonic limits

Harmonic order	$h < 11$	$11 \leq h \leq 17$	$17 \leq h \leq 23$	$23 \leq h \leq 35$	$h \geq 35$	**THD**
%	4.0	2.0	1.5	0.6	0.3	5

Table 2.4: DC current limits

Standard	**IEEE1547**	**IEC61727**	**G59**	**G83**
Limit	< 5% of rated RMS current	< 1% of rated RMS current	< 0.25% of rated RMS current	< 0.25% of rated RMS current

G59 define the harmonic distortion limits in accordance with the standard BSEN 61000-3-2 [52] [54]. In the Germany, VDEARN4105 standard defines the harmonic limit for the LV connected PV where as for the MV connected PV limits are defined in BDEW [53]. BDEW standard defines the permissible harmonic limits for each of the voltage level 10kV, 20kV and 30kV. The dc current is also usually measured as a part of a power quality analysis. There are limits on the value of dc current which can be injected by a PV inverter. These limits are shown in Table 2.4 [52] [54].

Unbalance

The connection of PV generation may cause an unbalance in a network. The standard G83 in the UK which is applicable for PV generation injecting per phase current less than 16A does not define any unbalance limits. However, the standard G59 in UK which is applicable to a PV generation having higher capacity defines these limits. The level of the unbalance for each of the voltage levels defined in G59 is shown in Table 2.5 [62]. European Standard EN50160 defines the maximum allowable unbalance to be 3% [63]. German standard VDEARN4105 allows maximum 4.6kVA unbalance connection between the three phases. The maximum single phase PV power connected should be less than or equal to 10kVA. The three phase connection is mandatory if a PV plant capacity is greater than 30kVA. All the standards prohibit the occurrence of a voltage flicker due to the

Table 2.5: Permissible level of voltage unbalance as per G59

PCC Voltage	$< 33kV$	$\leq 132kV$
Limit	$< 1.3\%$	$< 1\%$

intermittent PV generation.

2.3 Grid support features

The network operators are expecting increased participation from the PV generations into the grid support operations. This is due to the vast growth of the PV generation units. The grid support features expected from a PV generation are described in some of the standards. These can be subdivided into two major categories, namely the dynamic grid support features and the steady state grid support features.

2.3.1 Dynamic grid support

This category of features includes the services provided by a PV generation during system disturbance events. The major services expected in various grid codes are the low voltage ride through, the fault reactive current injection and the frequency support.

Dynamic voltage support

The PV plants were expected to disconnect from a grid during voltage dips in the older version of the grid codes. This can result in the loss of significant generation in the case of large PV integration scenarios. The low voltage ride through (LVRT) expects continuation of a PV power injection for a short period of time to avoid the nuisance tripping of a PV plant. This avoids loss of large PV active power injection, and in turn avoids further network collapse. The LVRT for MV grid code in Germany (BDEW) is shown in Fig. 2.3 as an example. This LVRT requirement is consistent with the transmission grid code in Germany [55].

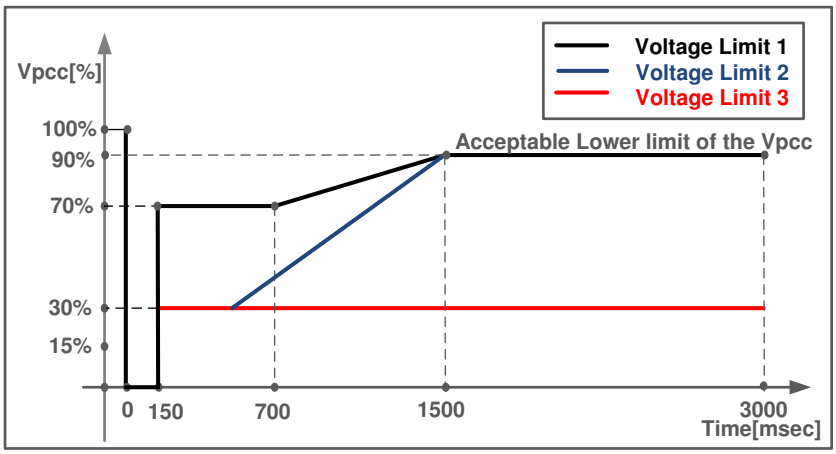

Figure 2.3: PV plant ride through capability

- The PV plant must not disconnect even if the PCC voltage drops to zero for the duration of the first 150msec. This is sketched by the *voltage limit 1* in Fig. 2.3. The PV plant must not disconnect from the network if the PCC voltage value is above the *voltage limit 1*.

- The voltage drops above the *voltage limit 2* and below the *voltage limit 1*, should not lead to disconnection of a PV plant. The disconnection of PV plant and resynchronization within 2 sec is also another option. Upon resynchronization, the active power increment must have a minimum gradient of 10% of the rated capacity per second. The value of injection of current during this time from a PV plant should be agreeable to a network operator. The *voltage limit 2* can be shifted/adjusted to suit the requirement of a network operator.

- If voltage drops above *voltage limit 3* and below *voltage limit 2*, the plants should be disconnected upon agreement with a network operator. The longer resynchronization time (greater than 2 sec)can be adopted. Similarly shorter gradient (less than 10%) can be also adopted to suit requirements.

- The plant can be disconnected for a voltage drop below *voltage limit 3*

There is also the specification in the grid code about minimum reactive current that must be injected during a balanced fault in order to offer a voltage support [64].

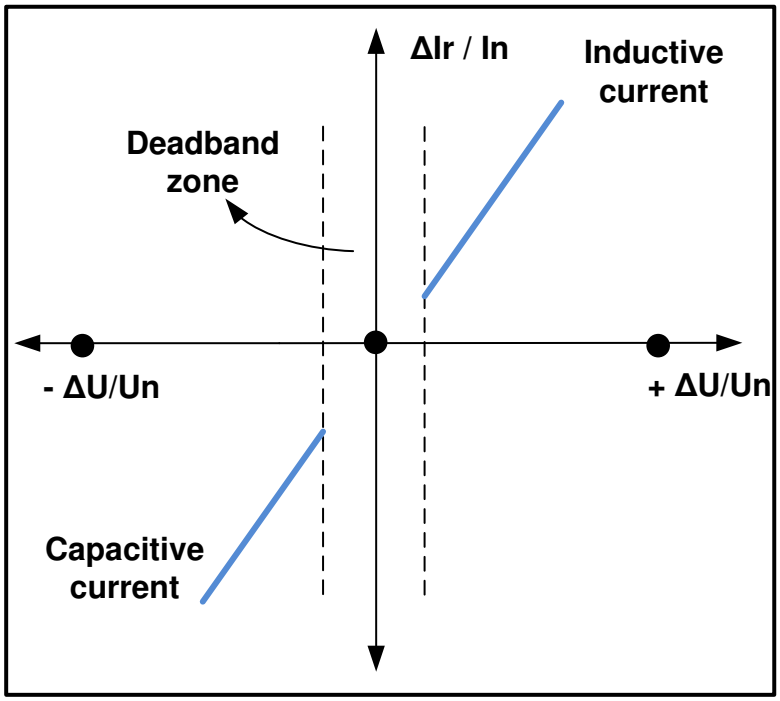

Figure 2.4: PV plant reactive current injection

This is shown in Fig.2.4. The supply of the reactive current should be at least 2% of the PV plant rated current for a per percent voltage variation. The requirement can be mathematically explained by the following equation,

$$\frac{\Delta I_r / I_n}{\Delta U / U_n} > 2\% \tag{2.1}$$

In the above equation, I_n and V_n respectively represent the rated current and the rated voltage of a PV plant. ΔU is the difference between a voltage during a fault and a voltage prior to a fault. ΔI_r is the difference between a reactive current injected and a reactive current prior to a fault. The *deadband zone* represents $\pm 10\%$ of the voltage around the nominal (1pu), in which the reactive current inject requirement should not be activated. Similar to the above illustrative LVRT example by German operators, there are country-specific LVRT requirements. The *voltage limit lines* and a voltage support requirements during a fault are adjusted by the operators in different countries to suit their power system support needs [65].

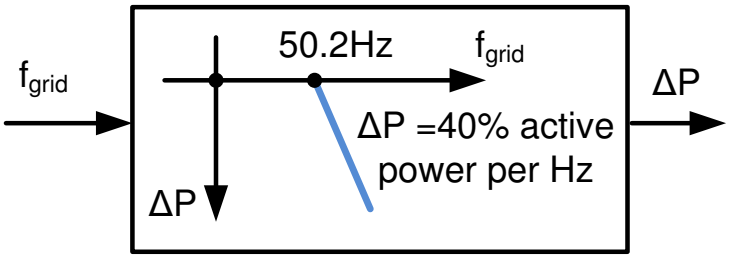

Figure 2.5: Active power reduction during over-frequency

Frequency support

The PV plants are disconnected from a network in case of an over-frequency event. This can result in the disconnection of a significant PV capacity in countries with large integration (for example Germany, Italy etc). This in turn can cause a cascaded effect and the power system may experience a black out as discussed in Chapter 1. This is avoided by defining a frequency support scheme from a PV plant. Such a service is defined in the German grid code BDEW. This is illustrated in Fig.2.5. The over frequency setpoint is at 50.2Hz in the Germany as explained in Chapter 1. German grid operators considered the possibility of loss of a large active power injection from the PV plants when the frequency exceeds 50.2Hz. This is mitigated by defining a power output reduction characteristic in an event of a frequency deviation. This is depicted in Fig.2.5. PV plants must reduce the available active power at the rated 40% per Hz. The increment in active power is not permitted till the frequency becomes 50.05Hz. The PV plant should be disconnected if the frequency is above 51.5 Hz.

The German example of the gradient active power reduction provision during an over-frequency event is illustrative. There are other standards which employ such a provision in different form. The frequency threshold VDEARN4105 and BDEW standards is 50.2Hz as shown in Fig.2.5. European standard EN50438 recommends a default threshold frequency of 50.3Hz Various strategies for the active power-frequency control during an over-frequency event are proposed in the various standards. The gradient parameters and response when the frequency returns to

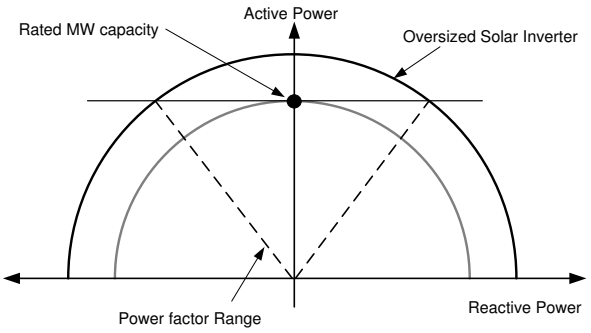

Figure 2.6: Solar generation capacity curve

the normal band etc. are different in different standards [66] [4].

2.3.2 Steady state voltage support

The most pressing steady state operational challenge faced by the distribution network operator is an intermittent overvoltage due to a PV plant. IEEE1547 expects a PV plant to operate at a unity power factor. The operation of a PV generation at an unity power factor means no contribution from a PV inverter towards the reactive power or the voltage support functionality. The network operators are increasingly demanding a contribution from PV generators towards a steady state voltage control functionality. The voltage support functionality by PV plant can be offered by an active power curtailment and a reactive power support. The voltage rise issue is addressed in German networks by 30% active power curtailment for plants smaller than 30kWp [45]. The contribution of a reactive power at the highest active power capacity of a PV plant necessitates an interface inverter overrating. This is indicated in terms of a PV generation capacity curve in Fig.2.6. The grid codes usually recommend a power factor range as shown in the capacity curve at which PV plant should be able to operate even at its maximum active power capacity. This determines an apparent power rating of a PV inverter. German LV grid code VDEARN4105 prescribes that PV plants having apparent power rating between 3.68 kVA and 13.8 kVA must be able to operate at 0.95 lead/lag power factor(pf). German MV grid code BDEW also suggests the same pf range. Italian grid code prescribes 0.95 lead/lag pf range for the PV plants having

apparent power rating between 3kVA to 6kVA where as above 6kVA 0.9 lead/lag pf range is recommended. UK standard G83 also states 0.95 lead/lag as the pf range.

The various LV and MV network standards both expect PV generation to offer a reactive power support as requested by a network operator. Most of the standards expect a reactive power support through the following different ways [55] [67].

1. Constant power factor (pf)
2. Constant reactive power (Q)
3. Variable power factor as active power varies (pf(P) characteristic)
4. Variable reactive power as voltage varies (Q(U) characteristic)

The *constant pf* mode and *constat Q* mode expect a PV plant to operate at a constant preset pf or a constant reactive power value when active power varies. However the other two modes of operational characteristics *pf(P)* and *Q(U)* adopt variable reactive power injections when active power or PV plant point of common coupling voltage varies.

pf(P) characteristic

The overvoltage condition in a power system typically occurs near the highest active power injection. In this scenario a PV inverter can offer an inductive reactive power support. The default *pf(P)* curve defined in VDEARN4105 is depicted in Fig.2.7. There is no reactive power support till a PV plant active power output reaches 50%. Then an inductive reactive power support is offered by a PV inverter by operating at a lagging pf. The PV plant is operated at a lagging pf limit of 0.95 at the rated active power output. A similar strategy with a PCC voltage check is implemented in Italian grid code. That is, a PV plant operates in a lagging pf if a PCC voltage is above a preset value [68].

Q(U) characteristic

This method monitors a PV PCC voltage. An appropriate value of a inductive or a capacitive reactive power support is offered to improve the PCC voltage profile. This

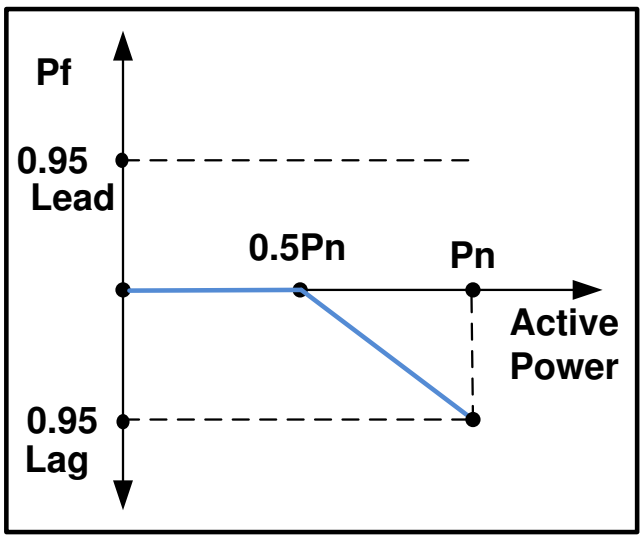

Figure 2.7: pf(P) characteristic as per voltage support

method of a voltage support through *Q(U)* characteristic is prescribed in BDEW standard. Typical characteristic as prescribed in BDEW is shown in Fig.2.8. There is a voltage deadband zone in the *Q(U)* characteristic where no reactive power support is offered [69] [70].

Both the *pf(P)* and the *Q(U)* characteristics consider a gradient to avoid sudden changes in a PCC voltage value. The BDEW guideline recommends that every individual network operator should decide either characteristic or target reactive power setpoints. Further, a remote control of the PV inverters to convey reactive power setpoints is recommended [25]. The *Q(U)* characteristic is defined in the Italian grid code as well.

2.4 Summary

- There are various country-specific grid codes. There are also different grid codes depending upon the voltage level at which a PV is integrated. Though the network operator specific settings are necessary there is a need for the harmonization of the grid codes.

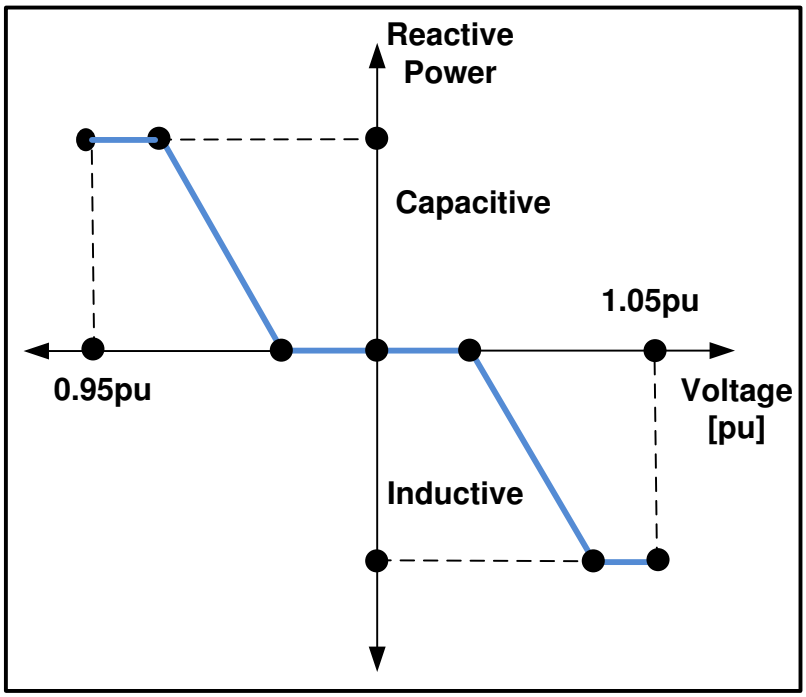

Figure 2.8: Q(U) characteristic for voltage support

- Those grid operators who are experiencing higher growth in the PV generations on to their networks are expecting PV to act in a grid support mode.

- Though it appears that grid operators wish to use PV inverter control features extensively in order to address the PV integration challenges, some of the standards are still evolving. For instance, IEEE 1547 recommends unity pf operation of a PV. The draft update of this standard is supportive of the reactive power support from a PV inverter.

- The reactive power support features for a steady state voltage support appear to consider PCC voltage magnitude only. That is if a PCC voltage is higher, an inductive reactive power support is recommended. The reactive power support from a PV inverter can be utilized for not only a voltage support but also an efficient operation of a feeder. There is no consideration for an optimal operation of a feeder in the standards.

- The enhanced utilization of the PV inverters in the voltage control mode is

still under consideration. The grid codes might consider it in future.

- Further steady state voltage support features recommended in the standards do not consider the challenges such as an adverse impact of a PV plant on the classical voltage control devices such as on-load tap-changers and voltage regulators.

Prior to the consideration of the steady state voltage control challenges, the detailed PV generation model is studied. A model suitable for the power system studies is developed. This is discussed in the next chapter.

Chapter 3

PV generation modeling

The previous chapters presented the challenges in integrating PV generation into a power system. A suitable model of PV generation is necessary to study how PV control integrates and interacts with those power system challenges. The PV generation models required for the power system studies can be classified as the dynamic and the steady state models. The model should adequately represent the various features of a PV generation such as its topology, control structure etc. This chapter discusses a typical PV generation topology, its component modeling and the control algorithm details. The dynamic model suitable for the power system studies is developed. This model is utilized in the case study to examine the impact of a PV generation on the *small signal stability* of a power system. The simulation results are presented in detail. The steady state models required to study power system operational challenge such as *steady state voltage control* are also discussed.

3.1 PV topology

A typical topology of a grid integrated PV and a control structure of its power inverter is shown in Fig.3.1. The topology comprises three main subsystems : a PV panel, a grid interface power converter and a converter control system. A PV panel converts solar energy into dc electrical energy. The dc electrical energy generated from a PV panel is injected into a power system at the nominal grid voltage and the nominal grid frequency by utilizing a power electronic converter. The control

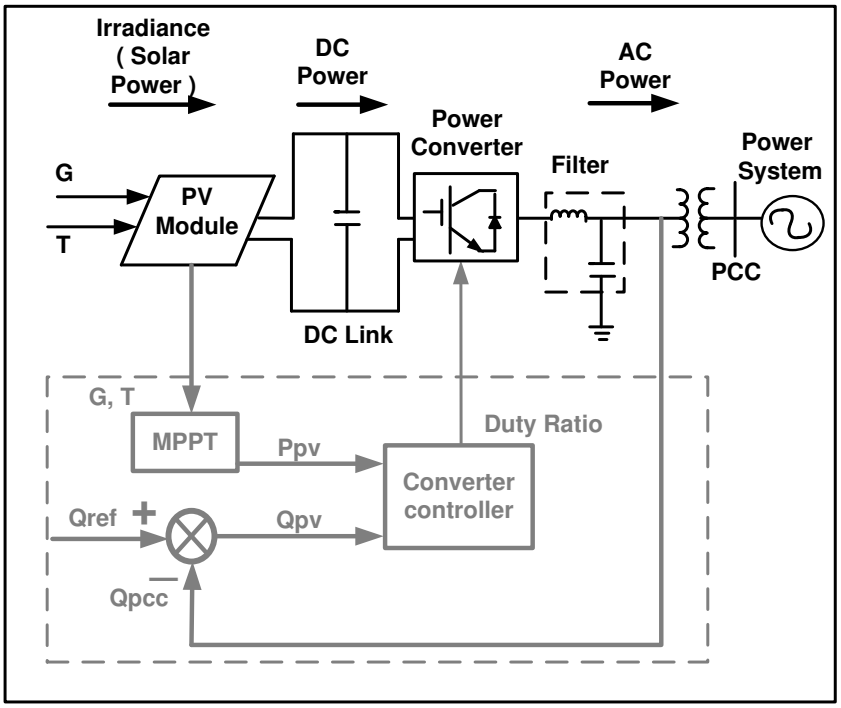

Figure 3.1: Generic grid integrated PV topology

structure of a power converter ensures an efficient operation and also incorporates the grid support features.

3.2 PV generation dynamic model

A dynamic model of a PV generation is necessary to study the impact of a PV plant on the power system stability and control. An appropriate mathematical representation of the above mentioned subsystems is essential to develop a suitable PV generation model. The following sections detail the modeling of these subsystems.

3.2.1 PV power circuit

The PV power circuit consists of two subsystems a PV panel and a power converter. The PV cell is the basic unit of a PV panel which converts an irradiance to an electrical energy. A PV cell usually produces power of the order of 1 or 2 watts. A series combination of the PV cells represents a PV module. A series-parallel

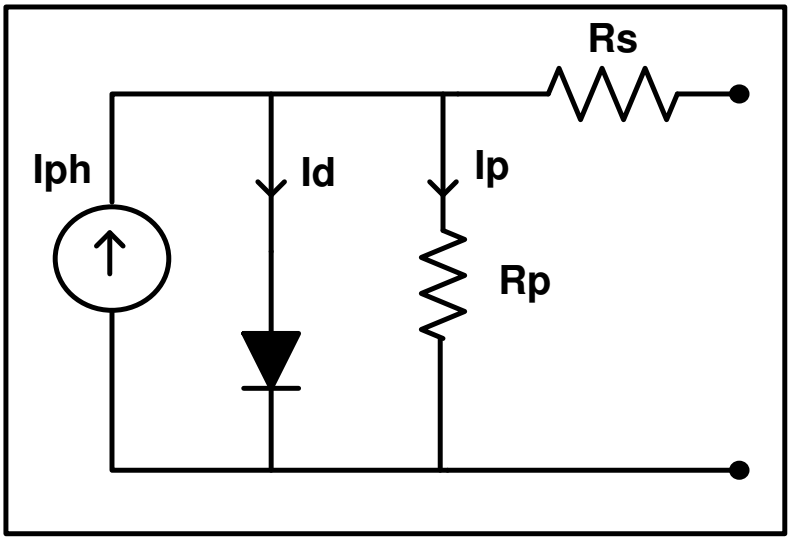

Figure 3.2: Equivalent circuit of PV module

combination of the several PV modules constitutes a PV panel. There are several mathematical models of the PV cells proposed in the literature. However, for power system studies a single diode model represented in Fig.3.2 is sufficiently accurate [73]. The PV module or the cell is represented as the current source in parallel with the antiparallel diode. It also consists of the series and the parallel resistances as shown in Fig.3.2. The current source represents the photon generated electrons and the holes. The antiparallel diode represents the diffusion of the minority carriers in the depletion region. The structural resistance of the PV module/cell and the leakage current are represented by the series and the parallel resistances respectively. A PV cell data provided by a manufacturer in a data sheet is at the standard test conditions (STC). The STC is defined as the condition in which the irradiance value is $1000W/m^2(G_{stc})$ and the cell temperature is 25^oC (T_{stc}). All STC data is at the specific air mass value 1.5. Air mass is defined as a relative path length of a direct solar beam through atmosphere. The air mass is calculated by sec(zenith angle). The air mass is 1.0 if the sun is at the zenith (exactly overhead at the zenith angle 0^o). The specific air mass value of 1.5 (at the zenith angle 48.2^o) has been selected for standardization purposes by the American society for testing and materials which is widely used [74] [75] [76].

A mathematical model of a PV panel can be described using Fig.3.2 and by defining following equations. The DC current output of a PV panel $I(V)$ which is a function of a voltage V across the PV module is calculated as,

$$I(V) = I_{ph}(G,T) - I_d(V) - I_p(V) \tag{3.1}$$

$I_{ph}(G,T)$ in (3.1) represents current generated by the PV, as a function of a temperature T and a irradiance G. $I_d(V)$ represents the current flowing through the antiparallel diode and the loss current is $I_p(V)$. Further substituting detailed expression for the diode current (Shockley equation) and the loss current,

$$I(V) = [I_{ph}(G,T)] - [\{I_o(T)\}.\{e^{\frac{\beta(V+R_sI)}{a}} - 1\}] - [\frac{(V+R_sI)}{R_p}] \tag{3.2}$$

In (3.2), $I_o(T)$ represents the diode reverse saturation current which depends on a temperature T, R_s is the series resistance, R_p is the parallel resistances, and a is the diode ideality factor. The inverse thermal voltage β in (3.2) depends on the temperature T and the electron charge q.

$$\beta(T) = \frac{q}{N_s k T} \tag{3.3}$$

In (3.3) k is Boltzman's constant and N_s is the number of series connected PV cells. The short circuit source current which depends on the irradiance G_{stc}, the temperature T_{stc} and the short circuit current $I_{sc,stc}$ at the STC is calculated as,

$$I_{ph}(G,T) = [I_{sc,stc} + K_I(T - T_{stc})]\frac{G}{G_{stc}} \tag{3.4}$$

K_I in (3.4) represents the short circuit current coefficient. The open circuit diode reverse saturation current $I_o(T)$ introduced in (3.2) also depends upon the temperature T_{stc} and the open circuit voltage $V_{oc,stc}$ at the STC.

$$I_o(T) = \frac{[I_{sc,stc} + K_I(T - T_{stc})]}{e^{\frac{\beta}{a}(V_{oc,stc} + K_V(T - T_{stc}))} - 1} \tag{3.5}$$

K_V in (3.5) represents the open circuit voltage coefficient. The parameters

introduced in equations (3.1)-(3.5) are PV panel datasheet parameters. The parameters used in this study are given in Appendix A. The equations (3.1)-(3.5) are used to mathematically represent a PV panel.

The power generated by a PV panel is in the DC form. The main purpose of a power converter is to convert this dc power to the ac form. The power converters can be single stage or two stage. A two stage power converter has a dc-dc converter in order to boost the dc voltage and then a dc to ac power inverter stage. A single stage converter consists of a dc to ac inverter stage only. The single-stage PV system has only one power conversion stage hence they are expected to be more economical. This system is also widely used in three phase utility interfaced applications for megawatt class PV plants. Utility interfaced PV plants is the focus of this study. Hence a single stage model of a PV generation is considered here. Typically dc to ac conversion in a single stage PV is achieved by a voltage source converter (VSC). A VSC is interfaced with a grid using a low pass filter and an interconnection transformer. Usually, Insulated-gate bipolar transistors (IGBTs) are used as power electronic switches in a VSC. A VSC converts power from dc to ac form by switching of IGBTs. The turn-on/off command for IGBTs are issued through a pulse-width modulation (PWM) strategy. A PWM technique varies the duty ratio of switches at high frequency to achieve the regulated lower frequency VSC output voltage. There are variety of different PWM techniques reported in litreture [77].

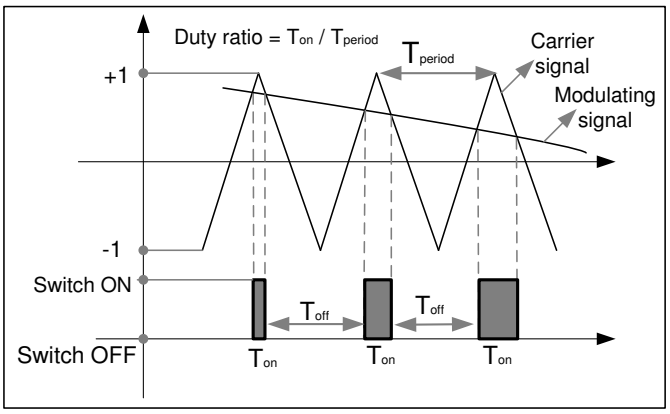

Figure 3.3: Typical PWM strategy for a VSC

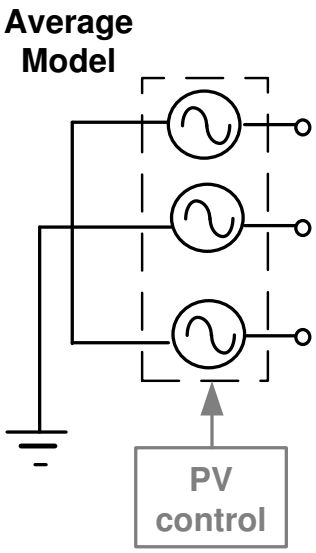

Figure 3.4: Converter circuit represented by voltage sources (average model)

Most widely used PWM strategy compares a carrier signal (high frequency periodic triangular wave) with a modulating signal (slow varying waveform). This is shown in Fig. 3.3. A carrier signal is a periodic waveform having amplitude ± 1 and period T_{period}. A modulating signal is the main control signal from a PV controller. The intersection of these two waveforms determines the on time of a VSC switch. The fraction of the switching period T_{period} during which the switch is on is called the duty ratio.

A VSC can be modeled as a three phase controlled voltage source neglecting power electronic switches. Such a model of VSC is known as the dynamic average model [78]. This is depicted in Fig.3.4. VSC terminal voltages and currents are represented by moving average values in averaged model simulations. In average models algebraic relationship between controller modulation signals and VSC variables (dc and ac voltages, currents) is established. A modulation signal which is the main control signal is determined by a PV controller. A typical PV controller incorporates a vector control strategy in the *dq reference frame*. This control strategy is explained in the next section.

3.2.2 PV control structure

The converter control ensures an efficient operation of a grid connected PV system. There are two basic functional blocks of a PV control structure. The first functional block is a Maximum Power Point Tracking (MPPT) algorithm. The MPPT achieves the best possible efficiency of a PV system by setting the appropriate value of the dc link voltage reference at the particular value of the temperature and the irradiance. The dc link voltage controller helps to track this reference value set by the MPPT. Typically, the dc link voltage control consists of an inner active power control loop. The inverter is also capable of offering a reactive power support. This is achieved by a reactive power control loop [79] [78]. The PV reactive power control loop can also achieve a dynamic voltage control of a PCC voltage. Typically well developed pulse width modulation (PWM) techniques are utilized to control AC output of a converter. A PWM technique varies duty ratios that is percentage on times of various power converter switches in one period. From an average model point of view which does not consider detailed representation of power electronic switches duty ratios can be considered as output signals from the control system to voltage sources represented in Fig.3.4.

Maximum power point tracking (MPPT)

A typical PV power against voltage or current characteristics is shown in Fig.3.5 This PV characteristic varies with a randomly varying solar irradiance and a temperature. The objective of a MPPT technique is to track the V_{MPP} at the every value of the irradiance and the temperature so the maximum power output P_{MPP} can be injected into a power system grid. There are several MPPT techniques available to achieve this namely, perturb and observe technique, incremental conductance technique, fractional open circuit voltage or short circuit current etc. Some of the techniques are discussed here.

Perturb and observe technique:

A closer observation of the characteristics in Fig.3.5 can explain the basic strategy behind the Perturb and Observe technique ($P\ and\ O$) technique. An increase in PV voltage results in an increase in PV output power till an operating point is on

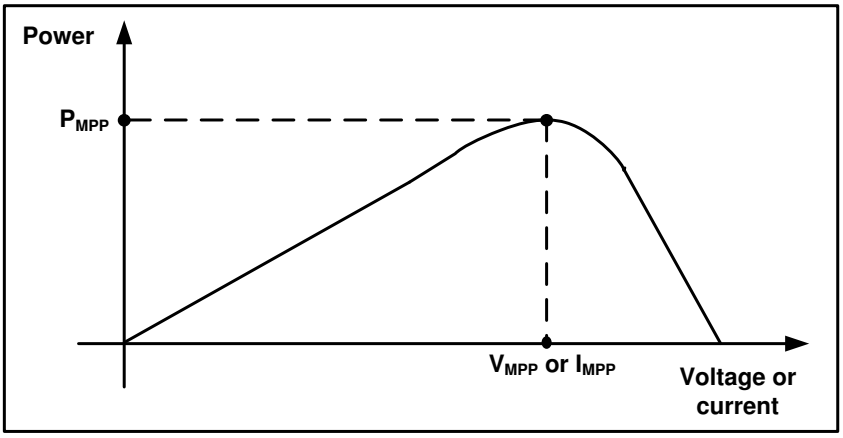

Figure 3.5: Power against voltage or current characteristics.

the left to the maximum power point (the point represented by V_{MPP} and P_{MPP}). Similarly if an increase in a PV voltage is resulting in a decrease in PV power then an operating point is on the right side of *the maximum power point*. The *P and O* technique uses this particular feature. The flow chart of the*P and O* algorithm is shown in Fig.3.6.

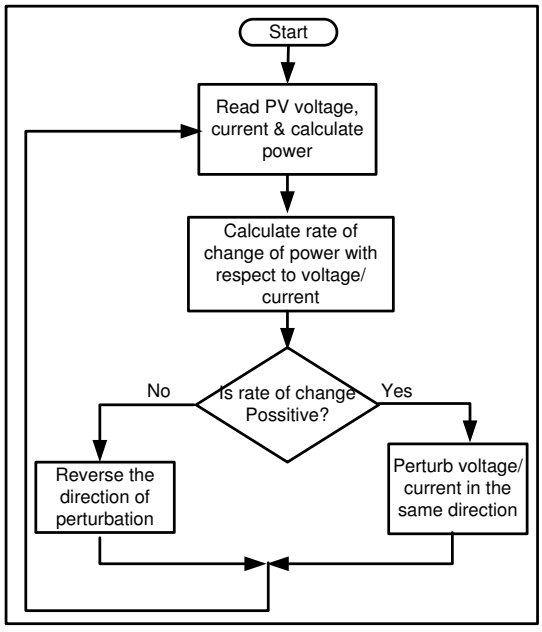

Figure 3.6: Perturb and observe MPPT technique

A DC voltage value across the PV is continuously perturbed and the PV Power

is observed. The change in voltage is maintained in the same direction if a change in the PV voltage value is increasing the PV power, otherwise the dc link voltage is changed in the reverse direction. This process is continuously operational until *the maximum power point* (MPP) is reached. A PV current also can be perturbed in order to achieve *the MPP* instead of a PV voltage. This perturbation in a PV voltage value or a current value is achieved by varying the duty ratio of the power converter.

Incremental conductance technique:

The incremental conductance technique continuously monitors the conductance value in order to achieve the MPP. The mathematical model detailing this technique can be derived observing Fig.3.5 characteristic. It can be said that at *the MPP*, the rate of change of the PV power P_{pv} with respect to the PV voltage V_{pv} is zero,

$$\frac{d}{dV_{pv}}(P_{pv}) = 0 \tag{3.6}$$

The rate of change of the PV power with respect to the PV voltage also can be expressed as,

$$P_{pv} = V_{pv} \times I_{pv}$$

$$\frac{d}{dV_{pv}}(P_{pv}) = I_{pv} + V_{pv}\frac{d}{dV_{pv}}(I_{pv}) \tag{3.7}$$

Hence the following expression can be written in the three regions of the PV characteristics. At *the MPP*, the following expression is true:

$$\frac{\triangle I_{pv}}{\triangle V_{pv}} = -\frac{I_{pv}}{V_{pv}} \tag{3.8}$$

The left hand side of *the MPP* when the PV power increases with the increase in PV voltage, the following expression is true:

$$\frac{\triangle I_{pv}}{\triangle V_{pv}} > -\frac{I_{pv}}{V_{pv}} \tag{3.9}$$

The right hand side of *the MPP* when the PV power decreases with the increase in

PV voltage, the following expression is true:

$$\frac{\triangle I_{pv}}{\triangle V_{pv}} < -\frac{I_{pv}}{V_{pv}} \tag{3.10}$$

Thus comparing the instantaneous conductance value, a reference voltage can be set for a PV in order to achieve P_{MPP} using the expressions (3.8)-(3.10).

Fractional open circuit voltage or short circuit current:

The fractional open circuit voltage method makes use of the fact that the open circuit voltage V_{OC} and the MPP voltage V_{MPP} have a linear relationship amongst them. The PV short circuit current I_{SC} and the MPP current I_{MPP} also have the linear relationship.

$$V_{MPP} = K_1.V_{OC}$$

$$I_{MPP} = K_2.I_{SC} \tag{3.11}$$

The constants of proportionality K_1 and K_2 in (3.11) can be computed by an empirical determination of the open circuit voltage and the MPP voltage at different temperature and irradiance values (or by determining the short circuit current and the MPP current). Once these proportionality constants are calculated, during the operation of a PV, an open circuit voltage V_{OC} can be measured by momentarily shutting down the power converter (or a short circuit current I_{SC} can be measured by momentarily shorting the PV terminals through a switch). Thus by using the values of V_{OC} (or I_{SC}) and K_1 (or K_2) the MPP values of V_{MPP} (or I_{MPP}) can be computed.

Several other techniques which are improved versions of the above techniques are available in the literature. The techniques have their relative advantages and disadvantage. The cost of hardware, the computational complexity and the performance etc. are some of criteria based on which these techniques are compared. A comprehensive review of MPPT techniques is presented in [80]. MPPT is one of the important feature of a PV topology. In this work the perturb and observe technique is implemented. This MPPT algorithm sets the dc link voltage reference. The DC link voltage control loop to track this reference is explained next.

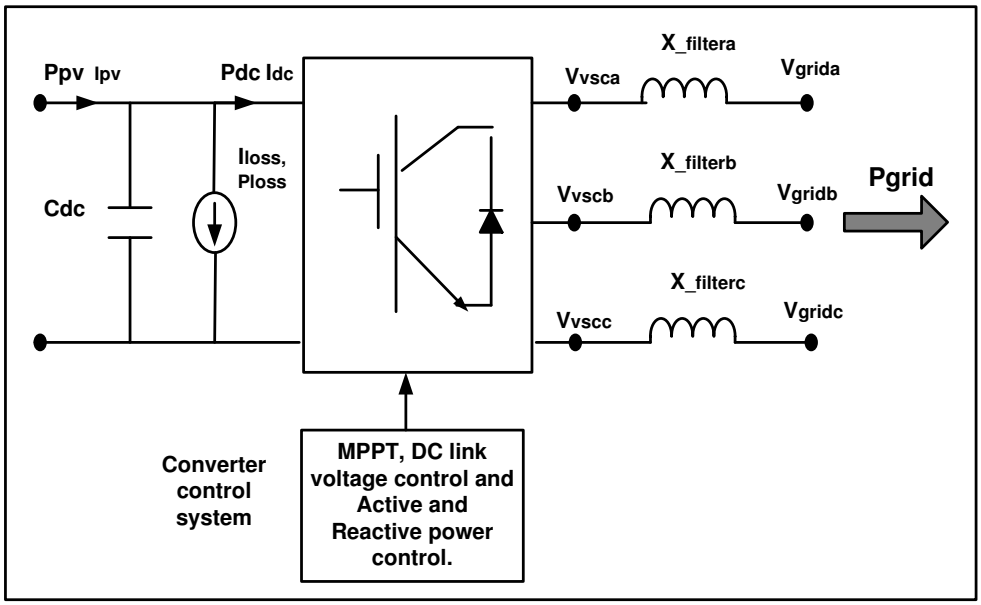

Figure 3.8: Schematic of dc link and grid interface

DC link voltage control

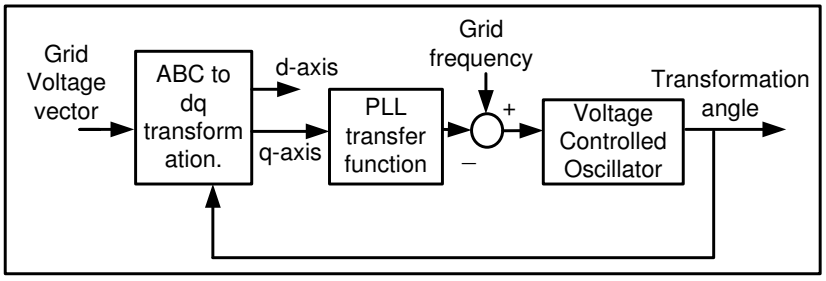

Figure 3.7: Phase locked loop

The control of a PV inverter is carried out using a vector controlled strategy in the d-q reference frame. The transformation angle calculation and the grid synchronization is achieved through a phase locked loop (PLL). The control block diagram of a PLL is shown in Fig. 3.7. The VSC modeled as a controlled voltage source is connected to the grid through a filter and a transformer. A schematic of the dc link and the grid interface with all variables is shown in Fig.3.8.

The following equations illustrate the dc link voltage dynamics. The dc link

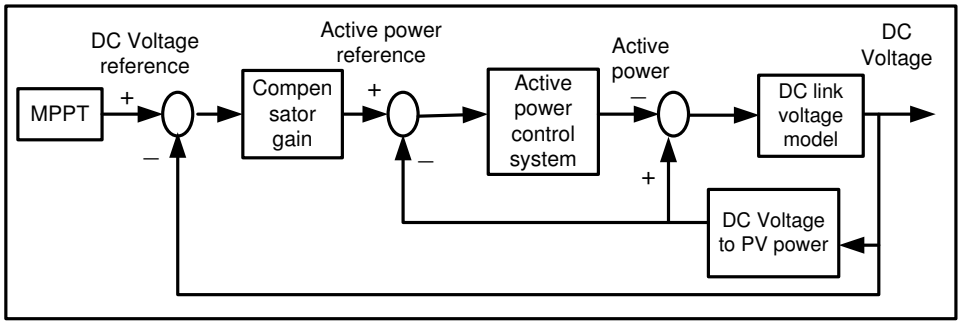

Figure 3.9: DC link voltage control

power P_{dc} indicated in Fig.3.8 can be calculated as follows :

$$P_{dc} = P_{pv} - P_{loss} - \frac{d}{dt}(\frac{1}{2}CV_{dc}^2) \tag{3.12}$$

In 3.12, P_{pv} is the power generated by a PV plant, the derivative term in (3.12) indicates the rate of change of energy of the dc link capacitor and P_{loss} is the negligible power loss associated with the capacitor. The power injected to AC grid P_{grid} is equal to P_{dc}, if a lossless VSC and filter are assumed.

$$P_{grid} = P_{pv} - P_{loss} - \frac{d}{dt}(\frac{1}{2}CV_{dc}^2) \tag{3.13}$$

$$\frac{C}{2}\frac{d}{dt}(V_{dc}^2) = P_{pv} - P_{loss} - P_{grid} \tag{3.14}$$

The above equation (3.14) shows the VSC AC side power P_{grid} (neglecting the losses) can be considered as the control input, the dc link voltage term V_{dc}^2 as the output and the power terms P_{pv} and P_{loss} as the disturbance inputs. The control block diagram of the system is shown in Fig.3.9.

The main task of the dc link voltage controller is to track the dc link voltage reference set by the MPPT scheme. This voltage reference is achieved by the control of the active power flowing through the VSC (P_{grid} or P_{dc}). The error between the DC link voltage reference set by the MPPT and the actual dc link voltage is processed by the compensator. This outputs the real power reference for the real power control system as shown in Fig.3.9. The real power control

system which is explained in the next section processes this reference and tracks the active power P_{grid} or P_{dc}. Further, P_{dc} is processed by the dc link voltage dynamics (illustrated by eq.(3.12)-eq.(3.14) above) to calculate the dc link voltage. The PV power characteristics demonstrates that the photovoltaic power P_{pv} depends upon V_{dc}. Hence an estimate of P_{pv} as shown in control blocks can be added to the real power reference value as shown in the control block diagram Fig.3.9 by the *dc voltage to PV power block*. In the dynamic situation the difference between the PV power and the VSC ac side power will flow through the dc link capacitor which will result in the change in a dc link voltage. As discussed above the dc link voltage controller has an active power controller as its nested loop.

Active and reactive power control

The primary objective of the active power controller is to track the active power reference. The primary objective of the reactive power controller is to control the power factor/voltage at the PCC. Let us denote w_g as the grid frequency then the three phase grid voltages from Fig.3.8 can be expressed as follows.

$$\begin{aligned} V_{grida}(t) &= V_{peak}cos(w_g t) \\ V_{gridb}(t) &= V_{peak}cos(w_g t - \frac{2\pi}{3}) \\ V_{gridc}(t) &= V_{peak}cos(w_g t - \frac{4\pi}{3}) \end{aligned} \tag{3.15}$$

The following equation can be written neglecting filter losses, if the grid voltage vector $\overrightarrow{V_{grid}}$, the VSC terminal voltage vector $\overrightarrow{V_{vsc}}$ and the filter current $\overrightarrow{I_{filt}}$ flowing through the filter inductance L_{filt} are considered.

$$L_{filt}\frac{d}{dt}\overrightarrow{I_{filt}} = \overrightarrow{V_{vsc}} - \overrightarrow{V_{grid}} \tag{3.16}$$

The above eq.(3.16) is in the three phase *abc reference frame*. The same equation in the *dq-reference frame* using the transformation angle ϕ is expressed as,

$$L_{filter}\frac{d}{dt}I_{dq}e^{j\phi} = V_{vscdq}e^{j\phi} - V_{peak}e^{jw_g t} \tag{3.17}$$

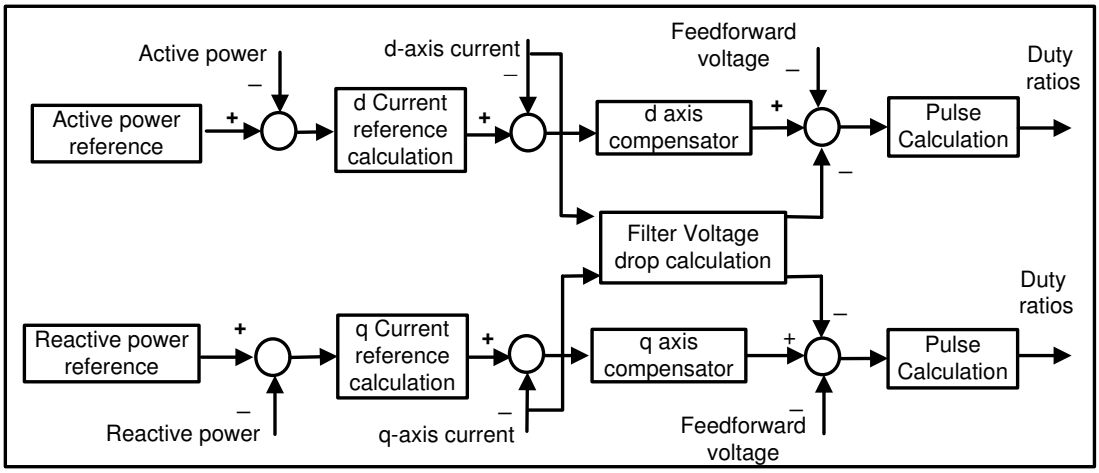

Figure 3.10: Active and Reactive power control topology

Separating the d-axis and the q-axis components results into following,

$$L_{filt}\frac{d}{dt}I_d = V_{vscd} - V_{gridd} + L_{filt}w_g I_q$$

$$L_{filt}\frac{d}{dt}I_q = V_{vscq} - V_{gridq} + L_{filt}w_g I_d \tag{3.18}$$

The active power P_{grid} and the reactive power Q_{grid} in the *dq-reference frame* is given by [78],

$$P_{grid} = \frac{3}{2}[V_{gridd}I_{gridd} + V_{gridq}I_{gridq}]$$

$$Q_{grid} = \frac{3}{2}[-V_{gridd}I_{gridq} + V_{gridq}I_{gridd}] \tag{3.19}$$

The PLL modeled here always sets the V_{gridq} component to zero that simplifies (3.19) further,

$$P_{grid} = \frac{3}{2}V_{gridd}I_{gridd}$$

$$Q_{grid} = -\frac{3}{2}V_{gridd}I_{gridq} \tag{3.20}$$

The above equations show that, the active power at the PCC can be controlled by controlling I_{gridd} and the reactive power can be controlled by controlling I_{gridq}. The control block diagram for the active and reactive power controllers is shown in Fig.3.10. The active power reference value is set by the DC link voltage control.

Further, the direct axis current reference is calculated using the active power reference. The reactive power reference calculates the quadrature axis current reference. The errors in the direct and quadrature currents are processed by the compensator. The compensator calculates the VSC duty ratios required to track the reference values. All the above controllers have saturation blocks for the various signal (dq- currents, dc link voltage etc) in order to have the protection. These saturation limiters are not shown in the control block diagrams. The presented PV dynamic model is used in the case study which is discussed next.

3.2.3 Case study : small signal stability analysis

The discussed dynamic model is utilized to analyze the impact of PV generation on the small signal stability of a power system. Two system models, the single solar infinite bus (SSIB) system and the solar connected in multi-machine system are studied. The SSIB system models the dynamics of the PV system connected to an infinite bus. The multi machine system considers the conventional power plants by modeling the synchronous machine dynamics along with the discussed dynamic PV model.

Single solar infinite bus model

The dynamic PV generation system and all its control features explained are modeled in detail. The model has irradiance, temperature and reactive power reference as inputs. And the active and the reactive power injections to the grids are outputs. Appendix A presents the detailed PV panel parameters and PV inverter parameters for this simulation study [81].

The perturb and observe MPPT algorithm is modeled to track the maximum power point under varying irradiance (G) and temperature (T). The developed dynamic model is tested by applying a step change in the irradiance, the temperature and the reactive power demand. A solar inverter rating of 1.5MVA is considered. The response of the MPPT algorithm is shown in Fig.3.11. The step change in irradiance happens at 4sec from $800W/m^2$ to $200W/m^2$. The step change in temperature is introduced at 8sec from 40^oC to 15^oC. The MPP tracking using

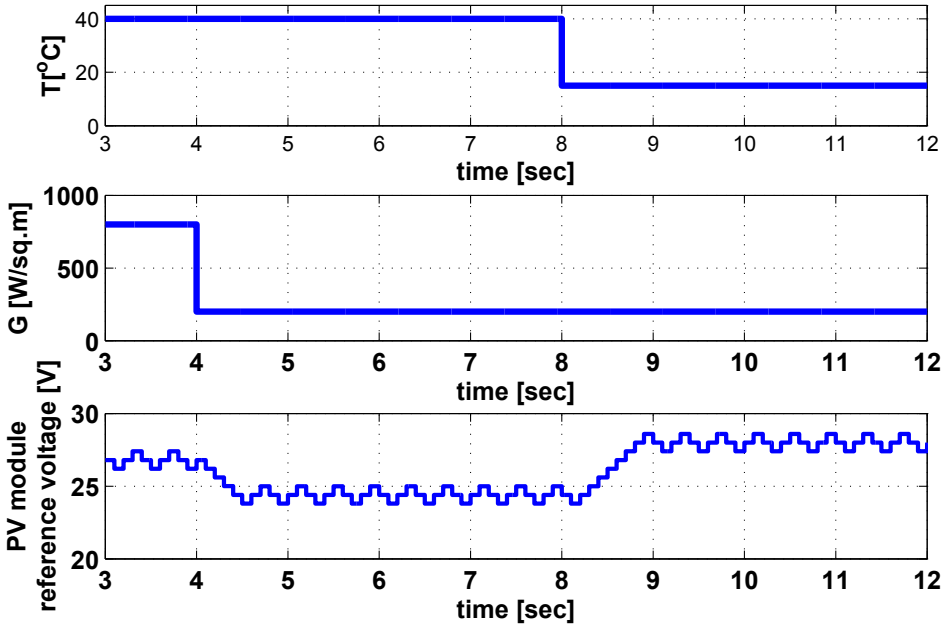

Figure 3.11: MPPT performance : PV module reference voltage

the perturb and observe algorithm can be seen in Fig.3.11. It can be observed that there is a perturbation around the maximum power point. This perturbation can be reduced by considering a smaller perturbation step size. A perturbation step size of $0.6V$ is considered in Fig.3.11. The consequence of the smaller step size is demonstrated in Fig.3.12. The smaller perturbation step size of $0.3V$ is considered. As expected perturbations around the maximum point are reduced. However it takes around 1 sec to track the maximum power point when irradiance changes and around 1.5 sec to track the maximum power point when the temperature changes. It can be observed from Fig.3.11 that it takes 0.5sec to track the irradiance change and around 1sec to track the temperature change when perturbation step size is $0.6V$. Thus reduced size minimizes the perturbations around the maximum power point but slows down the tracking process. This case study considers a perturbation step size of $0.3V$. Along with the change in the irradiance and the temperature, 100kVAr capacitive reactive power support is demanded from the PV inverter at 1.5sec. The injected active and reactive power to the grid are shown in Fig.3.13. Thus the proposed model takes into account MPPT and active- reactive power control dynamics in PV inverter. The objective is to study the impact of PV dynamics on

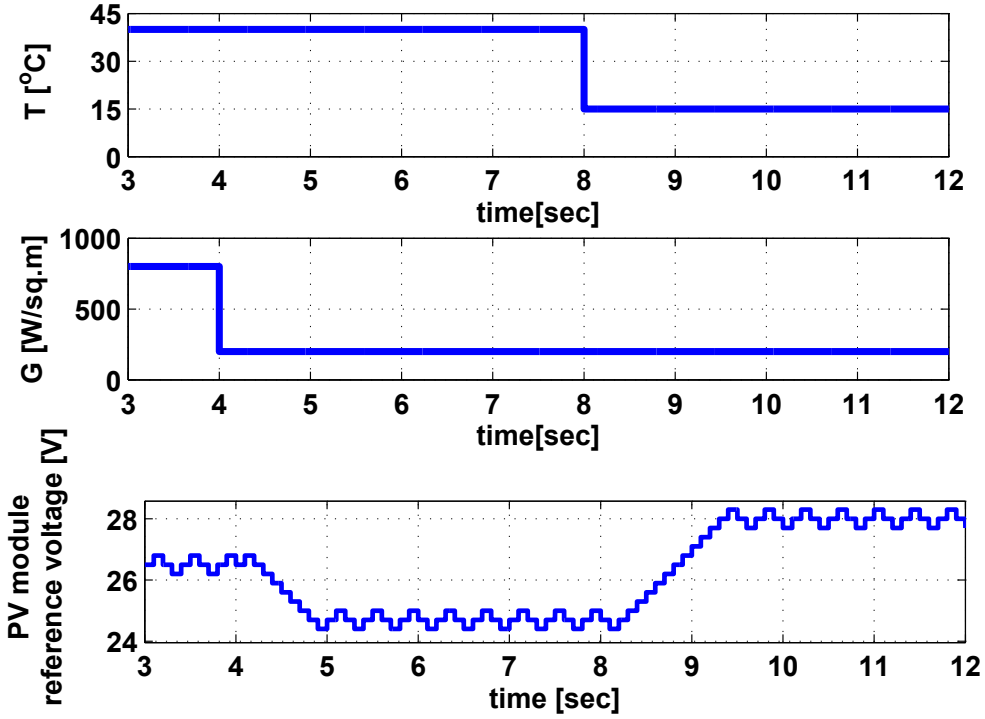

Figure 3.12: MPPT performance with a smaller perturbation step

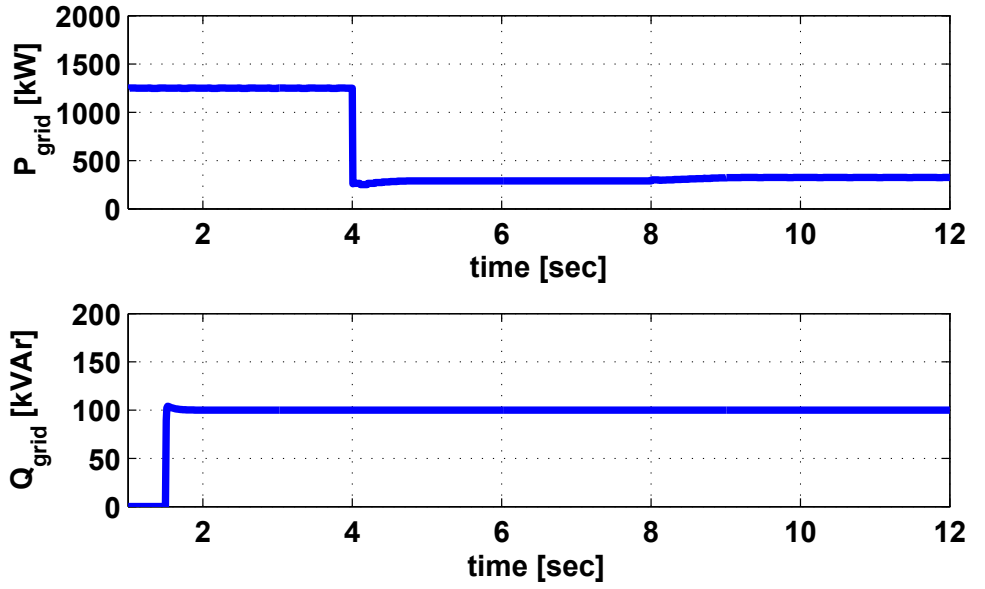

Figure 3.13: PV plant active and reactive power injection

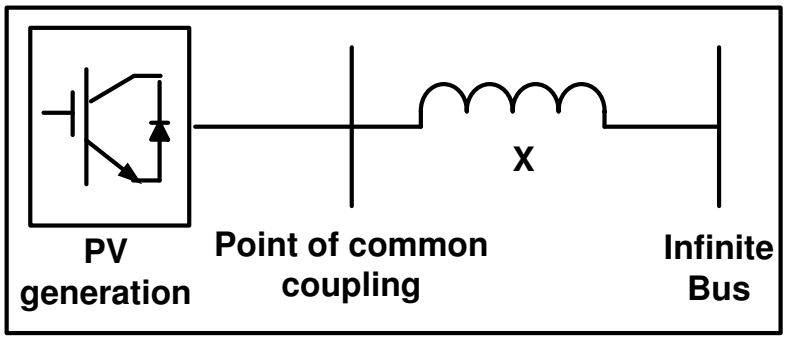

Figure 3.14: Single solar infinite bus model

the power system. The single solar infinite bus model (SSIB) system is analyzed. The schematic diagram of the SSIB system is shown in Fig.3.14. The PV power converter is connected to the point of common coupling(PCC) using the grid filter and transformer. The PCC and the infinite bus are connected with the transmission line. This is represented by the series inductance X. The active power P_{grid} and reactive power Q_{grid} exchange between the grid and the generator are modeled by the following equations,

$$P_{grid} = \frac{V_p V_b sin\theta}{X}$$
$$Q_{grid} = \frac{V_p^2 - V_{pcc} V_b cos\theta}{X} \tag{3.21}$$

In (3.21), V_p represents PV plant terminal voltage and V_b and θ represent the magnitude and the angle of the infinite bus voltage. The mathematical model of the SSIB system can be written as a set of differential and algebraic equations.

$$\frac{dx}{dt} = f(x, a, u)$$
$$g(x, a, u) = 0 \tag{3.22}$$

The schematic representation of the SSIB system differential and algebraic equations is shown in Fig.3.15. In eq.(3.22) x represents state variables, a represents algebraic variables, and u represents input variables. The differential and the algebraic equations vector is represented by f and g respectively. In small-signal analysis,

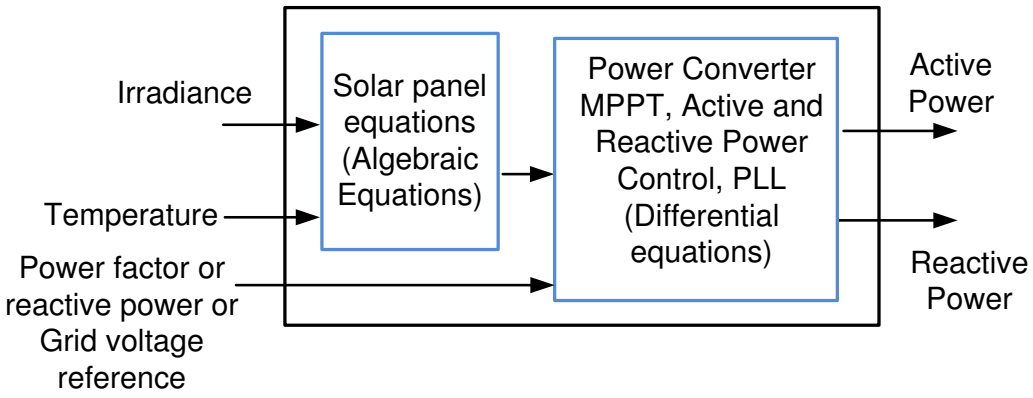

Figure 3.15: PV algebraic and dynamic equations

eq.(3.22) is linearized by a Taylor series expansion around an operating point (x_0, a_0, u_0). The system state matrix A_{sys} is obtained by eliminating the algebraic variable. The SSIB system state matrices are obtained as follows:

$$x = [I_a, I_b, I_c, V_{dc}, Control_{Vdc}, I_d, I_q]$$

$$u = [G, T, V_b, Q_{ref}] \tag{3.23}$$

x represents different states due to SSIB dynamics. I_a, I_b, I_c represents the current flowing through the impedance Z. V_{dc} in the state vector x represents the dc link voltage dynamics. The dc link voltage control state is represented by $Control_{Vdc}$. I_d and I_q represent the current controller states. The matrix u represents the SSIB model inputs: the irradiance G, the temperature T, the infinite bus voltage V_b, and the reactive power reference to the PV inverter Q_{ref}.

The base case SSIB system test results are obtained in order to compare the system performance under different scenarios. The operating point with standard test conditions (STC) for weather, the grid voltage of 1 pu and no reactive power support from the PV plant is considered as the base case. The solar and the grid converter systems are considered to be connected to an infinite bus as explained earlier. The base case eigenvalues and the corresponding participation factors are shown in Table.3.1 and Table.3.2. The dynamics consist of the five stable modes, one of which is oscillating with a high frequency. The participation factors indicate

the dominant states for each mode. The high frequency mode is mainly contributed by the dc link voltage control dynamics. The detailed participation factor analysis equations as proposed in [82] [83] are utilized.

Table 3.1: SSIB system eigenvalues

Serial Number	**Eigen Values**	**Oscillation frequency [Hz]**	**Damping ratio**	**Time constant [s]**
λ_1	$-7943.92 \pm 8310.28i$	1322	0.69	0.00013
λ_2	-863.24	0	1	0.0012
λ_3	-181.69	0	1	0.0055
λ_5	-10.61	0	1	0.0943
λ_6	-10.02	0	1	0.0998

Table 3.2: SSIB system participation factors

Serial Number	I_a	I_b	I_c	V_{dc}	$Ctrl_{Vdc}$	$Ctrl_{Id}$	$Ctrl_{Iq}$
λ_1	0.0003	0.36	0.37	0.724	1	0.0006	0
λ_2	0.014	0.044	0.044	0.09	1	0.001	0
λ_3	1	0.25	0.25	0.048	0.022	0.003	0.09
λ_4	0.0375	0.009	0.009	0.0026	0	0.04	1
λ_5	0.0014	0.0004	0.0003	0.0023	0	1	0.04

It is important to study the effect of a change in the irradiance and temperature on the dynamic behavior of a PV plant. The irradiance level is varied from $400W/m^2$ to $1000W/m^2$. The eigenvalues of the system for the different irradiance levels are shown in Table 3.3. It can be observed that there is no impact of the change in the irradiance level on the PV plant dynamics. Though there is some change in the eigenvalues, it is insignificant. The eigenvalues indicate that the system remains stable at the different irradiance values. A similar study is carried out with the change in the temperature. Only the temperature is varied and the other system parameters remain the same as the base case. The temperature is varied from 25^oC to 65^oC. Table 3.4 shows the eigen values of the system for different temperature levels. It can be observed that there is no impact of the change in temperature on the PV plant dynamics. The eigen values in Table3.3 and Table 3.4 indicate that the PV

Table 3.3: PV plant dynamics at change in irradiance

Serial Number	$1000W/m^2$	$700W/m^2$	$400W/m^2$
λ_1	$-7943.92 \pm 8310.28i$	$-7942 \pm 79591i$	$-7939.78 \pm 7591.60i$
λ_2	-863.24	-867.43	-872.06
λ_3	-181.69	-181.37	-181.03
λ_4	-10.61	-10.61	-10.62
λ_5	-10.02	-10.02	-10.02

system remains stable at different irradiance and the temperature conditions. Table

Table 3.4: PV plant dynamics at change in temperature

Serial Number	25^oC	45^oC	65^oC
λ_1	$-7943.92 \pm 8310.28i$	$-7943.87 \pm 8301.13i$	$-7943.49 \pm 8233.14i$
λ_2	-863.24	-867.34	-864.14
λ_3	-181.69	-181.69	-181.62
λ_4	-10.61	-10.61	-10.61
λ_5	-10.02	-10.02	-10.02

3.5 indicates the effect of the change in the terminal voltage. The terminal voltage is changed from 0.9pu to 1.1pu. It can be observed that the system remains stable at the different voltage levels. The PV inverter can offer the reactive power support.

Table 3.5: PV plant dynamics at change in terminal voltage

Serial Number	$0.9pu$	$1pu$	$1.1pu$
λ_1	$-7938.61 \pm 7401.47i$	$-7943.92 \pm 8310.28i$	$-7948.08 \pm 9128.17i$
λ_2	-874.56	-863.24	-854.32
λ_3	-180.85	-181.69	-182.37
λ_5	-10.62	-10.61	-10.61
λ_6	-10.02	-10.02	-10.02

The impact of varied reactive power injections from the PV plant is shown in Table 3.6. The operating conditions remain the same as those of the base case. Only the reactive power reference is varied from 1 MVAr inductive to 1 MVAr capacitive. It can be seen that the system remains stable at different reactive power injections.

Table 3.6: PV plant dynamics at different reactive power injection

Serial Number	$1MVAr$ inductive	$0MVAr$	$1MVAr$ capacitive
λ_1	$-7959.022 \pm 8324.22i$	$-7943.92 \pm 8310.28i$	$-7928.7 \pm 8296.28i$
λ_2	-859.31	-863.2375	-867.32
λ_3	-153.08	-181.6900	-209.45
λ_4	-12.55	-10.6133	-9.9835
λ_5	-10.0066	-10.0231	-9.26

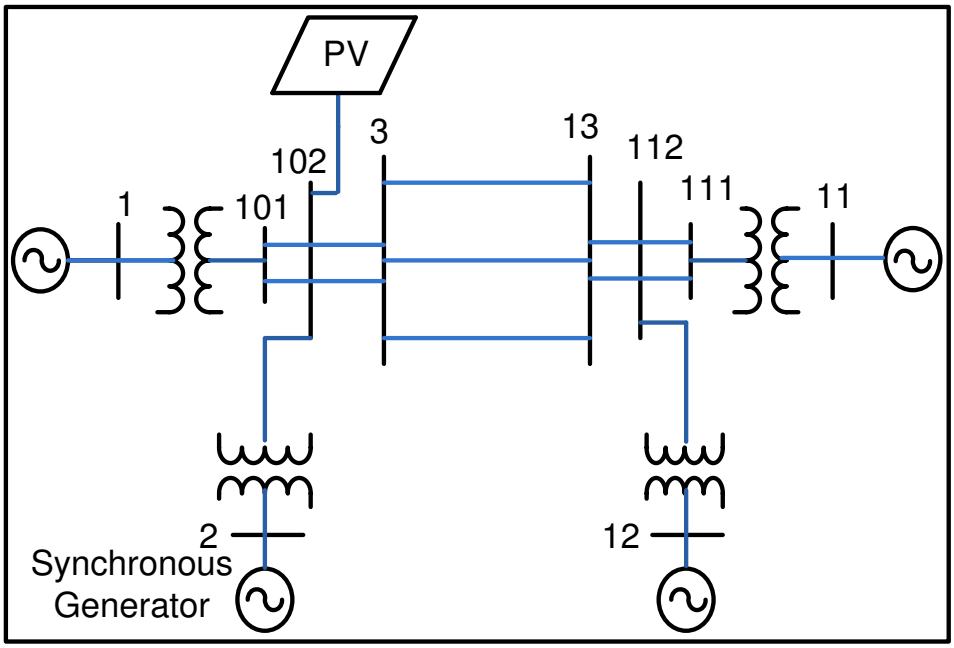

Figure 3.16: Four Machine two Area system with the PV plant

Multi machine power system

This case study formulates a simulation test set up to study the impact of PV on stability in a multi-machine transmission network. The developed PV dynamic model can be used for this purpose. The four machine two area system as shown in Fig.3.16 is considered. The system consists of four synchronous generators and two power system areas. A power base of 100MVA is assumed for the per unit (pu) calculations. All the four synchronous machines are generating 7pu. On bus 3 in area 1, 11.59 pu of the active and 2.12 pu of the reactive power load are considered. On bus 13 in Area 2, 15.75 pu of active and 2.88 pu of reactive power

load are considered. The detailed data of the system such as the transmission line impedances etc. is given in Appendix B. The PV plant is modeled as a negative load with no reactive power injection in the base case. The PV plant considered at bus 102 is injecting 0.9 pu of active power in the base case. Each of the PV inverter is of 0.015 pu capacity. There are 60 such inverters considered in the plant each operating at the same value of the irradiance and the temperature. Their control structure and converter dynamics for all the inverters is assumed identical. The initial operating point as discussed in eq.(3.22), (x_0, z_0, u_0) is calculated by solving Newton Raphson load flow. The synchronous generator data and dynamic equations as described in [82] [83] are utilized in modeling. The effect of the PV on the oscillatory stability of the power system is observed by considering two scenarios. The first scenario considers no PV plant and all the synchronous machines generating 7 pu. The second scenario considers the PV plant of 0.9 pu with the active power injection from the synchronous generator connected at bus 2 reduced to 6.1pu. Table3.7 shows the eigen values of the system with the PV plant at bus 102. It can be observed that consideration of the PV plant *does not* have a negative impact on the stability. Table 3.7 shows, the eigenvalues (which are close to the imaginary axis) and the dominant states calculated from the participation factor analysis. These eigenvalues are for the *base case* with the PV plant at bus 102. The consideration of PV plant introduces *two non-oscillatory stable modes*. The impact of an increase

Table 3.7: Eigen values with the PV plant at bus 102 (Base case)

Eigen values	**Dominant states**
$-0.756 \pm 6.638i$	Speed, Angle
$-0.836 \pm 5.97i$	Speed, Angle
$-0.033 \pm 4.007i$	Speed, Angle
-4.3205	Speed, angle
$-4.55 \pm 0.078i$	Exciter,field
-4.1658	Exciter, Field
-11.55	Exciter, field
-11.10	Exciter, field
-16.30	Dc voltage, $Ctrl_{Vdc}$, $Ctrl_{Id}$, $Ctrl_{Iq}$
-10.168	$Ctrl_{Iq}$

in active power injection by a PV plant on the stability margin is analysed for a two area four machine system. The generation capacity of an aggregated PV plant, located at bus no. 102 (Area 1), is increased by 2.1 pu i.e., from 0.9 pu to 3 pu while the capacity of synchronous machine based conventional generator at bus no. 2 (Area 1) is reduced by an equal amount. The associated changes in the parameters of the PV plant and the conventional generator (including inertia) have been considered for the stability studies. For a PV generation of 3 pu, the oscillatory inter-area mechanical mode shifts from the base case value of $0.0332 \pm 4.07i$ to $0.1 \pm 3.98i$. The stable non-oscillatory electrical mode moves from the base case value of -11.55 to -13.04. These results indicate overall improvement in the stability margin. However, these results are case specific as various factors such as capacities of the aggregated PV plant and the synchronous machine based conventional generation, associated machine parameters and control structures may have significant impact on the stability margin. Further, generator dispatches and inter area power flows can also have an impact. It is envisaged that the small signal stability aspects need a case specific examination to determine the impact of increase in PV generation.

Next, the location of the PV generation is altered from bus no. 102 to bus no. 112 to examine the impact on the small signal stability margin. The PV active power generation of 3 pu is considered at bus no. 112 while the active power output from the synchronous machine connected at bus 4 is reduced by 3 pu. All other parameters remain same as that of the base case to observe the impact of changing the location of PV plant. The improvement in the stability margin of the inter area mode can be observed when the PV plant is in Area 2 i.e., at bus no. 112. The eigenvalues for both cases are shown in Fig. 3.17. *This is due to the tie-line power flow.* The Area 2 has more load as compared to the Area 1. Hence, the PV generation connected in the Area 2 reduces the tie-line power flow. This improves the stability margin of the inter area mode.

Thus the case study demonstrates the proposed dynamic model that can be utilized to study the small signal stability. The Matlab/Simulink©is used as a simulation tool for this purpose. The next section discusses the steady state models

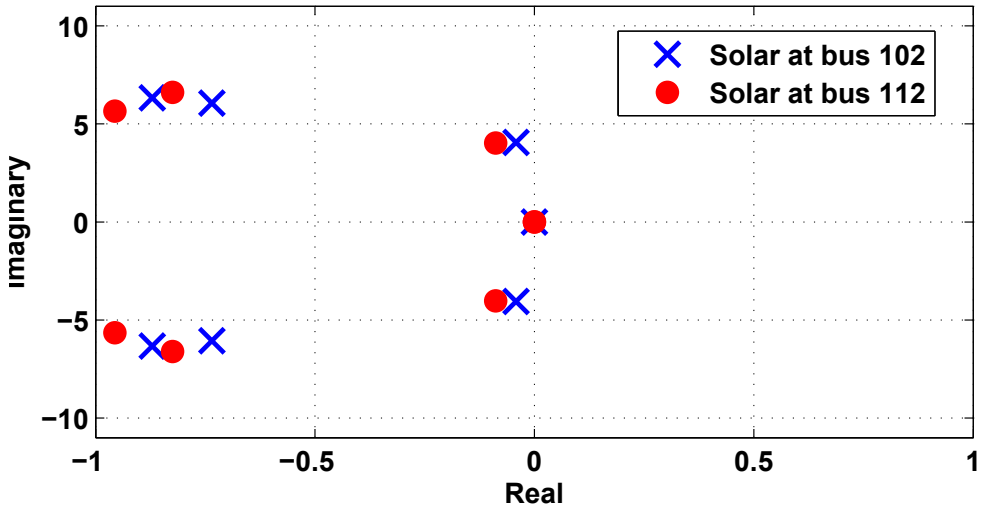

Figure 3.17: Eigen values with PV at bus 102 and bus 112

of the PV generation.

3.3 PV generation steady state model

Amongst various steady state operational challenges discussed in Chapter 1, the *voltage support* in the presence of a PV generation is the focus of this thesis. The typical tools needed to study *steady state voltage support* are *load flow analysis*, *optimal power flow analysis* etc. The steady state power injection models of the PV generator suffice to carry out a load flow or an optimal power flow analysis.

The PV generation injects an active power at the MPP and can offer an inductive or a capacitive reactive power support depending on the operator's choice. The PV generation can be modeled as a negative load, which is widely referred as $-P$, $\pm Q$ bus in the load flow studies. A sufficiently large PV plant connected to a weak power system bus can also control the voltage of a PCC. Under such a scenario the PV can be modeled as a generator bus for load flow studies. These models need to ensure that during normal operation of PV, active power injection must be equal to the MPP and the reactive power support from a PV inverter is limited by the operational capacity curve of Fig.2.6.

The unpredictable nature of a PV generation necessitates consideration of the stochastic power system studies such as for instance a *probabilistic power flow*. This necessitates accurate representation of the injected PV active power randomness using a probability distribution model. The PV irradiance probability density function (PDF) is typically modeled by Beta distribution for the long term stochastic planning studies. The PV irradiance PDF is modeled by Gaussian distribution for the day ahead or hour ahead planning study in stochastic framework.

3.4 Summary

- A dynamic model of PV generators is discussed in detail. This model is utilized to study the impact of PV generation on the small signal stability of a power system. The small signal stability margin is *not* affected by weather changes. The small signal stability margin is also *not* affected by small changes in grid voltage. The PV inverter controller parameters, however, should be carefully tuned to avoid negative impact on the stability. The solar system dynamics do *not* participate into the low frequency oscillation modes, but its location in the system has an impact on the overall stability margin of the power system.

- An optimal power flow and a stochastic optimal power flow are typical tools utilized to study *steady state voltage control* in the presence of PV generation. This necessitates use of steady state PV models. The PV generation can be modeled as negative load($-P$,$\pm Q$) in an optimal power flow. A PV active power injection can be modeled by a beta distribution for the planning studies in stochastic framework. A PV active power injection can be modeled by a Gaussian distribution for power system operational studies in stochastic framework.

The next chapter discusses *deterministic steady state voltage control* in the presence of PV generation. The detailed analysis of the different voltage control challenges is carried out.

Chapter 4

Deterministic voltage control

Most PV plants are getting connected to low/medium voltage distribution level as Distributed Generation (DG) as discussed in Chapter 1. However, this has led to many problems from the power system operation perspective. One of the operational problems is the variable voltage rise on distribution feeders due to DG [84]. This chapter deals in detail with *deterministic steady state voltage control* in the presence of PV generation. The detailed impact of PV on Voltage Regulators (VRs) and On-load tap changers (OLTCs) is also considered. A coordination strategy is proposed to mitigate the overvoltage and to alleviate the negative impact on OLTC and VR using reactive power option from a PV plant.

4.1 Motivation

The present day technique to manage overvoltage in the presence of a PV plant is by curtailing active power injection [44]. In a low voltage network this approach is required due to lower X/R ratio [85] [86]. Though necessary, this directly results in suboptimal capture of energy from the DGs. For instance, the German grid has approximately 30 GW of solar. However, because of the voltage rise issue only 70% of the total capacity is paid through feed-in-tariff for plants smaller than 30kWp. The result is that PV owners are discouraged from operating their plants at full capacity [45]. The PV voltage source converter (VSC) interface can offer reactive power support as discussed in Chapter 3. With the VSC interfaced DG, the option

of reactive power control is available in medium voltage (MV) networks [87]. Though till now PV operation is at unity power factor, some of the technical standards such as BDEW and updated draft version of IEEE 1547 are supportive of this feature to be utilised. This gives PV plants the opportunity to participate in voltage/reactive power control as explained while discussing the grid codes.

Distribution Network Operators (DNOs) maintain appropriate voltage profile across the network with the help of on load tap changers (OLTCs), voltage regulators (VRs) and capacitors. In most of the distribution feeders these devices are controlled based on the local signals, for example, bus voltage for OLTC and VR and time control or local bus voltage control for capacitors. In this conventional voltage control method all devices operate autonomously in a non coordinated manner. This non coordinated approach and unity power factor PV generation impacts the operation of OLTCs and VRs. The presence of PV on distribution feeders will lead to increased number of OLTC and VR operations and wear and tear of the devices [46] [88]. The result is an increase in the OLTC and VR maintenance/overhaul cost incurred by the DNOs. Under the scenario of significant power injection by PV, power flows can reverse on a distribution feeder. Some OLTC construction is such that permissible reverse power flow is less than the apparent power rating of the transformer [89]. Under specific operational scenario VR fails to control voltage at the regulated bus and reaches the lowest or highest tap limits. This phenomenon is widely referred to as reverse power *tap changer runaway* condition [47] [48]. This highlights the fact that in the presence of PV on the feeder, an appropriate consideration of OLTC, VR and their control settings are necessary for an effective voltage control strategy. Most of the recent approaches replace local autonomous control of the voltage control devices with communication based supervisory control [90] [49]. In [90] voltage control devices are remotely dispatched on an hourly basis through a communication channel to achieve flat voltage profile in the system without DG. Unity power factor PV in distribution systems is considered in [49]. Further, two way communication based real time smart grid Volt-Var control is proposed in [91]. Though the above mentioned schemes will certainly be able to alleviate the challenges, they require communication with all voltage control devices.

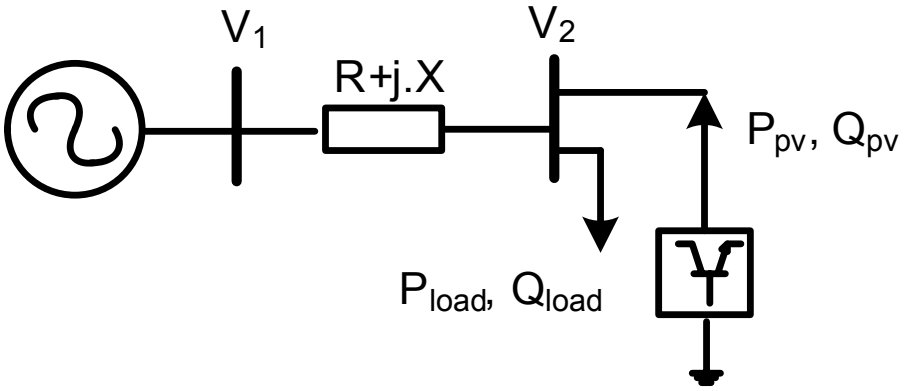

Figure 4.1: PCC voltage control by PV plant

However the operation of VRs is still autonomous based on local signals, without communication links on many distribution feeders [92]. The switched capacitors also lack communication links on some feeders and timer control is still operational in Europe [93] [94]. Considering this fact in [93], a combined local and remote voltage control strategy is discussed. It proposed that by opting for complete remote control of voltage control devices, they could lose their ability to react to load changes. A local communication-less Volt-Var control in the presence of synchronous machine based DG is considered in [94].

Most of the available literatures does not consider detailed impact of DG such as PV on autonomous local control setting of VR. It is also important to have an insight into what possible interaction a PV and its reactive power settings will have with the autonomous operation of a VR. This chapter investigates these challenges and proposes an optimal coordination strategy.

4.2 Radial feeder voltage variation

Fig.4.1 is a simple equivalent circuit of a radial feeder. The feeder has a connected load and a PV generator. The active/reactive power consumption by a load and the active power injection by a PV both will cause a voltage drop on a feeder. This voltage drop can be mathematically derived as follows. In Fig.4.1 V_1 is a constant substation voltage. The vector diagram of the operation of feeder is shown in Fig.4.2.

Current I flowing on the feeder can be calculated as :

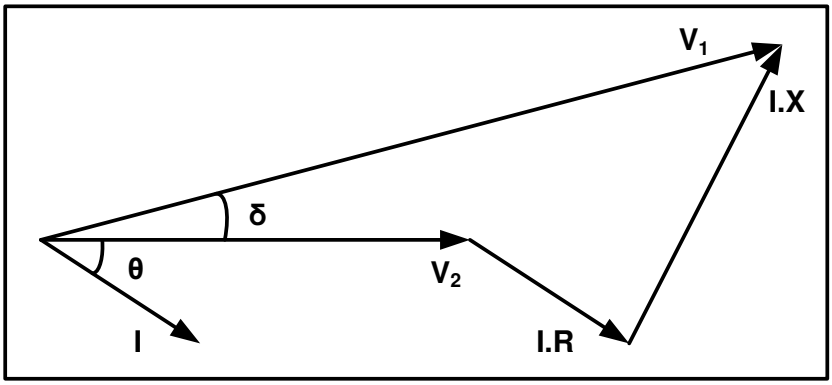

Figure 4.2: Vector diagram of radial feeder

$$I = \frac{(P_{load} - P_{pv}) - j.(Q_{load} \pm Q_{pv})}{V_2} \tag{4.1}$$

PV generation MPPT active power is denoted by P_{pv} and reactive power output is Q_{pv}. Load power is denoted by P_{load} and Q_{load}. $R + jX$ represent impedance of the line. Let us denote ΔV as the voltage drop across the feeder impedance $R+j.X$,

$$\Delta V = V_1 - V_2 = I.(R + j.X) \tag{4.2}$$

Substituting the eq.(4.1) in (4.2) :

$$\Delta V = \frac{R.(P_{load} - P_{pv}) + X.(Q_{load} \pm Q_{pv})}{V_2} + j.\frac{X.(P_{load} - P_{pv}) - R.(Q_{load} \pm Q_{pv})}{V_2} \tag{4.3}$$

The imaginary term in eq.(4.3) on the distribution feeders is typically very small and can be neglected. Thus voltage drop ΔV on the feeder can be calculated as :

$$\Delta V \approx \frac{R(P_{load} - P_{pv}) + X.(Q_{load} \pm Q_{pv})}{V_2} \tag{4.4}$$

The voltage drop equation in (4.4) signifies that there is ΔV voltage drop due to P_{load}, Q_{load} and P_{pv}. Further this ΔV voltage drop (and voltage V_2) will vary as the load power P_{load}, Q_{load} and the injected PV power P_{pv} will vary. The load power P_{load}, Q_{load} is not controllable to mitigate the voltage V_2 variation. Thus in order to control the voltage drop either P_{pv} needs to be curtailed or Q_{pv} needs to be controlled.

Q_{pv} control can mitigate the voltage drop by injecting either inductive or capacitive reactive power. The various reactive power settings of a PV plant have already been discussed in Chapter 2. The DNOs have an option of setting fixed reactive power(Q) or fixed power factor(pf) of PV plant as real power varies. The operator also has an option to define variable pf as active power varies (pf(P)), or variable reactive power as voltage varies (Q(U)). PV connected to a strong substation bus is controlled more effectively in these reactive power or power factor control modes. It is also important to note that depending on the capacity of PV plant and fault level at PCC, PV can be operated in voltage control mode. The PV can regulate the voltage of a weak bus having lower fault level. In the context of Fig.4.1 the PCC voltage V_2 can be controlled or kept constant by the PV plant [93] [95].

Besides this voltage variation introduced by PV active power injection, a PV plant active power injection has an impact on the operation of OLTC and VR. It is important to study operational details of these classical equipments to examine the impact from a PV plant. This is discussed in the next section.

4.3 Classical voltage control devices

4.3.1 On-load tap changer

The On-load tap changer (OLTC) is primarily responsible for feeder voltage control. OLTCs are typically installed in the substation from where a feeder emanates. Details of the technical operation of the OLTC mechanism can be found in [1]. The typical voltage control mechanism in an OLTC is represented in Fig.4.3. An operator will specify the particular voltage setpoint to control the voltage of a regulated bus. The turns ratio of a transformer can be adjusted in steps from the transformer windings. The OLTC controls the voltage of the regulated bus within the defined dead band settings. The regulated bus voltage is compared with user defined setpoint by the comparator. The tap is not varied if the measured voltage is within the deadband. The taps are moved after an operator defined time delay if the measured voltage is outside the deadband.

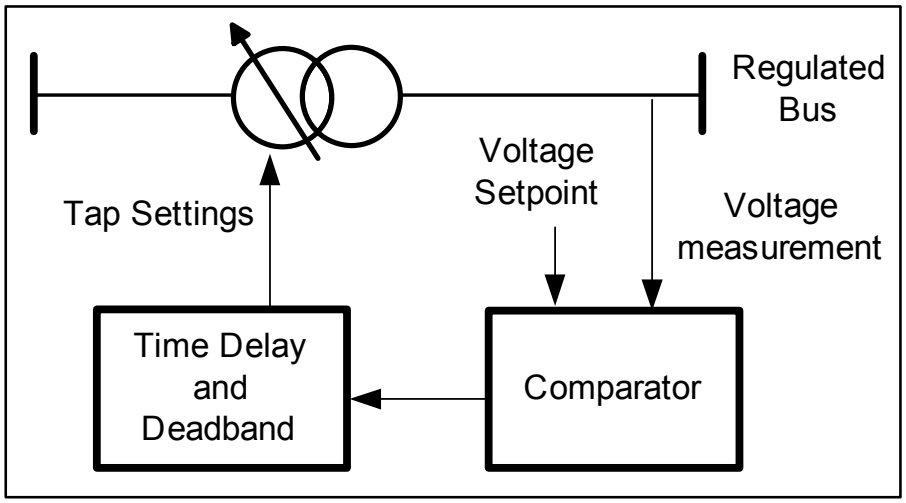

Figure 4.3: OLTC Voltage Control mechanism

4.3.2 Voltage regulator (VR)

A VR is typically an autotransformer with ±10% voltage regulation capability. The VR maintains the load terminal voltage at the set value by adjusting the tap position as the load current varies. The deadband and the delay time concept is similar to the OLTC. The typical VR schematic diagram is shown in Fig.4.4 which is widely referred to as *Type B* arrangement. The shunt winding of this type of regulator is connected to the series winding through the taps. The shunt winding is directly connected to the load. The boost of the voltage across the load is achieved by connecting the switch to the raise position. The following equation details the operation. Fig.4.4 shows the operation of the VR in the raise position.

$$\frac{E_1}{E_2} = \frac{N_1}{N_2} \tag{4.5}$$

The relationship between the load voltage V_L and the source voltage is calculated as follows :

$$V_L = E_1 = V_S + E_2 \tag{4.6}$$

$$V_S = V_L - V_L.\frac{N_2}{N_1} \tag{4.7}$$

The regulator ratio is expressed in terms of the shunt winding turns N_1 and the

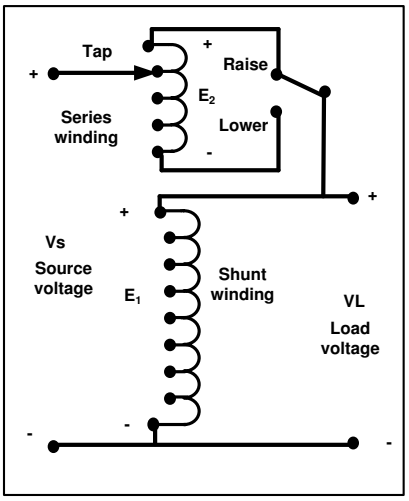

Figure 4.4: Voltage regulator in the raise position [1]

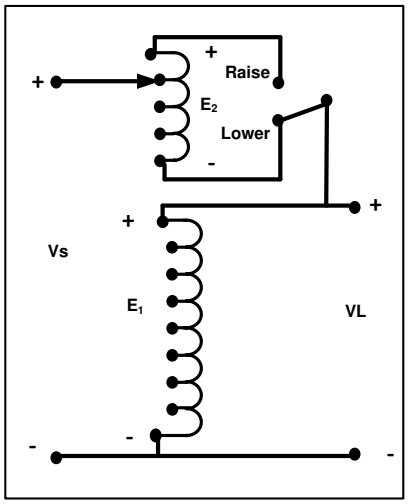

Figure 4.5: Voltage regulator in the lower position [1]

series winding turns N_2 in equations (4.7). Fig.4.5 shows the operation of the VR in the lower position. Similar to the above equations in the lower position of the VR following equations are true. If the VR is in the lower position. The relationship between the load voltage V_L and the source voltage is calculated as follows :

$$V_L = E_1 = V_S - E_2 \tag{4.8}$$

$$V_S = V_L + V_L.\frac{N_2}{N_1} \tag{4.9}$$

Equations (4.7) and (4.9) show how the load voltage can be raised or lowered by

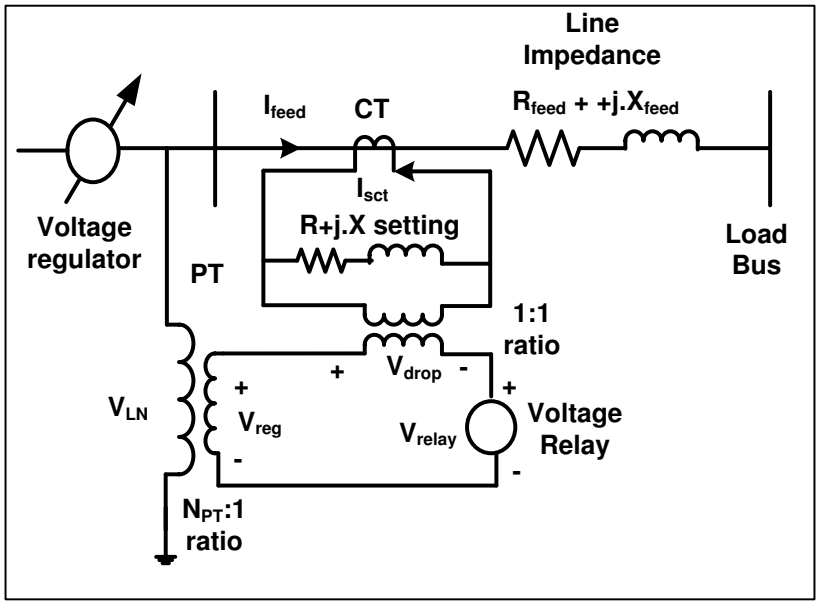

Figure 4.6: Line drop compensation [1]

adjusting the auto transformer turns ratio N_1/N_2 through the taps.

Line drop compensation (LDC)

This section discusses the most widely used VR feature the LDC. A VR is usually installed at a substation or on a feeder between a source and a load. The feeder itself has a voltage drop due to the feeder current flowing through the feeder impedance. The LDC mechanism calculates the feeder voltage drop and adjusts the source side VR tap position so that the voltage at the actual load bus improves. The schematic of the LDC mechanism is shown in Fig.4.6. The compensator $R+j.X$ setting values in Fig.4.6 must be representative of the feeder impedance $R_{feed}+j.X_{feed}$ to calculated the feeder voltage drop. This is achieved by designing the same value of the feeder per unit(pu) impedance Z_{puf} and the compensator pu impedance Z_{pur}. The calculation of the $R + j.X$ setting is as follows. The base impedance for the primary feeder circuit is denoted by Z_{basef}. The feeder current and the source voltage is measured through the current transformer (CT) and the potential transformers(PT) for the

relay circuit. The base impedance for the secondary relay circuit is Z_{baser}.

$$Z_{basef} = \frac{V_{LN}}{I_{feed}^{rated}}$$

$$Z_{baser} = \frac{V_{LN}}{N_{PT} I_{sct}^{rated}} \tag{4.10}$$

N_{PT} in eq.(4.10)is the PT turns ratio, I_{feed}^{rated} is rated feeder current, the CT secondary current is I_{sct}^{rated}, and V_{LN} is the source side feeder voltage. The pu value of the feeder impedance Z_{puf} is calculated as:

$$Z_{puf} = \frac{R_{feed} + j.X_{feed}}{Z_{basef}}$$

$$Z_{puf} = I_{feed}^{rated}.\frac{R_{feed} + j.X_{feed}}{V_{LN}} \tag{4.11}$$

The pu impedance of the feeder Z_{puf} and the pu compensator impedance Z_{pur} must be the same, hence the actual compensator impedance can be calculated by the following equation.

$$R + j.X = Z_{pur}.Z_{baser} = Z_{puf}.Z_{baser}$$

Substituting the value of Z_{puf} from eq.(4.11),

$$R + j.X = I_{feed}^{rated}.\frac{R_{feed} + j.X_{feed}}{V_{LN}}.\frac{V_{LN}}{N_{PT} I_{sct}^{rated}}$$

Hence, the compensator feeder impedance $R + j.X$ is given by:

$$R + j.X = (R_{feed} + j.X_{feed}).\frac{I_{feed}^{rated}}{N_{PT} I_{sct}^{rated}} \tag{4.12}$$

The compensator impedance calculated above is multiplied by the CT secondary compensator current to calculate V_{drop} in Fig.4.6. Thus voltage across the relay V_{relay} can be calculated considering the feeder voltage drop and accordingly appropriate tap setting can be achieved [1] [96]. Other than LDC settings, there are various VR control settings in which it can operate based on the feeder requirements. This is

discussed in the next section.

VR control settings

The VR control settings primarily define the expectation of an operator from the VR during a *reverse power flow* situation. The distribution network operator can choose various control settings for a VR through its control panel. The major settings available with most of the manufacturers are discussed here. The details of the operation varies as per the manufacturers. The idea here is to explain the principle.

The radial distribution feeders in which only a forward power flow is expected *locked forward operation setting* of VR is usually utilized. The operational details of this control setting are shown in Fig.4.7. There are two thresholds namely the *operational threshold* and the *indication threshold*. The VR tap changer operation is blocked when the reverse current is below the reverse current threshold as indicated in Fig.4.7. The indicative threshold usually issues an alert to an operator. This alert is usually flashing of the light on the control panel of a VR. The indicator flashing begins as soon as the current is below the negative (reverse) indication threshold and stops only when the current is above the positive (forward) indication threshold. The typical value of the indicative threshold can be $\pm 1\%$ or $\pm 2\%$. The VR can also be set to operate in *idle reverse mode*. This setting is useful when the reverse power flow is an abnormal situation. This operation is indicated in Fig.4.8. Here a VR tap changer operation is blocked as soon as the forward current is below the positive operational threshold. In the blocked operation, a VR continues to idle at the tap value attained just prior to the threshold violation. The feeders on which the reverse power flow is the abnormal situation can also utilize the *neutral reverse setting*. There control setting details are sketched in Fig.4.9. In this mode, when a VR current is below the negative operational threshold, VR taps up or taps down to the neutral position. The tap operation is blocked when the VR current is within the band between the positive operational threshold and the negative operational threshold. The VR operates normally when the current is above the positive operational threshold. There can be feeders on which the forward current

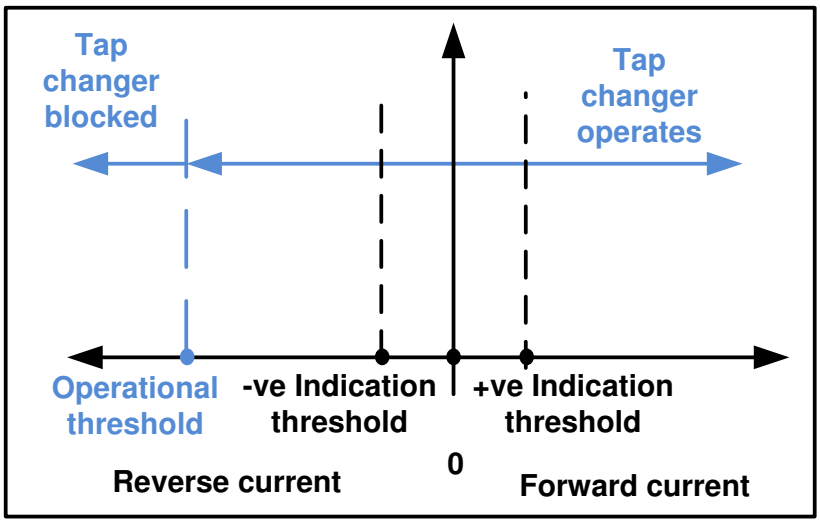

Figure 4.7: Locked forward mode

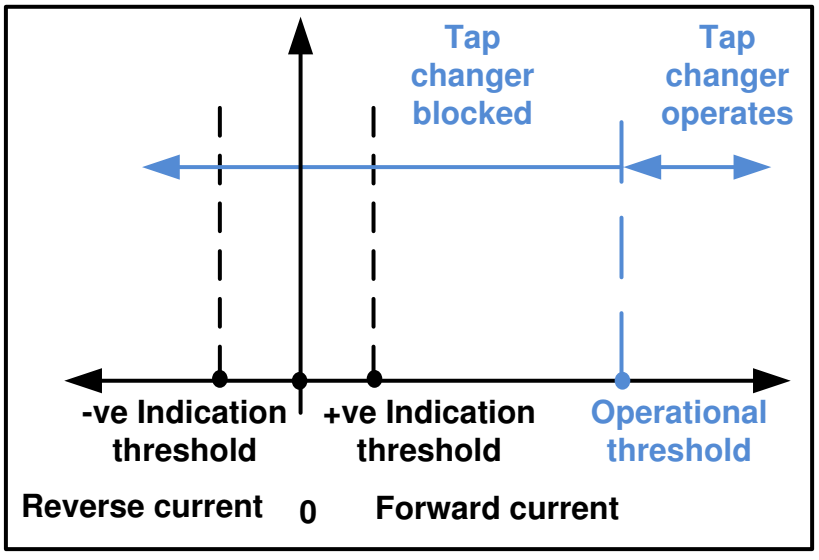

Figure 4.8: Idle reverse operation

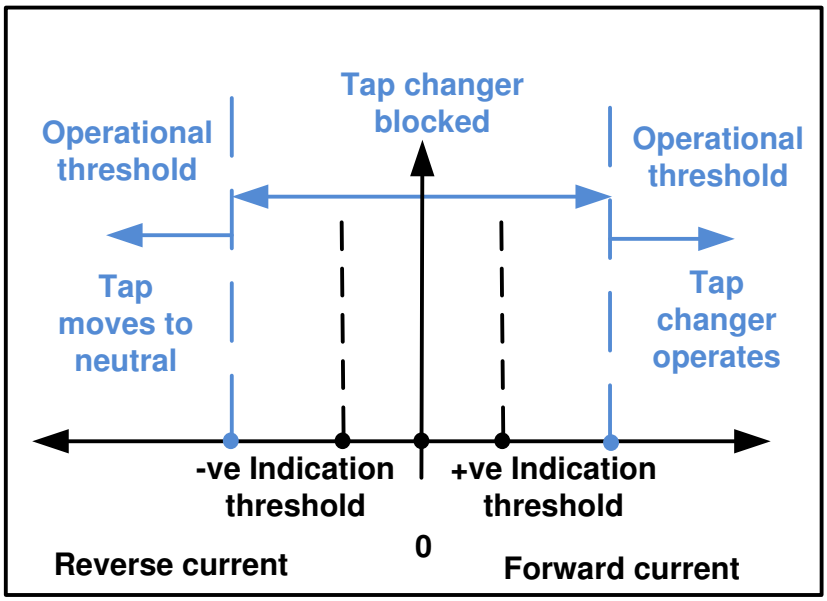

Figure 4.9: Neutral reverse operation mode

itself is an abnormal scenario and a reverse power flow is normal. On such a feeder, a VR can be set to operate in the *locked reverse mode*. This operation is indicated in Fig.4.10. The VR tap changer operation is blocked when a forward current is above the forward current threshold. This mode of operation is exactly opposite to the *locked forward mode*. There can be the scenarios in which a reverse power flow is expected and is a normal situation. The next operational modes are useful on the feeders where a forward and a reverse power flow both are expected. The VR can be set to operate into a *bidirectional mode* of operation. This mode of operation makes the VR to operate normally when the current is below negative threshold or the current is above the forward current threshold. The VR tap operation is blocked if the current is within the band between the positive operational threshold and the negative operational threshold. This mode of operation is shown in Fig.4.11. It needs to be noted that in this mode during the forward operation *VR regulates the voltage in the forward direction* (that of a forward connect bus) and during the reverse direction the *VR regulates the voltage in the reverse direction* (that of a reverse connect bus). Some of the manufacturers also offer the *reactive bidirectional setting*. The real and the reactive currents are measured and the thresholds are defined for

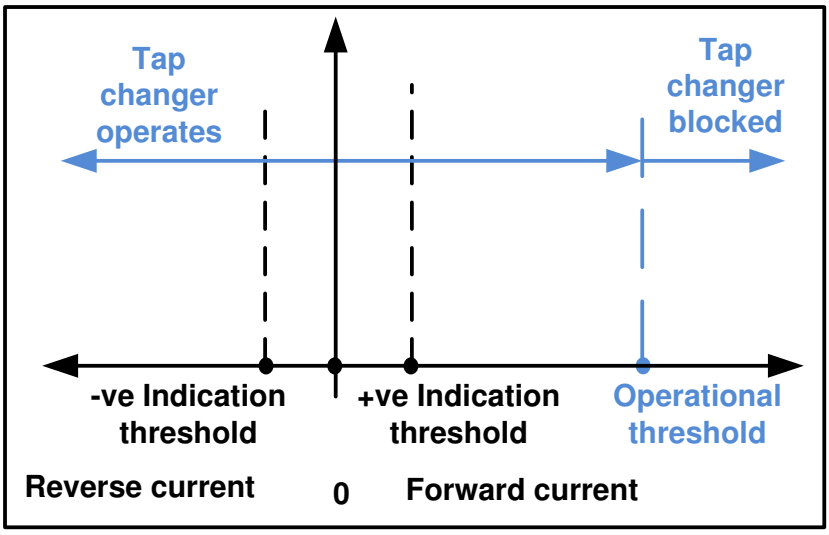

Figure 4.10: Locked reverse mode

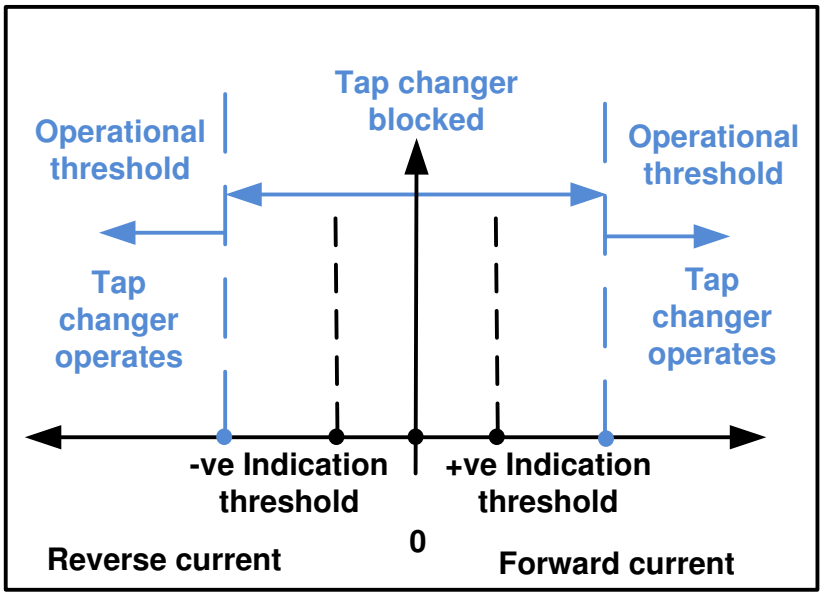

Figure 4.11: Bidirectional mode

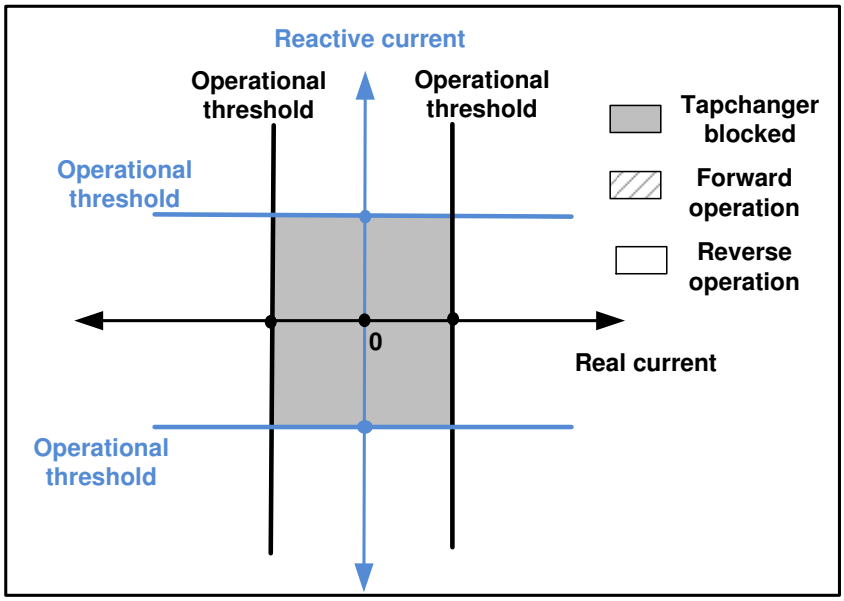

Figure 4.12: Reactive bidirectional mode

both of them in this mode. Fig.4.12 explains the reactive bidirectional mode. The various operating zones for the forward and the reverse operation are illustrated. The most common setting where a power flow is expected in the forward and the reverse direction is the *cogeneration mode*. This mode of operation is sometimes used in the presence of a distributed generation on the feeder downstream to the VR. The control setting is shown in Fig.4.13. The VR operation is blocked if the current is within the band between the positive operational threshold and the negative operational threshold. This mode of operation during the forward and the reverse current flow a *VR continues to regulate the voltage in the forward direction*. There are two different LDC settings selected one when the current is above the positive current threshold and the other when the current is below the negative current threshold. There is manufacturer specific variation in the availability of different control settings and their specifics as shown in Table 4.1 [97] [98] [99]. These control settings of the VR can interact with the PV plant giving rise to the operational challenges on a radial distribution feeder. These operational challenges are analyzed in detail in the next section.

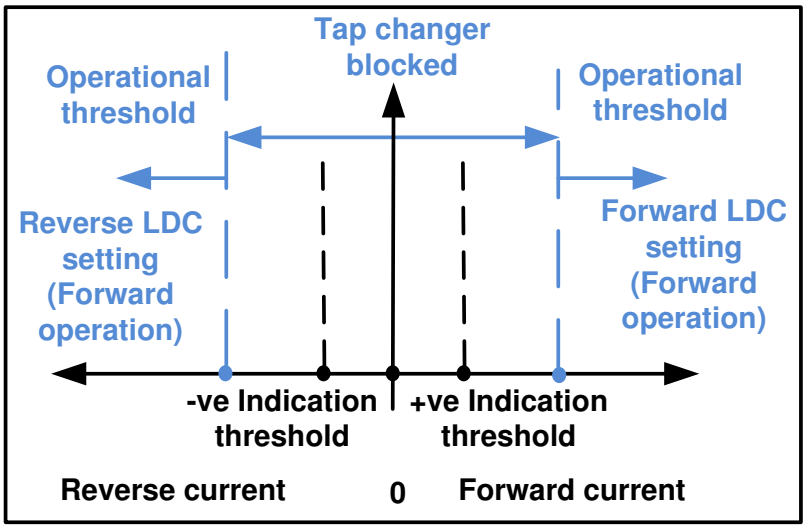

Figure 4.13: Cogeneration mode

Table 4.1: Comparison of VR controls of different manufacturer

	Cooper-CL6A	Siemense-MJX	Beckwith-M2001B	ICMI-UVR1
Reactive power Bidiecrtional	✓	×	×	×
Cogeneration	✓	✓	×	✓

4.4 Feeder operational challenges

A typical MV radial distribution feeder as shown in Fig.4.14 is under consideration here. This feeder has PV along with its reactive power control capability. The other voltage control devices available are OLTC and VR. The VR operates in an autonomous mode. It consists of normally open switch which connects to an alternate power feeding point. A grid integrated PV model is Fig.3.1. The converter control achieves the best possible active power capture through MPPT. Fig. 4.15 shows the equivalent circuit of the MV distribution feeder of Fig.4.14.

There is a possibility of power flows in the reverse direction towards the source substation OLTC, particularly when PV penetration is high. This causes a rise in the load voltage as can be seen from the vector diagram in Fig. 4.16.

The voltage control challenge will be more complex where a PV plant has a

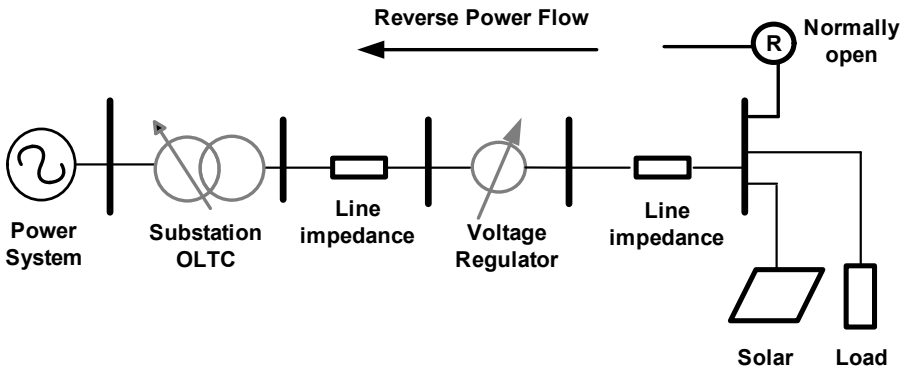

Figure 4.14: Radial system topology

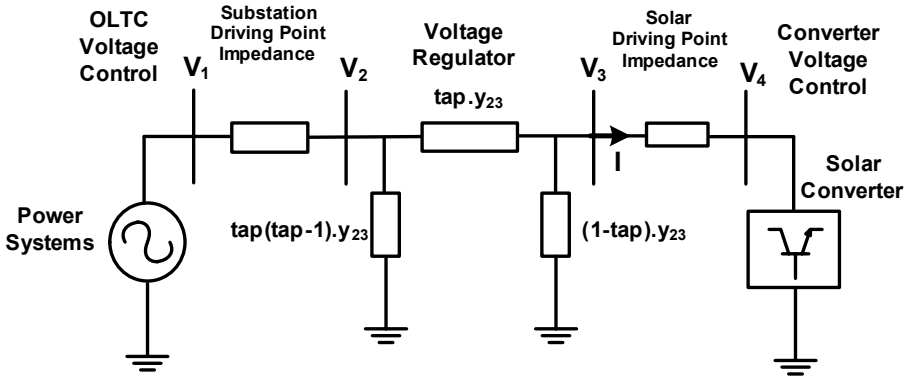

Figure 4.15: Equivalent circuit of a radial system with VR

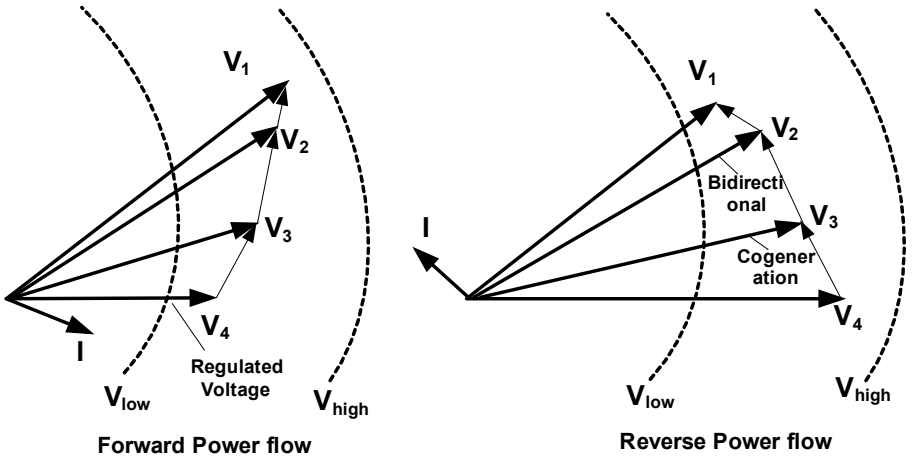

Figure 4.16: Vector diagram of a radial system

reactive power control option. There will be interaction between VR and PV voltage control. The nature of the control interaction between VR and PV and its overall effectiveness depends on various factors such as the driving point impedance, PV capacity, PV reactive power setting, VR setting, and system topology. Table 4.2 summarizes generic interactions between VR autonomous mode and PV reactive power setting [48] [99] [100]. It is not difficult to appreciate that for low driving point impedance i.e. strong voltage source there is a real risk of the *VR hitting its limit or operating in runaway condition* thus compromising its control effectiveness. There are primarily two autonomous operational modes of VR where they can potentially interact with a PV voltage control action. The details of the operational challenges during these VR operational modes are discussed next with reference to the model feeder topology of Fig. 4.14 and Fig. 4.15.

Operational challenges : Bidirectional mode

In this mode the VR will switch its target voltage control node depending on the direction of active power flow through it. In the context of Fig. 4.15 during forward active power flow VR regulates V_3 or V_4 and during reverse active power flow VR regulates V_2. This VR mode is useful when alternate feed is activated by changing the status of 'normally open' (NO) switch to 'normally closed' (NC) as shown in Fig.4.14. In the 'NO' position of switch, unity power factor PV can cause a reverse power flow through VR. This will make VR control the voltage V_2 on the substation side. If the substation is the stronger source, i.e. with low driving point impedance, VR fails to set the required voltage set point and reaches the highest or lowest tap position; i.e. runaway condition. Under this situation the VR is ineffective in providing voltage regulation which will result in voltages V_3 and V_4 outside the prescribed limit on the side of PV. In a scenario when the substation side driving point impedance is higher and PV is capable of supplying reactive power, the runaway situation can be avoided. However it should be noted that PV having a reactive power capability is *necessary but not sufficient*. The PV should inject *the optimum value* of reactive power and target optimum voltage setpoint V_4 so that the VR does not operate close to its limit. Any positive voltage control

contribution from the VR only helps to run the PV with reduced losses because of reduced reactive current.

Table 4.2: Interaction between PV reactive power support mode and VR autonomous setting

	PV plant setting : Unity pf	**PV plant setting : Constant Q or pf, pf(P) or Q(U)**	**PV plant setting : Constant voltage**
VR Setting : Bidirectional	**Caution:** Runaway during reverse power flow if low substation driving point impedance.	**Caution:** Runaway during reverse power flow if low substation driving point impedance and no optimum Q from PV.	**Caution:** Runaway during reverse power flow if low substation driving point impedance and no optimum voltage set point from PV.
VR Setting : Reactive Bidirectional (Not available with all manufacturers)	Mostly for loop distribution systems. No impact on reactive current setting of VR due to PV.	Mostly in loop distribution systems. **Caution:** Reactive current set point of VR can be impacted by PV.	Mostly in loop distribution systems. **Caution:** Reactive current set point of VR can be impacted by PV.
VR Setting : Co-generation	**Caution:** Interference with the line drop compensator setting.	**Caution:** Interference with the line drop compensator settings	**Caution:** Runaway for forward/reverse active power flow if PV driving point impedance is low for high capacity PV.

Operational challenges : Co-generation mode

In this mode the line drop compensator settings are altered at the time of reverse power flow. In the context of Fig.4.15, during forward power flow the VR regulates voltage V_4. During reverse power flow it regulates voltage V_3. When voltage control option from a large PV plant is available the VR should always regulate V_3 in this mode as it will have little influence on the voltage V_4. High capacity PV with lower driving point impedance can even drive the VR into a runaway situation while the VR is controlling the voltage V_3. In this mode, regardless of the direction of active power flow the VR continues to regulate the voltage in the forward direction that is V_3 or V_4. In the context of Fig.4.14, where alternate feed is activated by changing normally open (NO) switch to normally closed (NC), this mode will still continue to regulate voltage V_3 which is not appropriate from the feeder operation point of view. The operational requirements with respect to OLTC and VR in the presence of PV are summarized as follows :

- The VR should not run away under any system scenario described in Table 4.2.
- The voltage control in distribution system has to be achieved with minimum tap counts of OLTC and VR. This requires optimal control coordination.

4.5 Optimal Coordination

4.5.1 Control Strategy

With reference to the equivalent circuit of Fig. 4.15 one possible situation can be that the PV is of high capacity and both sources, substation and PV, are controlling voltages V_1 and V_4 respectively. Usually field settings should be such that the weaker source (higher driving point impedance values) side voltage is regulated by the VR. For weaker substation source, during reverse power flow, the VR will be set to regulate V_2. During forward power flow, for the cases with weaker PV source, VR can regulate V_3 effectively. V_1 and V_4 are tightly regulated by substation OLTC and large

PV plant when both sources are stronger (smaller driving point impedance values), and in that situation the VR will neither be able to control V_2 nor V_3. However, the VR will still be useful for reactive power flow control. By varying the tap value, the shunt element $(1 - tap)y_{23}$ and $tap(tap - 1)y_{23}$ will change their admittance. This will make the PV plant and substation OLTC to alter their reactive power injections. From Fig. 4.15, it can be seen that where both the PV and substation will have realistic driving point impedance values, VR runaway can be avoided by adjustment of OLTC bus voltage V_1 and PV bus voltage V_4. This is achieved through coordinated and optimum voltage set point adjustment of OLTC and PV.

4.5.2 Optimization

The coordination between PV reactive power control capability and voltage control option of OLTC and VR is an optimization problem. The goal is to contain excessive/unnecessary operations of OLTC and VR and avoid VR runaway situation. This is formulated in this section as optimal reactive power dispatch problem subject to meeting the various network operational constraints.

Objective function

The objective is to minimize the total number of tap operations over the 24 hours subject to various equality and inequality constraints

$$Minimize f_{count} = \sum_{t=1}^{t=N} \sum_{T=1}^{T=N_{tr}} |Tap_{t,T} - Tap_{t-1,T}| \tag{4.13}$$

where t is time instant, N number of time instants considered in a day. The total number of time instants N will depend on the size of the time interval between instants t and $t + 1$. T is the transformer number, N_{tr} is total number of OLTCs and VRs. The constraint related to VR runaway is included as a penalty in the objective function which is discussed later.

Constraints

The different equality and inequality constraints are as follows:

Current balance: Equality constraints are represented by a set of nodal current injection equations formulated in rectangular coordinates. For generic load bus l connected with generation bus g, the mathematical model and Newton Raphson algorithm can be represented in schematic form as :

$$\begin{bmatrix} \Delta I_{iml}^{abc} \\ \Delta I_{rel}^{abc} \\ \Delta I_{img}^{abc} \\ \Delta I_{reg}^{abc} \end{bmatrix} = J \begin{bmatrix} \Delta V_{rel}^{abc} \\ \Delta V_{iml}^{abc} \\ \Delta V_{img}^{abc} \\ \Delta Q_{g}^{abc} \end{bmatrix} \tag{4.14}$$

In (4.14) ΔI_{re}^{abc} and ΔI_{im}^{abc} are real and imaginary current mismatch, ΔV_{re}^{abc} and ΔV_{im}^{abc} are real and imaginary voltage mismatch, and J is the Jacobian. The detailed algorithm of the current injection method and modeling of voltage control devices are formulated as per reference [101] and [102]. The current injection method can be utilised in unbalanced radial or meshed distribution systems.

Voltage limits: Steady state voltage at all the buses in the distribution system must be maintained within the prescribed limits.

$$V_{low} \leq V_t \leq V_{high} \tag{4.15}$$

Branch flow constraints: In steady state, the maximum amount of current flow on the line is constrained by feeder thermal limit, hence for each feeder,

$$I_t \leq I_{max} \tag{4.16}$$

Transformer capacity constraints: The maximum amount of apparent power flow through a transformer will be limited by its MVA rating. As explained earlier and described in [89], the mechanical construction of OLTC in certain transformers will limit the reverse power MVA to less than its MVA rating. DNOs should include this particular constraint based on the OLTC mechanism in the transformer. Hence

forward and reverse power flow constraints are as follows,

$$S_{tr,f,t} \leq S_{MVA} \tag{4.17}$$

$$S_{tr,r,t} \leq S_{rev,MVA}$$

Where $S_{tr,f,t}$ and $S_{tr,r,t}$ are forward and reverse apparent power flow through the transformer, S_{MVA} is MVA rating of the transformer and $S_{rev,MVA}$ is reverse power flow permissible through transformer.

Solar generation constraints:

The reactive power output and hence PCC voltage control capability of PV will be limited by the inverter apparent power rating. The capability curve Fig. 2.6 is discussed in the Chapter 2. In order to give reactive power support at peak active power injection, overcapacity of the inverter is necessary. There are equality and inequality constraints associated with PV plant operational performance. The PV owner will always prefer to inject maximum possible active power as it is linked to revenues. The solar generation reactive power support will be limited by its inverter rating. Hence, the equality and inequality constraints should be considered as,

$$P_{solar,t} = P_{MPPT,t} \tag{4.18}$$

$$\sqrt{P_{solar,t}^2 + Q_{solar,t}^2} \leq S_{solar}. \tag{4.19}$$

In (4.18) $P_{solar,t}$ and $Q_{solar,t}$ are the solar active and reactive power respectively. The solar inverter MVA rating is denoted by S_{solar} and $P_{MPPT,t}$ is active power output set by MPPT. In this study, the PV is considered in the voltage control mode. It is also assumed that DNOs will be able to issue a daily voltage set point schedule for the PV plant. PV inverter overrating to offer this voltage support is considered such that PV is able to operate at 0.95 lead or lag power factor at rated active power output [55].

Tap limits: Tap changer winding has limited number of tap positions for both OLTC and VR. Typically a tap winding has a total of 32 number of steps. Each step is designed to change 0.625% of voltage. Tap changer turns ratio of each transformer

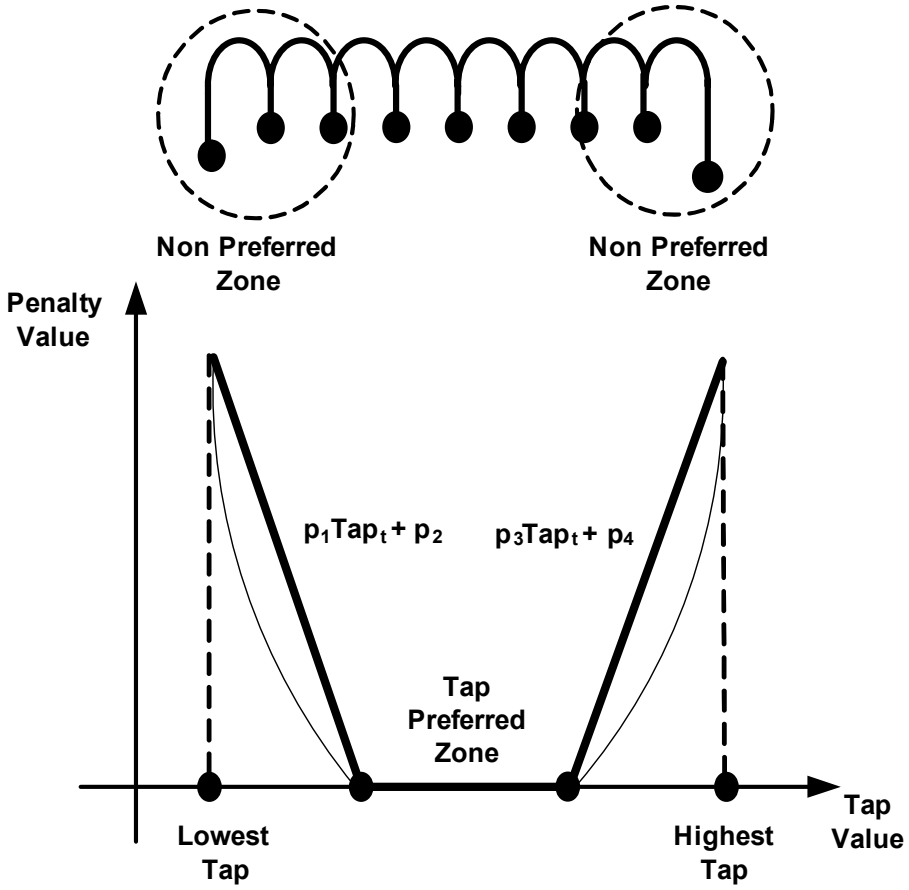

Figure 4.17: Proposed penalty function to avoid runaway

must satisfy the following constraints,

$$Tap_{low} \leq Tap_t \leq Tap_{high} \tag{4.20}$$

In order to solve the above optimization problem described by Eq.(4.13)-(4.20), the primal-dual interior point technique is chosen due to its features such as fast convergence, efficient handling of sparsity and ease of dealing with the inequality constraints. The OLTC and PV control set points are calculated based on the day ahead irradiance and load profile. The implementation of the proposed strategy assumes that one day ahead forecast of PV and load are known with sufficient accuracy. The VR operates in autonomous mode whereas PV and OLTC in the substation have access to a communication link that can help coordinate the voltage control in the system. In the primal-dual interior point method, the inequality constraints are handled by the introduction of barrier parameter and logarithmic

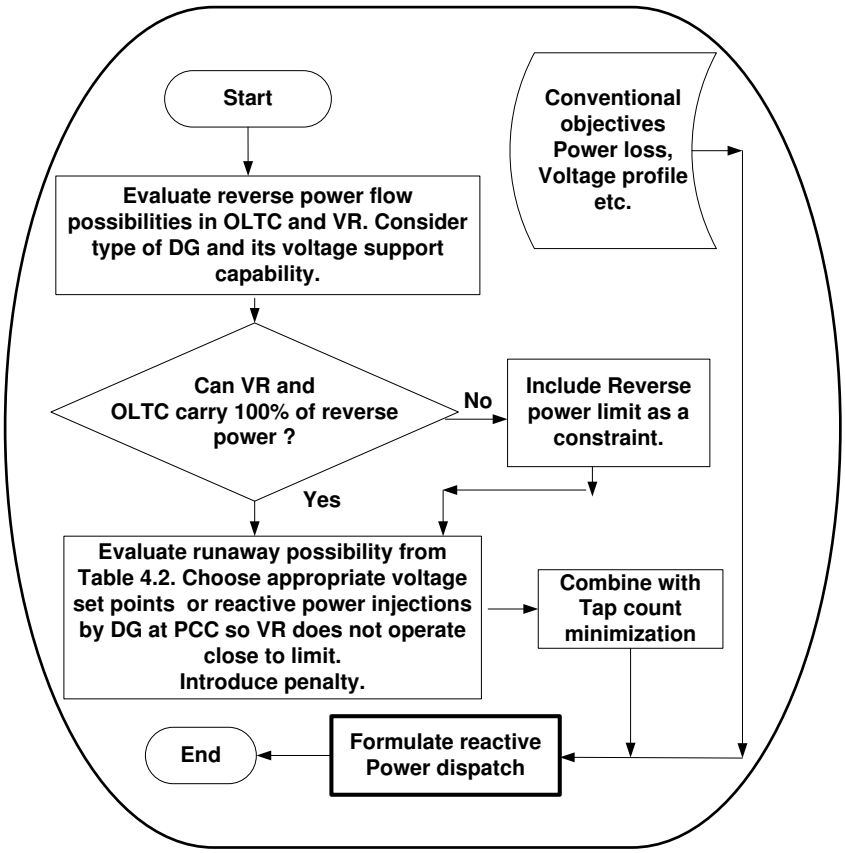

Figure 4.18: Problem formulation considering impact on OLTC and VR

barrier function. In order to reduce the operation of the tap close to its limit, an additional non-preferred zone of operation around the tap limit is defined. This penalty function can be quadratic or piece wise linear as shown in Fig. 4.17. The piece wise linear penalty function is included in the objective function in (4.13) as follows :

$$f_{tap} = W_c \sum_{t=2}^{t=N} \sum_{T=1}^{T=N_{tr}} |Tap_{t,T} - Tap_{t-1,T}| + W_r \sum_{t=1}^{t=N} |P_t| \tag{4.21}$$

$$P_t \geq 0, P_t \geq p_1 Tap_t + p_2, P_t \geq p_3 Tap_t + p_4$$

In (4.21), W_c and W_r are scalar weights, P_t is the penalty, p_1, p_2, p_3 and p_4 are penalty function parameters. The proposed objective function can be combined with the conventional objective function such as power loss minimization but this work mainly focuses on tap operation counts minimization.The overall generic optimization problem formulation in the radial distribution system of Fig. 4.14

having OLTC, PV and autonomous VR is conveyed through a flow chart in Fig. 4.18. The load and solar irradiance pattern will have a major change due to change of season. The set points of communication-less devices are readjusted seasonally. The daily variations in irradiance and load are taken care of by communicating voltage set points to OLTC and PV. The next section describes a case study to demonstrate the application and effectiveness of the proposed scheme.

4.6 Case study

4.6.1 System model

The UK Generic distribution system (UKGDS) is considered. All the 95 buses in the system are at 11kV voltage level. The network parameters and load data are obtained from [103]. The topology of the UKGDS is shown in Fig. 4.19. This test system considers a typical bus which serves a mixture of four types of consumers: domestic unrestricted, domestic economy, industrial and commercial. The load profiles for each consumer class are defined in this system. The load profiles at different buses are generated based on the data and procedure discussed in [103]. The resultant load profile on 100kW base is shown in Fig. 4.20. There are two PV plants considered in this system each of 1 MW capacity. The PV plants can operate at 0.95 lead/lag power factor during peak active power injection. Appropriate inverter overrating is considered. The solar active power output profile on 100kW base is shown in Fig.4.21. The same irradiance profile is considered for both the plants. Half hourly load variations data are considered from [103]. The solar active power output is adopted from practical 30 second based measurements at Loughborough, England in the month of August 2012. It is assumed that at night times solar continues to offer reactive power support in a STATCOM mode. In Fig. 4.19, two VRs are connected between bus 24 and bus 23 and between bus 54 and 75 and control the voltage of the same buses. The system voltage values at different buses without PV are shown in Fig.4.22.

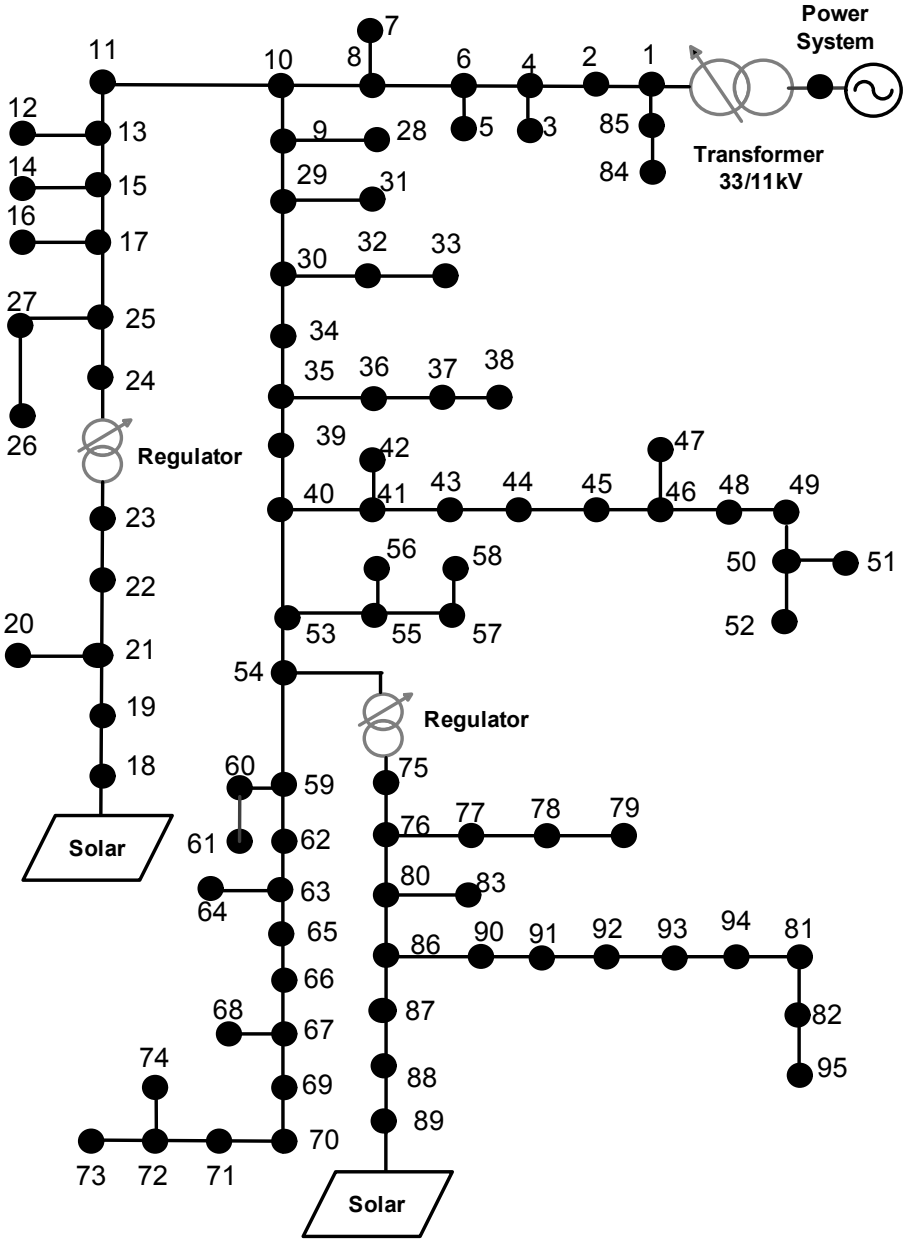

Figure 4.19: UKGDS 95 bus test system

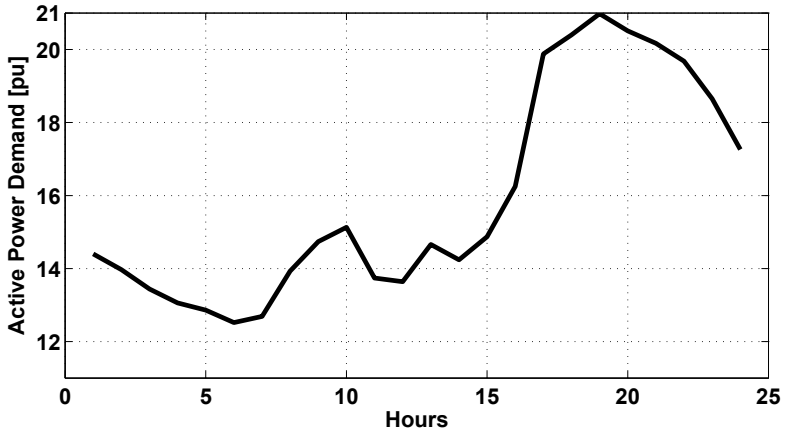

Figure 4.20: UKGDS system load profile

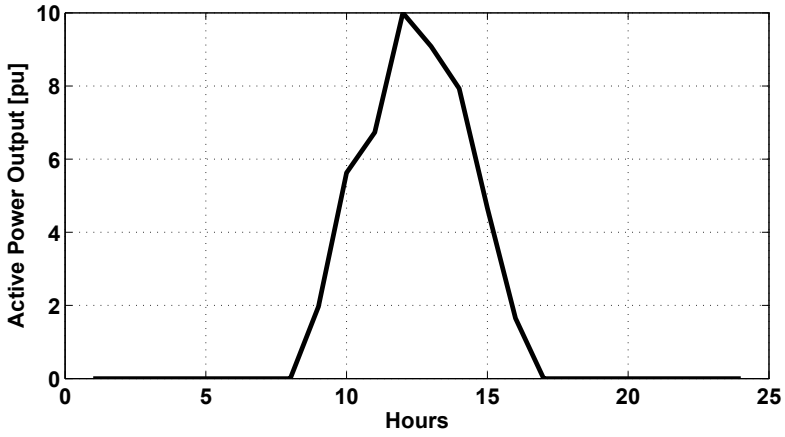

Figure 4.21: Solar active power profile

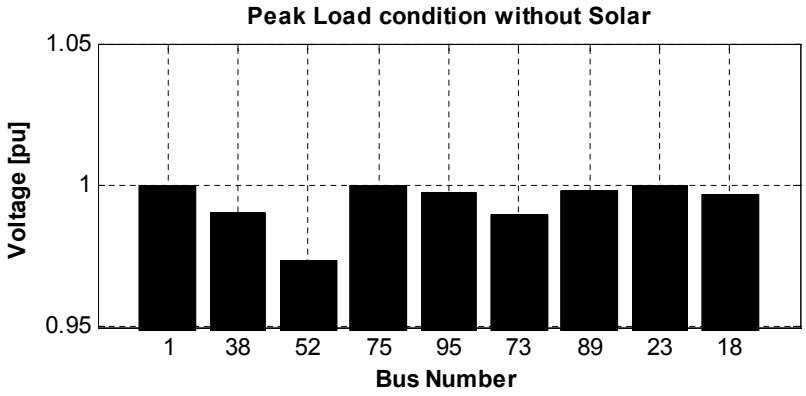

Figure 4.22: UKGDS system voltages during peak load condition without PV (nominal voltage at bus 1)

4.6.2 Results

The UKGDS system considers two DGs at bus 18 and 89. The PV generation plants are considered at the same locations. The VR is considered in an autonomous mode. Both OLTC and PV generation plants are coordinated to achieve the voltage control. The objective function guarantees reduced tap counts and reduced operation of VR in non preferred zone in a preferential manner formulated using weighted combinations. The scalar weights W_c and W_r are varied such that $W_c + W_r = 1$. Table 4.3 and Table 4.4 demonstrates simulation results for different values of weights. In Table 4.3, VR 1 represents VR connected between bus 54 and 75, and VR 2 represents VR connected between bus 24 and 23. Parameters for the penalty function are chosen such that, the penalty function value should not be too small or too large as compared to base case tap count objective function when equal weights are assigned for both objective functions. At the end of the control range for the voltage regulator (at tap position ± 16), the penalty value is significantly higher than the tap count objective function (when the weight W_r corresponding to the voltage regulator runaway is non zero). This ensures that even for the smaller value of Wr the voltage regulator operation at absolute limit is avoided. In order to maintain the control margin for the voltage regulator and avoid runaway, a higher tap non-preferred zone is defined. The preferred zone for both VR is considered to be between tap positions $+10$ to -10.

Table 4.3: UKGDS 95 bus system performance

Case	**Weights**		**Total tap count of all equipments**	**Nonpreferred zone operations**
	Wc	**Wr**		
Case 1	-	-	76	19
Case 2	0.0	1.0	61	8
Case 3	1.0	0.0	33	21
Case 4	0.8	0.2	41	12

Case 1 is considered at unity power factor non-coordinated operation. It can be observed that in Case 1 the total number of tap count is 76 and number of operations of VR1 in the non preferred zone is 11 and that for VR2 is 8. The next

Table 4.4: OLTC and VR performance

	Tap count			**Nonpreferred zone operations**	
Case	OLTC	VR1	VR2	VR1	VR2
Case 1	40	19	17	11	8
Case 2	40	4	17	0	8
Case 3	29	2	2	9	12
Case 4	25	14	2	12	0

case demonstrates the minimization of tap operation in the non preferred zone. The weight W_r is set to 1 and no weight is attached to tap counts. It can be observed that all the operation of the VR1 occurs in preferred zone. But the total tap count remains 61 which is high. In the third case weight W_c is set to 1 and no weight is attached to the penalty function. Tap counts are reduced to 33 but tap operation instances in the non preferred zone are 9 for VR1 and 12 for VR2. This case demonstrates the benefits of penalty function. Conventional objective functions do not consider the proposed penalty. It can be observed that though tap counts are reduced, tap operation happens close to its limit. Case 4 gives the most satisfactory value of the objective function. The following step by step procedure is considered while tuning weights.

Step 1: There are two objectives : tap counts minimization and avoiding operation in the non preferred zone. Tap count minimization is considered to be the preferred objective in this study. The weight tuning is done in preferential manner, so intuitively weight assigned for tap count minimization W_c has to be higher.

Step 2: W_c is set to 1 and W_r to 0 and the best possible objective value of the tap count is calculated. Table 4.3 shows the values achieved.

Step 3: W_r is set to 1 and W_c to 0 and the best possible objective value of the tap in the preferred zone is calculated. Table 4.4 shows the values achieved.

Step 4: The target reduction in tap counts from the base case is decided. In this simulation study it is considered 50.

Step 5: The values of W_c are varied in steps of 0.1 from 0 to 1. The values of both objective functions are noted. Fig. 4.23 shows the variation in both objective

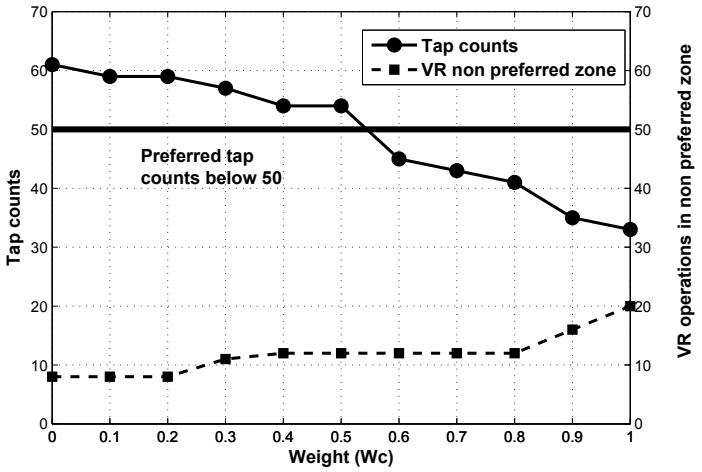

Figure 4.23: Variation in both objective function values at different weights

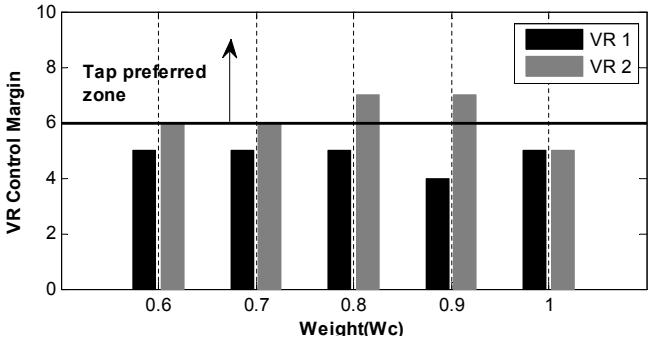

Figure 4.24: VR control margin at different weights

function values. Case 1 tap count is 76, considering target tap count reduction to 50, the weight range selected is W_c from 0.6 to 1.

Step 6: While selecting the final value of W_c (from 0.6 to 1) along with the frequency of operation of voltage regulators in non preferred zone, the voltage regulator control margin is also considered. The control margin of a voltage regulator is defined as the difference between the voltage regulator limit and the nearest operation of the voltage regulator to its limit.

Step 7: The voltage regulator preferred zone of operation is considered between tap values +10 to −10. Hence a value above 6 is a good control margin. For every value of weight W_c from 0.6 to 1, the control margin for both voltage regulators is plotted. Fig. 4.24 demonstrates the control margin for both VR in the system.

Step 8: It can be observed from Fig. 4.23 and Fig. 4.24 that W_c equal to 0.8 offers the same number of tap operations in non preferred zone as W_c equal to 0.7 and the

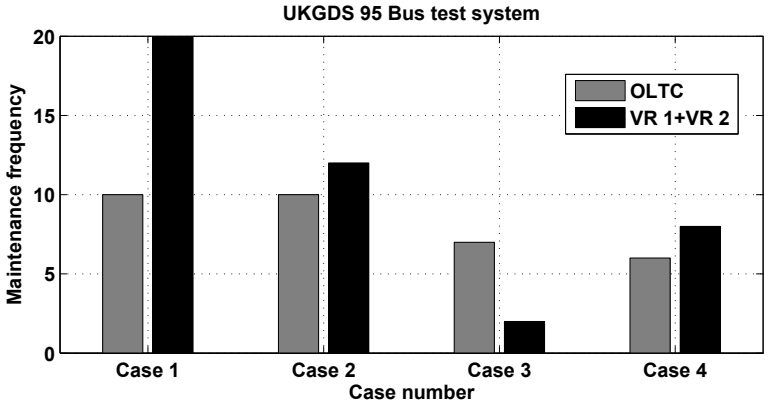

Figure 4.25: OLTC and VR maintenance interval

same control margin as can be achieved by W_c equal to 0.9, hence the final selection of weights is W_c is equal to 0.8 and W_r is equal to 0.2. Thus the final optimal weight tuning is achieved for Case 4 of Table 4.3.

The results of Table 4.3 are confirmed with 30 sec time step load flow. Table 4.5

Table 4.5: Percentage reduction in OLTC and VR tap count

Case	2	3	4
OLTC	0%	27.5%	37.7%
VR1+VR2	41.66%	88.9%	55.56%

shows the percentage reduction in the OLTC and VR tap counts. Typical life of transformer and VR is 30 years. The typical maintenance interval of OLTC and VR is after 3 years. So in the base case, a total of 10 maintenance schedules are considered for each VR and OLTC. Fig. 4.25 shows a reduction in maintenance intervals for this test system if the daily percentage reduction as in Table 4.5 is achieved. Fig.4.26 shows voltage values at different buses for Case 4 during the peak solar injection and the peak load. It can be observed that in both operating conditions, the voltage profile across the feeder is maintained within ±5%. Table 4.6 shows OLTC and VR set points. The hourly voltage set points for both PV plants are shown in Fig. 4.27.

Table 4.7 shows benefit of reactive power support from PV inverter at zero irradiance. Table 4.7 demonstrates Case 3 for which W_c is 1 and W_r is 0. The comparison with case 3 in Table 4.3 shows that, there is significant increase in tap

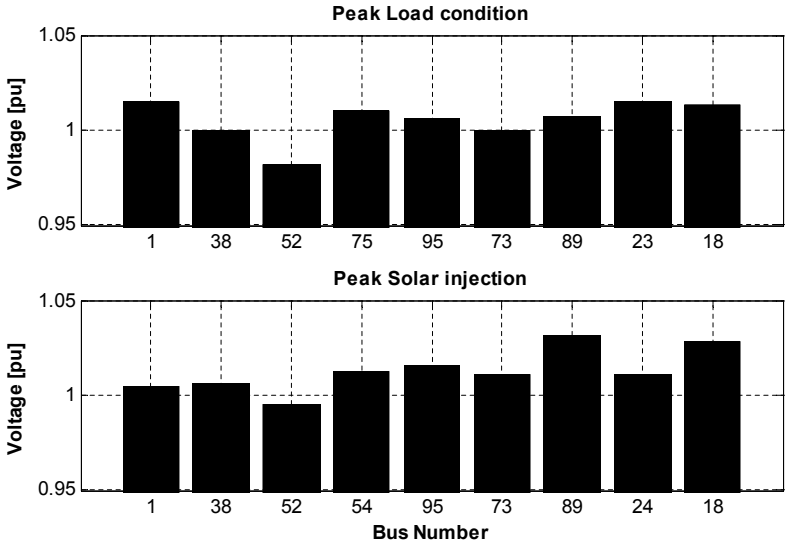

Figure 4.26: Voltages during peak load condition and peak solar injection (Optimal case W_c =0.8 and W_r=0.2)

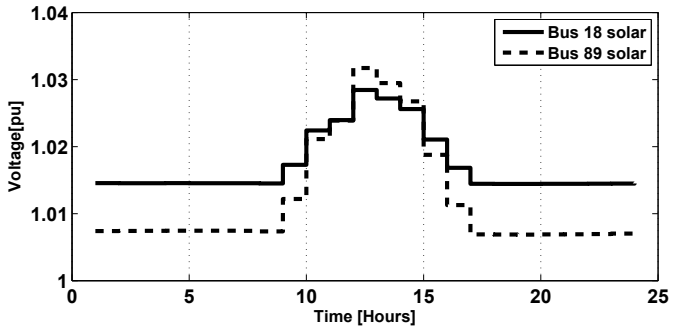

Figure 4.27: Hourly PV plant voltage setpoints

Table 4.6: OLTC and VR Set Points

	Set Points	**Dead Band**
OLTC	1.01	0.02
VR1, VR2	1.02	0.02

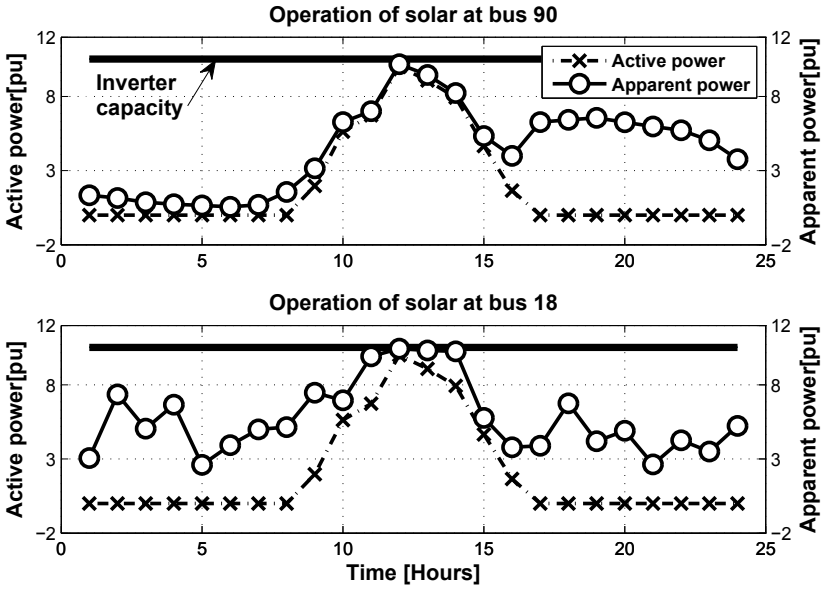

Figure 4.28: PV plant operation

counts when no reactive power support is considered from PV at zero irradiance.

Table 4.7: Tap count with no reactive power support from solar at zero irradiance

OLTC	VR1	VR2	Total
29	10	11	50

The operation of both PV plants for a particular day under consideration is represented in Fig. 4.28. The active power and apparent power consumption of both the PV plants is represented in Fig. 4.28. The solid line represents the inverter capacity. Fig.4.28 demonstrates sufficient reactive power margin available at all the operating values. Also PV plant operates at MPPT at all instants. As can be observed from Fig. 4.27 there are in total 24 optimal voltage set points calculated. The impact of PV active power variability on PCC voltage and hence on OLTC and VR is mitigated by these constant optimal voltage setpoints. On a day having higher variability frequent dispatch of PV voltage set points can be

carried out by considering more PV active power states. This will ensure that MPPT equality constraint in (4.18) is enforced frequently. Even with shorter time interval, underlying principle remains the same that tap count minimization and mitigation of runaway is possible with optimum setpoint selection.

It can be observed from Fig.4.22 that the voltage at bus 52 is acceptable but lower during peak load condition. Distribution static synchronous compensator (STATCOM) is connected at bus 52. A PV inverter reactive power control is similar to that of a STATCOM [95]. The STATCOM capacity is considered to be 250kVAr and voltage set point is considered 1pu. This will ensure that voltage at bus 52 is 1 pu. Both VR and STATCOM are in autonomous mode. So, based on the daily load and irradiance profile, OLTC and PV reactive power set points are coordinated. Again similar to the base case, scalar weights W_c and W_r are varied such that $W_c + W_r = 1$. Table 4.8 and Table 4.9 demonstrates simulation results for different values of weights. The weight tuning is carried out by a similar procedure as explained before.

Table 4.8: UKGDS 95 bus system with STATCOM at bus 52

Case	**Weights** **Wc**	**Wr**	**Total Tap Count of all equipments**	**Nonpreferred zone Operations**
Case 1	-	-	60	20
Case 2	0.0	1.0	52	4
Case 3	1.0	0.0	25	18
Case 4	0.6	0.4	39	8

Table 4.9: OLTC and VR performance STATCOM at bus 52

Case	**Tap Count** OLTC	VR1	VR2	**Nonpreferred zone operations** VR1	VR2
Case 1	29	14	17	12	8
Case 2	27	9	16	4	0
Case 3	19	3	3	9	9
Case 4	21	16	2	8	0

It can be observed that Case 4 gives the most satisfactory value of the objective function. The comparison between the results of Table 4.3, Table4.4, Table 4.8 and

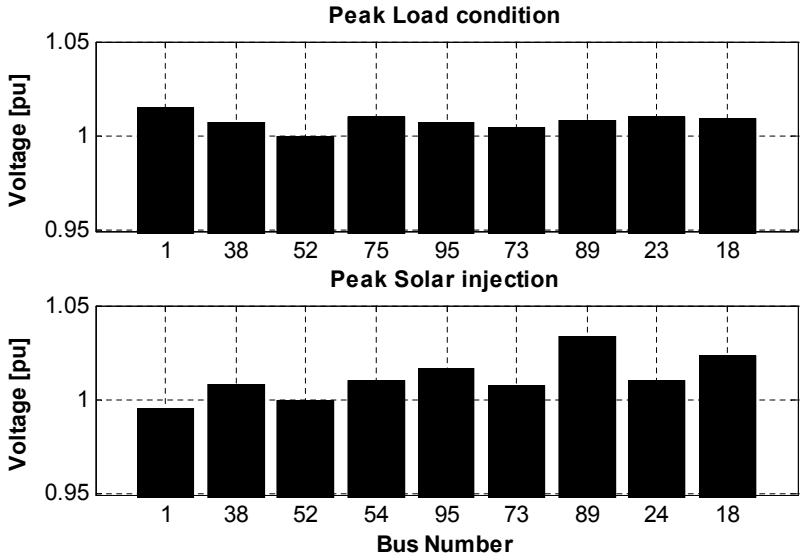

Figure 4.29: Voltages during peak load condition and peak solar injection with STATCOM

Table4.9 indicates that for all operating cases, tap count and number of operation in non preferred zone are lowered when STATCOM is considered. Fig.4.29 shows voltage profiles at different buses for Case 4 during peak solar injection and peak load. It can be observed that in both operating conditions, the voltage profile across the feeder is maintained within ±5%. In Case 4, the coordination is achieved with OLTC and VR set points as described in Table 4.10. The hourly voltage set points for both PV plants are shown in Fig. 4.30. The operation of both PV plants for a particular day under consideration is represented in Fig. 4.31. The active power and apparent power consumption of both the PV plants is represented. Solid line represents the inverter capacity. The comparison between Fig.4.28 and Fig.4.31 indicates that there is less reactive power utilization from PV generation when STATCOM is present in the system.

Table 4.10: OLTC and VR Set Points

	Set Points	**Dead Band**
OLTC	1.005	0.02
VR1, VR2	1.02	0.02

The following advantages are observed with the inclusion of STATCOM :

- The number of tap counts is to achieve voltage control is lower when

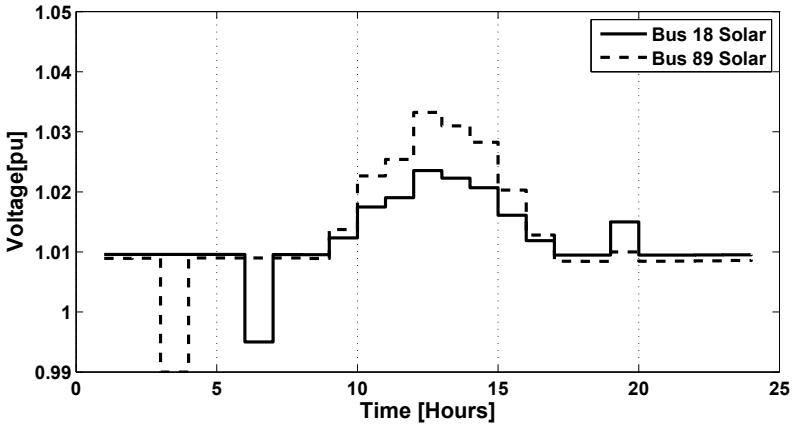

Figure 4.30: PV plant voltage setpoints with STATCOM

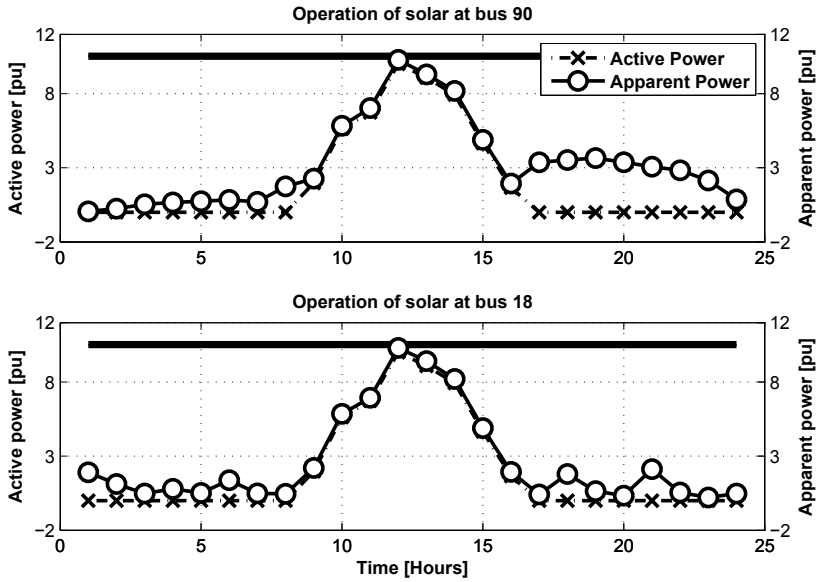

Figure 4.31: PV plant operation with STATCOM at bus 52

STATCOM is placed at Bus 52.

- The number of operations of the voltage regulator in the non preferred zone is reduced with the presence of STATCOM
- Reactive power utilization from PV inverter is less when STATCOM is considered.

Similarly distribution feeders are sometimes equipped with switched capacitors. Hence, at this bus, two switched capacitor banks are installed instead of STATCOM. The capacitor banks C1 and C2 each has rating of 200 kVAr at rated voltage (1 pu). In Europe, timer controlled switched capacitors are prevalent [94]. In order to simulate this scenario, Capacitor C1 is switched on at 17:00 hrs and switched off at 3:00 hrs. Capacitor C2 is switched on at 17:00 hrs and switched off at 8:00 hrs.

Table 4.11 and Table 4.12 display simulation results for the base case and the optimal case. Fig. 4.32 shows the PV plant voltage set points for the optimal case. It can also be seen from Fig. 4.33 that voltages at all buses remain within the prescribed limits.

Table 4.11: UKGDS 95 bus system with capacitors at bus 52

Case	**Weights** **Wc**	**Wr**	**Total Tap Count of all equipments**	**Nonpreferred zone Operations**
Case 1	-	-	69	13
Case 2	0.5	0.5	45	6

Table 4.12: OLTC and VR performance with capacitors at bus 52

Case	**Tap Count** OLTC	VR1	VR2	**Nonpreferred zone operations** VR1	VR2
Case 1	31	21	17	5	8
Case 2	27	16	2	6	0

The case studies demonstrate reduction in tap counts and operation of VR without runaway using the proposed optimization procedure. The reduction in OLTC and VR maintenance cost comes at the cost of solar inverter over capacity. There can be a scenario in which a feeder is supplied by only one OLTC substation

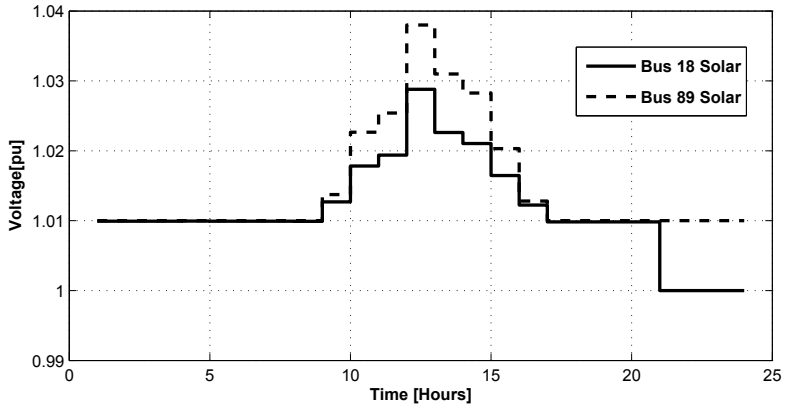

Figure 4.32: PV plant voltage setpoints with capacitors at bus 52

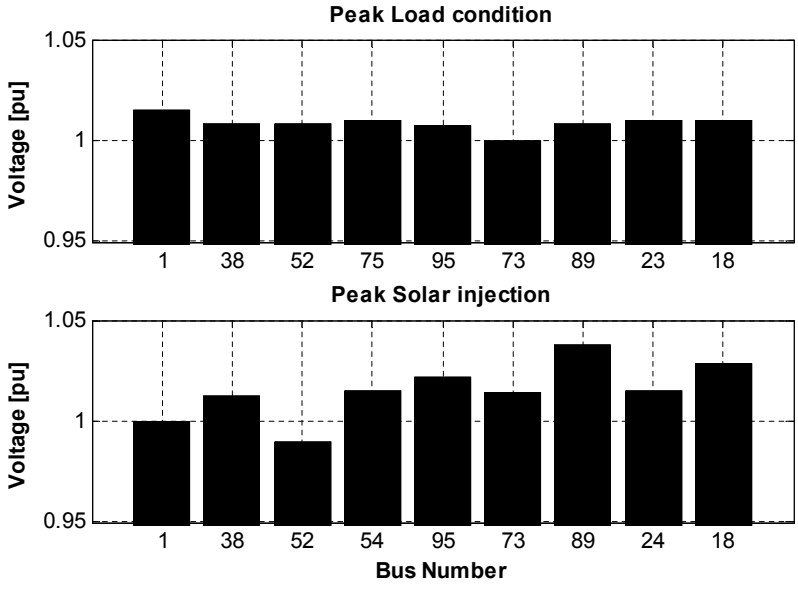

Figure 4.33: Voltages during peak load condition and peak solar injection (Timer controlled capacitor case)

transformer. The OLTC maintenance in this area will require a feeder disconnection and the revenue will be lost. However, to have reactive power support from solar its inverter needs to be oversized. The cost benefit analysis needs to be carried out while planning inverter over capacity. Implementation of additional fast control devices such as STATCOM had a positive impact on the tap changer operation. However, STATCOM is a costly equipment. Hence it is recommended that costly equipment such as STATCOM should be implemented only after detailed cost benefit analysis during planning study. The conventional STATCOM or switched capacitors if present on the feeder can be considered in the proposed optimization procedure.

4.7 Summary

- The operation of VR in autonomous mode can result in VR *runaway* in the presence of a PV power injection. The *runaway* depends upon PV plant capacity, control modes of a VR and PV plant, driving point impedance values and voltage control device set points. An increase in an OLTC and a VR tap counts is possible in the presence of a PV plant.

- This chapter has proposed a strategy that ensures smooth operation of line voltage regulators in autonomous mode. The voltage control is achieved by designing optimum voltage control set points for OLTC and PV plant.

- The problem is solved by formulating weighted tap counts minimization objective subject to power flow and other constraints including limits on node voltages, tap and maximum power tracking from solar. The non preferred operating zone of VR is modeled as a penalty function in the optimization process.

- The effectiveness of the scheme is tested through simulations on a realistic distribution network model. The case study demonstrates that with the optimal daily proposed coordinated reactive power dispatch, tap counts are reduced without detrimental impact on the feeder voltage. The operation of

VR in non preferred zone is also limited and proper operation of VR without runaway is ensured.

- Further, the definition of non preferred zone in penalty function ensures control margin for VR. It is believed that the proposed approach is useful to Distribution Network Operators to achieve voltage control in the presence of PV and autonomous VR while ensuring better operating life of OLTC and VR.

The PV generation forecast and the load forecast are utilized in many deterministic techniques as in this Chapter. The deterministic techniques assume that the forecast errors are absent and the available forecast is accurate. The consideration of forecast errors into steady state voltage control challenges is discussed in the next chapter.

Chapter 5

Stochastic voltage control

PV generation forecast suffers from inherent errors. The challenge of the *steady state voltage control* is further intensified due to the presence of the PV forecast errors. Since there is an element of randomness associated with the forecast errors, it is necessary to deal with this problem via stochastic approaches. This chapter proposes a *stochastic distribution voltage control* strategy. A stochastic operation considering voltage regulator(VR) *runaway* is formulated here as a classical chance constrained optimization (CCO) problem. The consideration of VR *runaway* in a CCO problem formulation needs appropriate stochastic indices. Two stochastic indices are defined which assist consideration of VR *runaway* in the stochastic formulation. The solution strategy to solve the CCO is developed. A case study is presented which demonstrates the effectiveness of the approach.

5.1 Motivation

The classical approach to deal with randomness in power system operation is through probabilistic load flow (PLF). The PLF analysis to evaluate the impact of PV generation is already proposed in [107]. Further, probabilistic optimal power dispatch considering uncertainty in the presence of PV generation is formulated in [108]. However, both of these studies considered the transmission network. The major focus of this thesis is on the voltage control challenges in a distribution system. One of the important objectives of the distribution voltage control is the feeder

power loss reduction. In the presence of stochastic PV generation the expectation of power loss needs to be minimized. The characterization of renewable output through the probability distribution function (PDF) and the minimization of power loss expectation is formulated in [109]. However, this formulation did not include different constraint violations in a stochastic sense. There is a probability of bus voltage violation or feeder current violation during the operation of a distribution feeder. This needs to be considered in the stochastic operation. A constrained probabilistic load flow (CPLF) which examines constraint violations while carrying out reactive power coordination is proposed in [110] [111]. Another method to solve the stochastic distribution system operation problem is through analytical PLF based chance constrained optimization as proposed in [112]. Monte carlo simulation (MCS) based stochastic optimization to calculate renewable energy power factor (pf) setpoints can be employed instead of analytical PLF based stochastic optimization [33].

These approaches do not consider the detailed impact of the PV generation on On-load Tap Changer (OLTC) and VR. The stochastic impact of renewable energy sources on voltage control devices is considered in [34]. But the available literature does not consider the VR *runaway* in system operation, including the forecast errors. A stochastic framework that minimizes the risk of VR *runaway* is proposed in this Chapter.

5.2 Chance constrained optimization (CCO)

The stochastic operation of the radial feeder shown in Fig.4.14 is under consideration here. In order to achieve an optimal operation, DNOs should consider different objectives and risks. A chance constrained optimization (CCO) based problem is formulated to achieve these objectives in the presence of PV generation and load forecast errors. The problem is mathematically formulated as follows.

5.2.1 Optimization objective

DNOs wish to operate distribution feeders such that the losses are minimum. The expected value of power losses should be minimized in order to account for randomness in forecasting errors i.e.

$$Minimize\ E(P_{loss}) \tag{5.1}$$

In (5.1) $E(P_{loss})$ represents the expected value of power losses in the time horizon under consideration.

5.2.2 Probabilistic constraints

1. **Bus voltage:** The primary objective of any feeder operational strategy is to maintain acceptable bus voltages. When the forecast errors are considered, the bus voltage violation risk needs to be accounted for. Variance minimization can be utilized if DNOs insist on maintaining a flat voltage profile. Generally, the bus voltages are required to stay within the specific band ($0.95pu$ to $1.05pu$). Therefore, minimizing the probability of violation of this band results in an acceptable voltage profile. The voltage violation probability should be below the tolerance prescribed by a DNO. $Pr(V \leq V_{limit}^{up}) \geq \alpha_V^{up}$ is defined as a constraint for the upper limit of the voltage:

$$Pr(V > V_{limit}^{up}) \leq 1 - \alpha_V^{up} \tag{5.2}$$

Similarly for the lower limit of the voltage:

$$Pr(V < V_{limit}^{low}) \leq 1 - \alpha_V^{low} \tag{5.3}$$

In (5.2) and (5.3), V_{limit}^{up}, V_{limit}^{low}, α_V^{low} and α_V^{up} are design parameters. These can be changed to suit the requirements of the DNO. $1 - \alpha_V^{up}$ and $1 - \alpha_V^{low}$ indicate voltage violation probabilities. Typically, a bus voltage violation is restricted below 5%. This violation probability is as per the European standard

EN50160.

2. **Feeder current:** The feeder current thermal capacity needs to be considered in the following manner:

$$Pr(I_{feed} > I_{feed}^{limit}) \leq 1 - \alpha_I^{feed} \tag{5.4}$$

Typically α_I^{feed} can be 95%. I_{feed}^{limit} changes from season to season. α_I^{feed} and I_{feed}^{limit} can be adjusted as per the operator needs.

3. **PV generation:** From a PV generation owner's perspective, revenue should be maximized. This necessitates that the injected active power should always satisfy the maximum power point tracker (MPPT) criterion as discussed in Chapter 4. However, in order to manage an overvoltage, active power curtailment is unavoidable in some cases. The situation can be best addressed by keeping the expectation of active power curtailment below a specific limit ($\epsilon_{pcurtail}$) i.e.

$$E(P_{curtail}) \leq \epsilon_{pcurtail} \tag{5.5}$$

This active power curtailment is typically 30% in Germany. However one should aim for less active power curtailment. The tolerance $\epsilon_{pcurtail}$ an be adjusted by the DNO. Further, the PV generation reactive power support is limited by its inverter apparent power rating as per capability curve shown in Fig.2.6 in Chapter 2.

4. **OLTC and VR:** The details of OLTC and VR mechanisms and impact of PV generation on these mechanisms are discussed previously in Chapter 4. One of the challenges in the presence of PV generation is the excessive number of tap operations which results in an increased frequency of maintenance as explained earlier. Therefore voltage control should be achieved with a minimum number of tap operations:

$$E(Tap_{counts}) \leq \epsilon_{Tapcounts} \tag{5.6}$$

In (5.6), $E(Tap_{counts})$ represents the expected value of tap counts in the time horizon under consideration. The maximum permissible tap counts is defined by $\epsilon_{Tapcounts}$.

The consideration of the VR *runaway* challenge is also important in a stochastic operation. The VR *runaway* needs to be avoided under all scenarios in Table 4.2 described in Chapter 4. As discussed earlier this phenomenon results in the operation of the VR either at the lowest or at the highest tap position. Hence avoiding the operation of a VR at the extreme tap position is essential. A tap violation probability for VR is defined to mitigate the VR *runaway*, according to the following constraints:

$$\begin{aligned} Pr(Tap > Tap^{up}_{limit}) &\leq 1 - \alpha^{up}_{Tap} \\ Pr(Tap < Tap^{low}_{limit}) &\leq 1 - \alpha^{low}_{Tap} \end{aligned} \tag{5.7}$$

The regions beyond the Tap values Tap^{low}_{limit} and Tap^{up}_{limit} are denoted as the *non preferred zones*. DNOs can mitigate the *runaway* and maintain VR control margins by specifying Tap^{low}_{limit}, Tap^{up}_{limit},α^{up}_{Tap} and α^{low}_{Tap}. The problem is solved through coordination amongst various reactive power devices in the network. The following section details the solution strategy of this chance constrained optimization (CCO) problem.

5.3 CCO solution strategy

The proposed CCO solution algorithm to solve the above CCO problem has three major routines; namely sample selection, set point calculation and set point validation. These three subroutines are as follows:

1. **Sample selection:** Both load and PV generation forecasting errors are considered in the particular time horizon. The time horizon can be day ahead or hour ahead based on the operators' choice. In order to solve the CCO problem, N independent identically distributed sample scenarios are selected. Let F^{lim}_{x} denote the probability for which constraints defined for

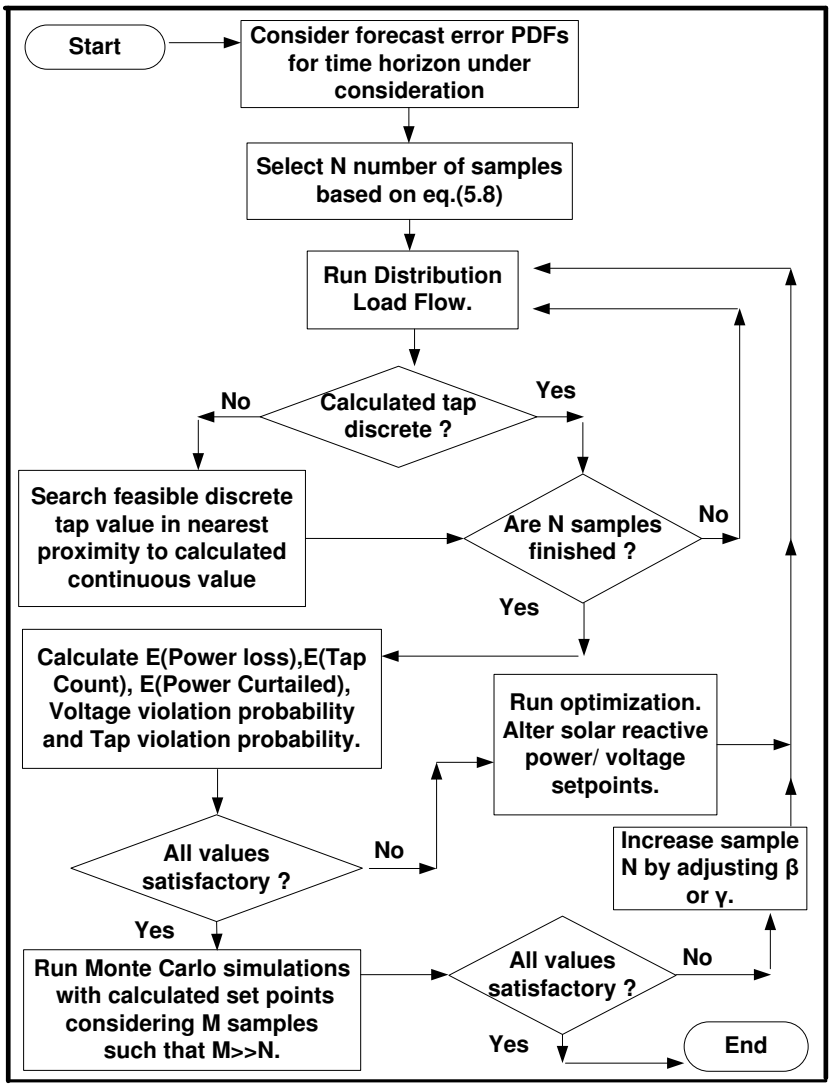

Figure 5.1: CCO Solution Strategy

decision variable vector x are violated. Let us also denote α as the acceptable probability level for which constraints are not violated. Hence the acceptable constraint violation probability β is calculated as $\beta = 1-\alpha$. A β-level robustly feasible optimization solution will satisfy $F_x^{lim} \leq \beta$. The number of N different samples to obtain a robust solution are selected as:

$$N \geq \frac{n}{\beta\gamma} - 1 \tag{5.8}$$

In (5.8), n represents the number of decision variables. The extraction of these N samples ensures that the obtained optimization solution is β-level robustly feasible with a probability no smaller than $1 - \gamma$ [113]. This result however requires the program to be convex, which is not the case here. Set point validation is therefore employed in Step 3.

2. **Setpoint calculation:** This subroutine calculates the setpoints of voltage control devices utilizing the N samples chosen in Step 1. It is based on the oriented discrete descent method [114]. First, the objective function is calculated for some initially assumed values of the control variables. The control variables are then altered in discrete steps along all possible search directions. Again for all the new control variable values, the corresponding new values of the objective functions are computed. The partial derivatives of the objective function with respect to all control variables are calculated. The partial derivatives are computed using the differences of the objective function divided by the corresponding variation in the setpoints. The control setpoint with the highest partial derivative is the best candidate to minimize the objective. Only the setpoint which corresponds to the highest value of the partial derivative is altered to minimize the objective. This procedure is repeated until satisfactory variables for the objective function and constraint violation probabilities are obtained.

3. **Setpoint validation:** The calculated setpoints in Step 2 are valid for N samples and they offer a β-level robustly feasible solution (with a minimum probability of (1-gamma)) only if the program is convex. The setpoint

validation is carried out in order to overcome this issue. The calculated setpoints are validated by choosing M samples such that $M \gg N$.

A Monte carlo simulation using the calculated setpoints is run. The objective function and constraint violation probabilities are checked for these M samples. The initially chosen N samples are increased if the validation results are not satisfactory. Upon increasing these N samples, Step 2 and Step 3 of the algorithm are rerun until a satisfactory result is obtained. The violation probability β or the confidence parameter γ in (5.8) can be reduced to increase the value of N.

Fig.5.1 details the flowchart of the proposed algorithm. As mentioned in the sample selection subroutine, the setpoints can be calculated for any time horizon. The operational strategy proposed here is subdivided into two distinct time horizons to minimize the impact of forecasting errors. Firstly a day ahead time horizon is considered. In this stage, the voltage setpoints of the OLTC and PV generation are calculated. The second stage is particularly useful when a day ahead PV forecast accuracy is lower. In the second stage, a shorter forecast horizon of one hour is considered. Hour ahead PV forecast errors are lower as compared to the day ahead forecast errors [50]. The readjustment of voltage setpoints is done considering hour ahead forecast. While readjusting, the OLTC setpoints calculated from the first stage remain the same. Only the PV generation setpoints are readjusted. Communicating voltage setpoints to OLTC and PV generation helps to achieve an efficient operation of a distribution system and mitigates the autonomous VR *runaway* risk.

5.4 Tap tail expectation(TTE)

The CCO discussed above considers VR *runaway* risks by enforcing constraints on tap violation probability. The proposed CCO implementation calculates reactive power set points such that the extreme values of taps lie in the tail region of the VR tap PDF. The parameters defined in (5.7) are designed to achieve this. However, its major disadvantage is due to the fact that CCO does not give information about the

scenarios where Tap values are beyond Tap^{up}_{limit} or Tap^{low}_{limit}. For instance, consider that the permissible probability of the tap value being beyond +13 is 5%. Then in 95% of cases it is ensured that a VR will not operate beyond the value +13. But the disadvantage is that in 5% of the cases there is no operational control at which tap position VR will operate. In 5% of cases, a VR can be operating even at +16, which indicates the runaway or lack of VR operational margin.

In order to mitigate this limitation, the *Tap tail Expectation (TTE)* index is defined. Fig. 5.2 demonstrates the concept of TTE for VR *runaway*. The mathematical definition of this risk measure is detailed as follows.
Let $F^{up}_{Tap}(z) = Pr\{Tap \leq z\}$ define the cumulative distribution function (CDF) of a variable Tap. The Tap^{up}_{α} with a confidence level $\alpha \in$ [0,1] is defined as,

$$Tap^{up}_{\alpha} = min\{z|F^{up}_{Tap}(z) \geq \alpha\} \tag{5.9}$$

Tap^{up}_{α} is a lower α-percentile of the random variable Tap. For example, suppose that the desired value of probability α is 95%. This indicates that for only 5% of instances, Tap attains a value greater than or equal to Tap^{up}_{α}. Similarly for the lower limit of the VR, if the CDF is defined as $F^{low}_{Tap}(z) = Pr\{Tap \geq z\}$ then,

$$Tap^{low}_{\alpha} = max\{z|F^{low}_{Tap}(z) \geq \alpha\} \tag{5.10}$$

The constraints defined in (5.7) can also be written as,

$$\begin{aligned} Tap^{up}_{\alpha} &\leq Tap^{up}_{limit} \\ Tap^{low}_{\alpha} &\geq Tap^{low}_{limit} \end{aligned} \tag{5.11}$$

The *Tap Tail Expectation* is an alternative risk measure that takes into account the tail of probability distribution of variable Tap. For the variable Tap and with confidence level $\alpha \in [0, 1]$, TTE is the mean of the tail distribution. If $F_{Tap}(Tap^{up}_{\alpha}) <$ 1 then there is a possibility of a VR operating in the *non preferred zone* that is above

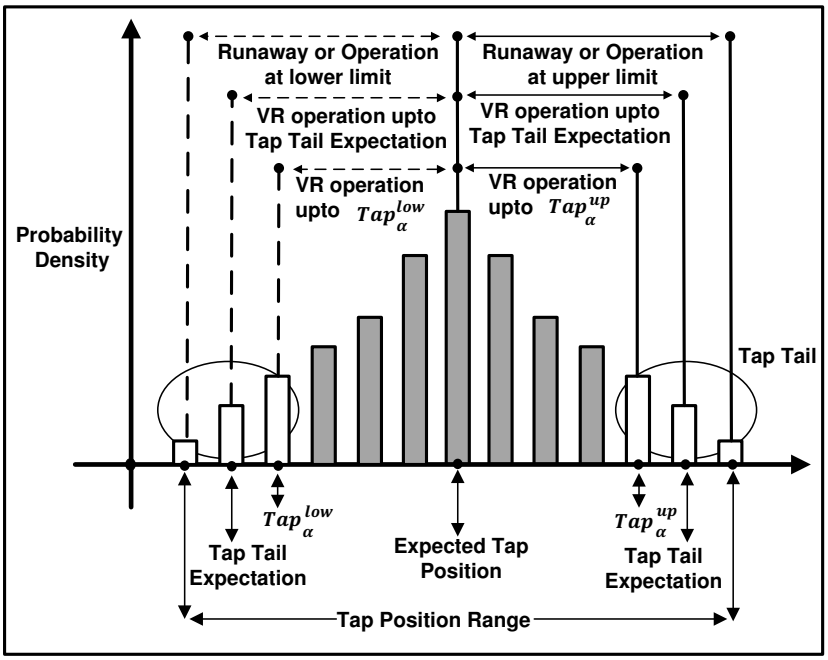

Figure 5.2: *Tap Tail Expectation* to mitigate VR *runaway*

Tap_{α}^{up} value. Then the *TTE* $E[Tail_{\alpha}^{up}(Tap)]$ is calculated as follows [115]:

$$E[Tail_{\alpha}^{up}(Tap)] = \Psi_{\alpha}(Tap)Tap_{\alpha}^{up} + \tag{5.12}$$
$$(1 - \Psi_{\alpha}(Tap))E[Tap|Tap > Tap_{\alpha}^{up}]$$
$$\Psi_{\alpha}(Tap) = \frac{F_{Tap}(Tap_{\alpha}^{up}) - \alpha}{1 - \alpha} \tag{5.13}$$

It should be noted that similarly for the lower limit of a VR $E[Tail_{\alpha}^{low}(Tap)]$ can be defined. The above *TTE* indices can be incorporated in the proposed CCO strategy by replacing the constraints in (5.7) by:

$$E[Tail_{\alpha}^{up}(Tap)] \leq \epsilon_{Taptail}^{up} \tag{5.14}$$
$$E[Tail_{\alpha}^{low}(Tap)] \geq \epsilon_{Taptail}^{low}$$

By selecting an appropriate value of $\epsilon_{Taptail}^{up}$, $\epsilon_{Taptail}^{low}$, the DNOs can control the shape of the VR tail probability distribution. All voltage control equipments and

PV inverter control features (for example reactive power injection, active power curtailment) need to be coordinated to achieve this. The effectiveness of modeling VR *runaway* in classical CCO and by using the *TTE* is demonstrated in the next section using a realistic distribution test system model.

5.5 Case study

5.5.1 System model

The UK generic distribution system (UKGDS), displayed in Fig.4.19, is considered again to evaluate the performance of the proposed CCO strategy. The system details and the PV generation location etc. remain the same as described in Chapter 4 case study. There are two PV plants considered in the system at bus 18 and bus 89 each of 1 MW capacity. The PV inverter MVA capacity is overrated such that the plant is able to operate at 0.95 lead/lag power factor during the peak active power injection. Two banks of switched capacitors namely, C1 and C2, each of rating 200 kVAr at rated voltage (1 pu), are assumed to be installed at bus 52. Capacitor C1 is switched on at 17:00 hrs and switched off at 3:00 hrs. Capacitor C2 is switched on at 17:00 hrs and switched off at 8:00 hrs. PV generation forecast errors are modeled by a Gaussian distribution [19]. The peak hour PV generation PDF for the PV at bus 89 is shown in Fig. 5.3. A correlation coefficient of 0.7 is considered between the two PV generators at bus 18 and bus 89. Load forecast errors are also modeled by a Gaussian distribution [51]. The peak hour load PDF is shown in Fig.5.4. The next section discusses various results obtained from this example.

5.5.2 Results

Three different cases are studied to evaluate the performance of the proposed strategy.

- Case 1 - Base case setpoint calculation
- Case 2 - Classical CCO

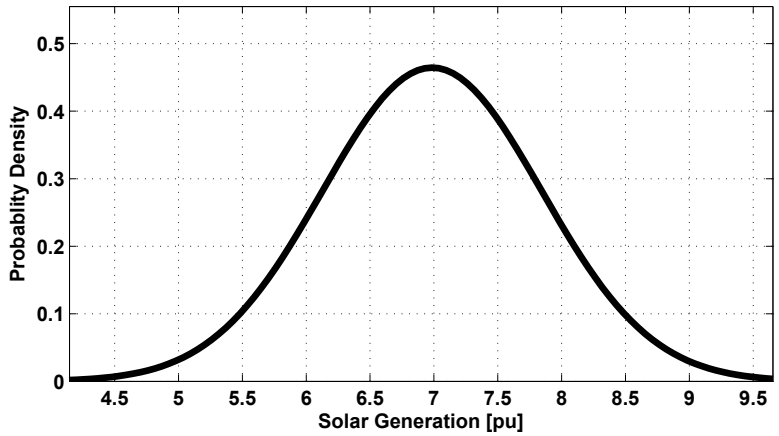

Figure 5.3: PV generation active power PDF during peak hour

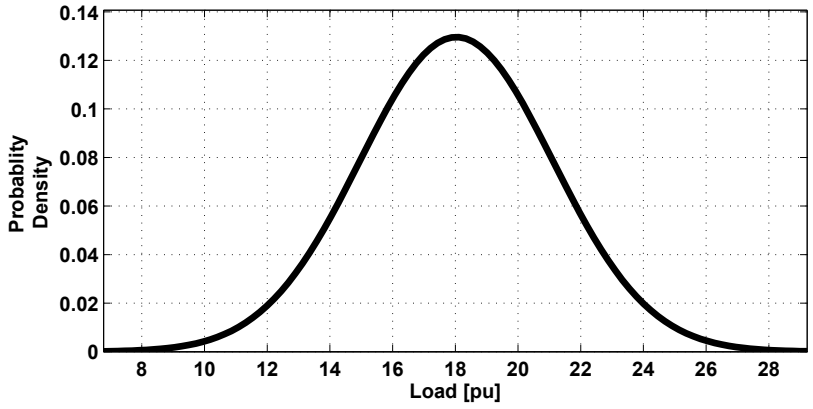

Figure 5.4: UKGDS system load PDF during peak hour

- Case 3 - CCO with *Tap Tail Expectation*

For these three cases, firstly voltage control device setpoints are designed. Then, using these setpoints a PLF is calculated to evaluate the operational performance of the system. The upcoming sections discuss the detailed results and the performance comparison.

Case 1 - Base case setpoint calculation

In this case, system voltage control is achieved by designing setpoints for the worst case scenario. Three worst case scenarios are considered. Namely, maximum output of the PV generator under minimum load demand, maximum load demand with no PV generation and maximum load demand with maximum PV generation [93] [116]. Non coordinated operation of OLTC, VR and PV plant is considered. Moreover the PV generation is operating at unity pf. Only the primary objective of maintaining the system voltage at all the buses is considered and setpoints are calculated. In reality, the PV generation and load forecasts will have errors. These errors are introduced and the PLF is run. The cumulative distribution function (CDF) curves of the voltage magnitudes at PV generation buses are shown in Fig. 5.5 for a day. It can be observed that the probability of violating voltage limits is zero. However, PDFs for both the VRs are shown in Fig. 5.6. It can be observed that the probability of operation at the tap position -16 (operational limit) for VR2 is 6.5%. This unsatisfactory operational performance of VR2 is due to the non coordinated operation of the voltage control devices. In order to alleviate this challenge, the following two cases evaluate the proposed CCO based strategies.

Case 2 - Classical CCO

In order to avoid VR *runaway* and maintain VR control margin, the classical CCO is used. To minimize the VR *runaway* probability, the constraints defined in (5.7) are considered. This exercise designates regions beyond Tap values of ± 10 of VR as *non preferred zones*. Ideally, the optimization should result in setpoints such that, the VR operation in the *non preferred zone* becomes a zero-probability event, or the non preferred zone Tap values should have very small probability. Hence, the setpoints

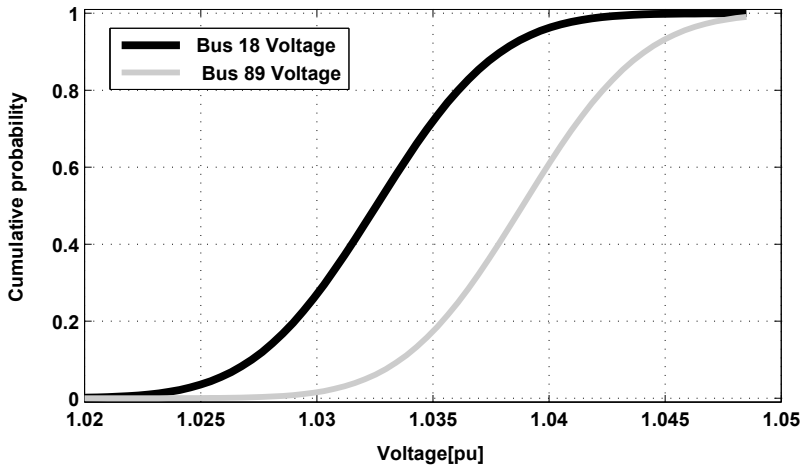

Figure 5.5: Case 1 : CDF curves of PV generation bus voltages

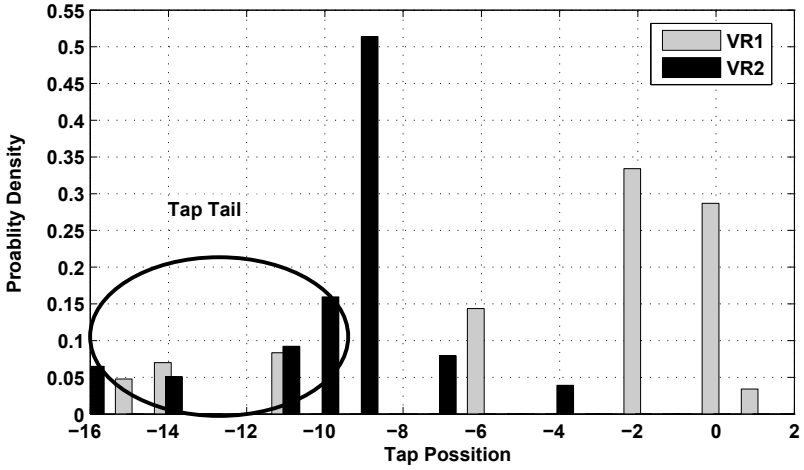

Figure 5.6: Case 1 : PDFs of both VRs Tap positions

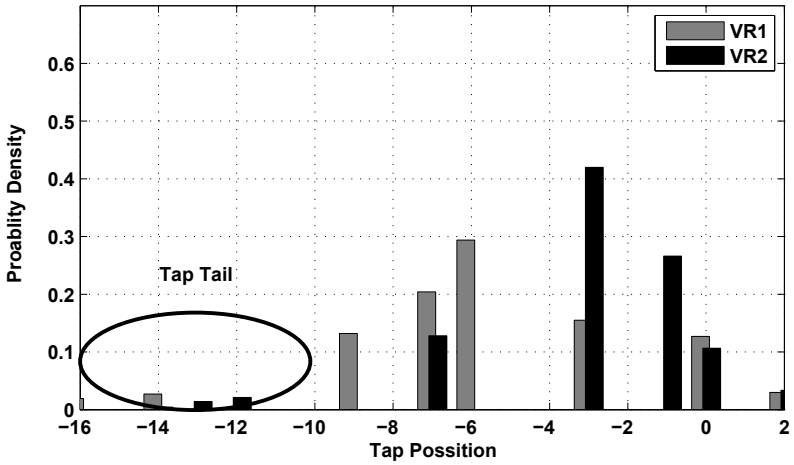

Figure 5.7: Case 2 : PDFs of both VRs Tap positions

should make the *non preferred zones* lie in the *tail* region of the VR Tap value PDF. In order to achieve this, the constraints in (5.7) are employed. A 5% violation probability is permissible beyond Tap values $+10$ and -10. Based on the operator's experience, an appropriate choice of violation probability and *non preferred zones* can be made to maintain a VR control margin. After defining these parameters, the Classical CCO based coordination is simulated. The resultant Tap PDFs for both VRs are shown in Fig. 5.7. The following observations can be made comparing 'Case 1' in Fig.5.6 and 'Case 2' in Fig. 5.7. It can be observed that there is reduction in the probability of VR operation in the non preferred zone beyond the Tap value ± 10. The probability of the operation below -10 is less than 5%. Similar to the VR operation, the violation probability is defined for the voltage. Fig.5.8 shows the CDF curves of UKGDS bus voltage magnitudes. It can be observed that the voltage at the buses is maintained between $0.95pu$ to $1.05pu$. The above classical CCO based reactive power coordination is achieved with optimal PV generation set points. Optimal PV generation setpoints for bus 18 and bus 89 are shown in Table 5.1. Thus the formulation helps minimizing the VR *runaway* probability and maintains bus voltages within their prescribed limits.

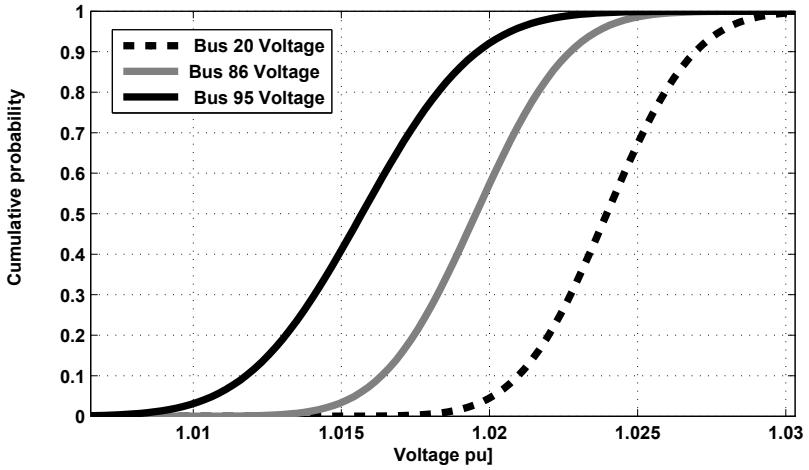

Figure 5.8: Case 2 : CDF curves of UKGDS bus voltages

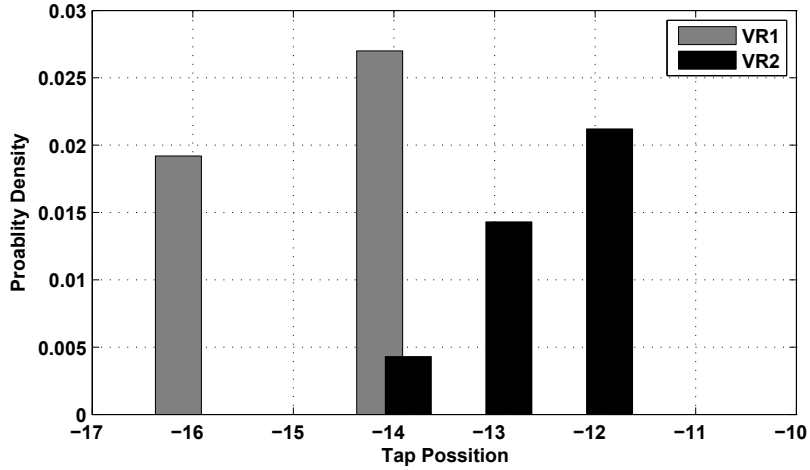

Figure 5.9: Case 2 : Tap tail distribution

Table 5.1: Case 2 : PV generation voltage setpoints [pu] from 11:00am to 12:00pm

	Voltage [pu]			
Bus 89	1.025	1.015	1.02	1.02
Bus 18	1.03	1.025	1.025	1.02

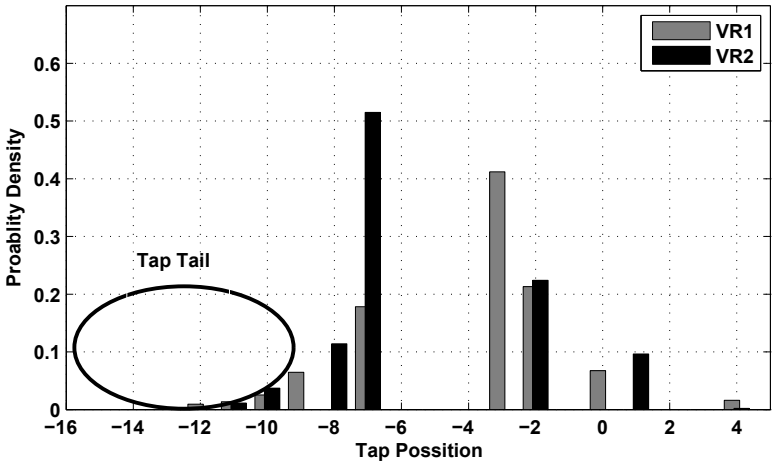

Figure 5.10: Case 3 : PDFs of both VRs Tap positions

Case 3 - CCO with tap tail expectation

Closer observation of Fig.5.9 indicates the limitation of the classical CCO. There is still a small probability of VR operation at -16 (approximately 2%). This shows that the modeling of the violation probability as per (5.7), reduces the probability of operation beyond the Tap value -10 to a value below 5%. But in the 5% of the scenarios, there is no control at which position VR will operate. As can be observed in Fig.5.9, this can very well be -16 indicating operation at the VR tap limit. Considering this limitation, the *tap tail expectation(TTE)* is used in the simulation. *Runaway* related constraints are replaced by (5.14). The $\epsilon^{up}_{Taptail}$ and $\epsilon^{low}_{Taptail}$ parameter values are considered to be ± 12. Fig.5.10 shows the effectiveness of the TTE. The probability of *runaway* is reduced further and the VR operational margin is improved. This is because the expected value of the Tap in the tail of the distribution is designed to be greater than -12. Therefore, defining constraints using the TTE offers control over the tail region of Tap. In this study, the TTE is defined only for VRs. The voltage optimization is carried out by defining the violation

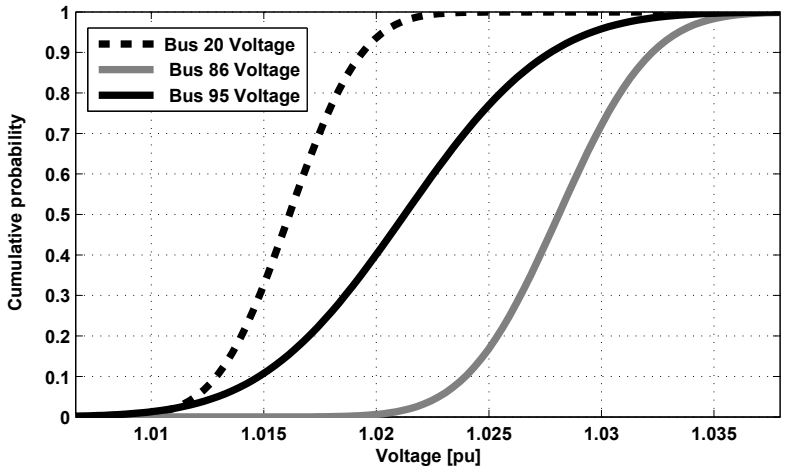

Figure 5.11: Case 3 : CDF curves of UKGDS bus voltages

probability. The resultant CDF curves of the UKGDS bus voltage magnitudes are shown in Fig.5.11. The optimal PV generation set points for bus 18 and bus 89, for this case are shown in Table 5.2.

Table 5.2: Case 3 : PV generation voltage setpoints [*pu*] from 11:00 am to 12:00pm

	Voltage [pu]			
Bus 89	1.035	1.025	1.025	1.03
Bus 18	1.015	1.02	1.025	1.02

Other operational targets such as power loss minimization and tap operational counts minimization are also considered in 'Case 2' and 'Case 3'. Table 5.3 shows the expected values of power loss in the network and the tap counts for all the cases. Both CCO based reactive power coordination strategies are able to reduce the power loss and tap counts as compared to 'Case 1' having non coordinated operation. Thus CCO based reactive power coordination through Classical approach and *TTE* approach are effective in improving the operational performance of the system such as, network losses and the number of tap movements.

Table 5.3: UKGDS 95 bus system operational performance

Case	E(Energy loss)	E(Tap counts)
Case 1	2.72MWh	48
Case 2	2.44MWh	25
Case 3	2.53MWh	29

5.6 Summary

- The conventional framework to achieve the distribution voltage control in the presence of PV generation does not consider inherent forecasting errors. It is essential to mitigate the operational risks such as overvoltage, excessive tap counts and VR Runaway, in the presence of PV and load forecast errors.
- This is achieved here via a stochastic optimization based voltage control strategy. Two variants of Chance Constrained Optimization (CCO) are proposed to minimize the risk of VR *runaway*. A classical CCO considers the *runaway* phenomenon by modeling the violation probability and by defining *Tap non preferred zones*. An improvement to this approach is proposed by defining the *Tap Tail Expectation* index as part of the CCO constraints.
- The problem is solved using a sample selection based approach. The simulation study carried out using a realistic distribution system model shows satisfactory results.
- Both CCO based approaches are able to reasonably minimize the probability of VR *runaway*. However, the classical CCO based approach does not control the shape of the tail probability distribution. In the classical CCO approach, the expected value of the tail can lie near the VR operational limit.
- The *Tap Tail Expectation* based approach offers control over the tail region of the *Tap* and offers a robust operational margin for VR. Both these approaches also minimize the power loss and excessive tap counts. These proposed CCO based strategies will be useful to DNOs to ensure efficient and risk averse network operation in the presence of PV generations.

Chapter 6

Conclusions

6.1 Introduction

A steady state voltage control of a distribution system is becoming challenging for network operators due to injection by intermittent photovoltaic (PV) generation. A variable voltage rise in the presence of PVs needs to be tackled. Classically voltages in a distribution network are controlled by devices such as on-load tap changes (OLTCs) and voltage regulators (VRs).The injection of PV generator active power impacts the operation of these mechanisms. Present day voltage control practices do not consider detailed impacts of PVs on these voltage control mechanisms. This thesis presents a detailed analysis of the impact of PV on OLTCs and VRs. Various voltage regulation strategies to tackle the possible adverse impact of PVs are also developed. The forthcoming sections summaries contributions of this thesis, and presents directions for future research.

6.2 Thesis contributions

1. The first contribution of the thesis is **detailed analysis of steady state voltage control challenges with the specific focus on the impact on classical voltage control devices** in the presence of a PV generation. The classical voltage control devices such as OLTCs and VRs are at the moment operational on many distribution feeders. A PV generation active power

injection impacts the operation of these mechanisms. One of the challenge is, **increase in number of tap counts** necessary to regulate the intermittent overvoltage due to a PV generation. The excessive number of tap counts increase the maintenance expense on these devices.

2. Another major challenge is VR *runaway*. The VR *runaway* happens due to the *control interaction* between a PV generation and a VR. A driving point impedance of a PV and a substation source, a VR control setting, capacity of a PV plant, and a PV inverter reactive power control setting are important parameters which will determine a possibility of VR *runaway*. A **detailed analysis of a VR runaway under various distribution feeder operating scenarios** is carried out in this thesis. The VR *runaway* phenomenon results in the operation of a VR at the lowest or the highest tap position. The extreme low or the extreme high voltage occurs on a feeder due to the VR operating at the extreme position. Thus the loss of VR controllability due to runaway needs to be avoided to seamlessly integrate a PV on a distribution feeder.

3. The conventional reactive power coordination approaches in the literature focused on maintaining the voltage on a feeder within the specified limits. This research work extends the conventional steady state voltage control formulations and takes into account the detailed impacts on the OLTCs and VRs. The **detailed deterministic operational strategy** formulation to solve these challenges is another contribution of the thesis.

4. This strategy ensures minimum number of tap counts of the OLTCs and VRs and mitigates the *runaway*. **The strategy defines the non preferred zone of operation around the VR extreme tap values to avoid runaway.** The strategy coordinates various voltage control devices and the PV generation reactive power support mode. One of the important conclusion of this research is that reactive power support from a PV generation is necessary but not sufficient. PV plant should provide **optimum reactive power support** in order to mitigate runaway and other challenges. The coordination of various reactive power sources including a PV generation is carried out by formulating

the optimization problem.

5. The optimization problem is solved through a primal dual interior point technique. The VR runaway is modeled in the optimization problem by defining **the penalty function for the extreme VR tap values.** The objective function in the optimization problem is weighted combination of tap counts and the penalty value. The considered constraints are bus voltage limits, feeder current limits, power balance constraints and PV generation capacity constraints. PV generation maximum power point tracking is modeled by an equality constraint in the optimization process. This ensures that active power curtailment is minimized and maximum possible clean energy from a PV generation is captured. A PV apparent power capacity is limited by its inverter rating. An additional inverter capacity is necessary to offer a reactive power support at the PV peak active power injection.

6. In order to select weights in the objective function a step by step weight tuning procedure is proposed in the thesis. **While tuning the weights, a VR control margin is also considered.** This approach helps in not only avoiding the runaway but also in maintaining a VR operational control margin. The proposed penalty function can be quadratic or linear. The penalty function parameters can be chosen by an operator based on a feeder operational experience. Thus the penalty function helps avoiding the VR *runaway.*

7. The realistic distribution feeder with the PV generation is simulated as a case study. The **case study demonstrates that the proposed reactive power coordination strategy is effective** in minimizing tap counts, avoiding the runaway and maintaining the feeder voltage within the specified limits. Further case study also considers a night time reactive power support from PV inverters. It is found that tap operations can be minimized by utilising reactive power support capabilities of PV inverters when PV active power output is zero.

8. PV generation forecasts are seldom accurate. The *forecast errors* intensifies the voltage control challenges. It is necessary to design setpoints of OLTCs and PV plants considering the load and irradiance forecast errors. The *stochastic operation* of a distribution feeder is essential due to this. The **thesis contributes a stochastic voltage control strategy for the distribution feeders with the PV generation**.

9. The proposed stochastic strategy is based on the**chance constraint optimization(CCO)**. The consideration of the voltage control challenges such as **runaway in the stochastic sense** is another contribution of the thesis. VR runaway is modeled in the CCO process by defining couple of stochastic indices. One of the index defined is a *tap violation probability*. Another index defined us the *tap tail expectation (TTE)*.

10. The CCO strategy anticipates the VR runaway and prevents it by minimizing a **tap violation probability**. The minimization of the tap violation probability forces the extreme values of VR tap in the *tail region* of the VR tap probability distribution function. This minimizes the probability of VR runaway. Where as **tap tail expectation (TTE)** based approach puts the constraint on the expected value of the tap tail. The detailed formulation of both the approaches is presented in the thesis. A distribution network operator can choose appropriate values of tap violation probability and tap limits in a *tap violation probability* based approach. Where as in TTE based approach expected value of the VR *tap tail* can be chosen by a network operator as a constraint for the CCO optimization process.

11. A sampled Monte Carlo simulation based strategy is proposed to solve this CCO problem. Other important stochastic constraints considered are **voltage violation probability, feeder current limit, solar generation capacity constraints.** There is also a constraint introduced on the active power curtailment probability of solar. This helps maximizing the clean energy capture. In order to improve the feeder operational performance **expected value of power loss and expected tap counts are minimized** in this

problem formulation.

12. A realistic case study demonstrating the effectiveness of the proposed approach is carried out. Both stochastic approaches that is tap violation probability and tap tail expectation based approach are able to minimize the probability of VR runaway. Though tap violation probability based approach is effective, it suffers from a drawback that expected value of VR *tap tail* can lie near the extreme position. In *tap tail expectation (TTE)* based approach, the operator can choose the expected value of the tap tail distant from the VR extreme tap positions. **TTE based approach is more convenient to maintain a robust VR control margin and offers a control over a tap tail.** Further case study demonstrates that with proposed stochastic strategy feeder operational performance improved. The expected value of the power loss and expected value of the tap counts both ere minimized.

Thus thesis contributes deterministic and stochastic steady state voltage regulation strategies in the presence of PV generators. It is believed that proposed strategies will be useful to distribution network operators. The strategies can be utilised in designing various voltage control devices setpoints and deciding control settings of OLTCs, VRs and PV generators etc during daily operation of a distribution feeder.

6.3 Future work

The approach to calculate the daily reactive power setpoints here is based on the day ahead forecasts and off-line simulation. Although the main issues associated with the steady state voltage control are addressed in this thesis, the future work will focus on the following aspects of the problem.

1. Most of the feeders have the voltage control equipments having local control settings without communication. The resetting of these setpoints is usually done seasonally. This is convenient for the network operators and is the existing network practice on some of the feeders. To calculate the local

seasonal setpoints for all the voltage control devices including a PV generation is challenging. This can be possibly carried out by extending the proposed stochastic formulation. However a PV generation is continuously varying due to the weather conditions. The calculated local setpoints must be robust and must mitigate a runaway and overvoltage risk under all the seasonal PV generation variations.

2. The timer control of capacitors which is prevalent on the European distribution feeders is considered in this study. The proposed formulation needs to be extended to consider the switched capacitors having the communication links. The proposed optimization framework can be used to carry this out. However additional programming is necessary.

3. The integrated volt-var control is an advanced distribution automation feature. This strategy carries out voltage control using the real time measurements. These real time measurement based smart grid volt-var control approaches should consider the various impacts of PV generation on the OLTCs and VRs. These algorithms should consider tap count minimization and VR *runaway*.

4. Both proposed strategies utilise the three phase current injection based load flow formulation. Hence both strategies can be used in unbalanced radial or meshed distribution network. However the UK distribution networks is reasonably balanced. The UKGDS test system is also balanced system. With single phase PV and new types of loads distribution systems are becoming unbalance. Though the proposed strategies are generic and can be used for unbalanced networks, a case study using unbalanced distribution test network is necessary in future to evaluate impacts of voltage/current unbalance.

5. Distribution system storage and demand response functions are under evaluation. Assessment of the impact of storage and demand response on proposed methodologies can be carried out in the future.

References

[1] W. H. Kersting, *Distribution system modeling and analysis.* CRC press, 2002.

[2] List of large scale photovoltaic power plants. [Online]. Available: http://www.pvresources.com/

[3] Proposal for a directive 2009/28/EC on the promotion of the use of energy from renewable sources the European parliament and council. [Online]. Available: http://ec.europa.eu/

[4] J. Appen, M. Braun, T. Stetz, K. Diwold, and D. Geibel, "Time in the sun: The challenge of high PV penetration in the German electric grid," *IEEE Power and Energy Magazine*, vol. 11, no. 2, pp. 55–64, Apr. 2013.

[5] Statstical report 2011 renewable energy power plants in Italy. [Online]. Available: http://www.gse.it/

[6] G. Masson, M. Latour, M. Rekinger, I. Theologitis, and M. Papoutsi, "Global market outlook for photovoltaics 2013-2017," Eurpean photovoltaic energy association(EPIA), Technical Report, Mar. 2013, [Online]. Available : http://www.epia.org/.

[7] UK solar PV strategy part 1: Roadmap to a brighter future, Department of Energy and Climate change. [Online]. Available: https://www.gov.uk/

[8] Installed capacity of sites generating electricity from renewable sources 2012, Department of Energy and Climate change. [Online]. Available: https://restats.decc.gov.uk/

[9] M. Vandenbergh, D. Craciun, V. Helmbrecht, R. Hermes, R. Lama, P. Sonvilla, M. Rekinger, G. Concas, H. Loew, C. Mateo, P. Frias, E. Collado, Z. Musilova, and D. Busek, "D3.1 Prioritisation of technical solutions available for the integration of PV into the distribution grid," Technical Report, Jun. 2013, [Online]. Available : http://www.pvgrid.eu/.

[10] China solar PV forecast for 2014. [Online]. Available: http://www.solarbuzz.com/

[11] D. Feldman and R. Margolis, "National survey report of PV power applications in the United States 2012," International energy agency co-operative programme on photovoltaic power systems, Technical Report, Nov. 2013, [Online]. Available : http://www.iea-pvps.org/.

[12] L. Sherwood, "U.S solar market trends 2012," Interstate renewable energy council, Inc. (IREC), Technical Report, Jul. 2013, [Online]. Available : http://www.irecusa.org/.

[13] USA Department of Energy, Energy efficiency and renewable energy. [Online]. Available: http://apps1.eere.energy.gov/

[14] Japanese act on the promotion of new energy usage amendment law number : Act No. 87 of 2005. [Online]. Available: http://www.japaneselawtranslation.go.jp/

[15] H. Yamada and O. Ikki, "National survey report of PV power applications in Japan 2012," International energy agency co-operative programme on photovoltaic power systems, Technical Report, May. 2013, [Online]. Available : http://www.iea-pvps.org/.

[16] Renewable energy (electricity) act 2000 - C2013C00237, Australia. [Online]. Available: http://www.comlaw.gov.au/

[17] Progress under Jawaharlal Nehru National Solar Mission. [Online]. Available: http://pib.nic.in/

[18] "Jawaharlal Nehru National Solar Mission phase II Policy document(draft)," Ministry of New and Renewable Energy, Technical Report, Mar. 2013, [Online]. Available : http://mnre.gov.in/.

[19] C. Breuer, C. Engelhardt, and A. Moser, "Expectation-based reserve capacity dimensioning in power systems with an increasing intermittent feedin," *10th International conference on the European energy market (EEM), Stockholm, Sweden*, pp. 1–7, May. 2013.

[20] E. T. Jauch, "Possible effects of smart grid functions on LTC transformers," *IEEE Trans. Industry Applications*, vol. 47, no. 2, pp. 1013 –1021, Apr. 2011.

[21] R. A. Jabr, A. H. Coonick, and B. J. Cory, "A primal-dual interior point method for optimal power flow dispatching," *IEEE Trans. Power Systems*, vol. 17, no. 3, pp. 654–662, Aug. 2002.

[22] S. J. Wright, *Primal-dual interior-point methods*. Society for Industrial Mathematics, 1997.

[23] W. J. Smolinski, "Equivalent circuit analysis of power system reactive power and voltage control problems," *IEEE Trans. Power Apparatus and Systems*, no. 2, pp. 837–842, Feb. 1981.

[24] S. Civanlar and J. J. Grainger, "Forecasting distribution feeder loads: Modeling and application to volt/var control," *IEEE Trans. on Power Delivery*, vol. 3, no. 1, pp. 255–264, Jan. 1988.

[25] Federal Ministry for the Environment, Nature conservation and nuclear safety (BMU), Germany, "Renewable energy sources act-EEG," Jan. 2012, consolidated (non-binding) version of the act, [Online]. Available : http://www.erneuerbare-energien.de/en.

[26] M. A. E. Kady, B. Bell, V. F. Carvalho, R. C. Burchett, H. H. Happ, and D. R. Vierath, "Assessment of real-time optimal voltage control," *IEEE Trans. Power Systems*, vol. 1, no. 2, pp. 98–105, May. 1986.

[27] M. Liu, S. K. Tso, and Y. Cheng, "An extended nonlinear primal dual interior-point algorithm for reactive-power optimization of large scale power systems with discrete control variables," *IEEE Trans. Power Systems*, vol. 17, no. 4, pp. 982–991, Nov. 2002.

[28] M. B. Liu, C. A. Canizares, and W. Huang, "Reactive power and voltage control in distribution systems with limited switching operations," *IEEE Trans. Power Systems*, vol. 24, no. 2, pp. 889–899, May. 2009.

[29] S.Paudyal, C. A. Canizares, and K.Bhattacharya, "Optimal operation of distribution feeders in smart grids," *IEEE Trans. Industrial Electronics*, vol. 58, no. 10, pp. 4495–4503, Oct. 2011.

[30] T. E. McDermott, "Modeling PV for unbalanced, dynamic and quasistatic distribution system analysis," in *2011 IEEE Power and Energy Society General Meeting, San Diego, USA*, Jul. 2011, pp. 1–3.

[31] M. Fila, G. A. Taylor, M. R. Irving, J. Hiscock, P. Lang, and P. Aston, "Systematic modelling and analysis of TAPP voltage control schemes," in *42nd International Universities Power Engineering Conference 2007, UPEC 2007, Brighton, UK*, Sep. 2007, pp. 349–356.

[32] A. Malekpour and A. Pahwa, "Reactive power and voltage control in distribution systems with photovoltaic generation," in *IEEE North American Power Symposium (NAPS 2012), Champaign, USA*, Sep. 2012, pp. 1–6.

[33] P. Chen, S. Pierluigi, B. Jensen, and Z. Chen, "Stochastic optimization of wind turbine power factor using stochastic model of wind power," *IEEE Trans. Sustainable Energy*, vol. 1, no. 1, pp. 19–29, Apr. 2010.

[34] N. Hatziargyriou, T. Karakatsanis, and M. Papadopoulos, "The effect of wind parks on the operation of voltage control devices," *Paper no. 438, 14th International Conference and Exhibition on Electricity Distribution (CIRED 1997), Birmingham, UK*, Jan. 1997.

[35] "IEEE Recommended practice for utility interface of photovoltaic PV systems," *IEEE Std 929-2000*, Aug. 2002.

[36] E. Ela, M. Milligan, and B. Kirby, "Operating reserves and variable generation," National Renewable Energy Laboratory, Technical Paper NREL/TP-5500-51978, August 2011, [Online]. Available : http://www.nrel.gov/.

[37] E. Ela, V. Diakov, E. Ibanez, and M. Heaney, "Impacts of variability and uncertainty in solar photovoltaic generation at multiple timescales," National Renewable Energy Laboratory, Technical Report NREL/TP-5500-58274, May 2013, [Online]. Available : http://www.nrel.gov/.

[38] J. Boemer, K. Burges, P. Zolotarev, J. Lehner, P. Wajant, M. Furst, R. Brohm, and T. Kumm, "Overview of German grid issues and retrofit of photovoltaic power plants in Germany for the prevention of frequency stability problems in abnormal system conditions of the ENTSO-E region continental Europe," *1st International Workshop on Integration of Solar Power into Power Systems, Aarhus, Denmark*, Oct 2011.

[39] Solar energy grid integration systems (SEGIS). [Online]. Available: https://www1.eere.energy.gov/

[40] P. Denholm, B. K. E. Ela, and M. Milligan, "The role of energy storage with renewable electricity generation," National Renewable Energy Laboratory, Technical Report NREL/TP-6A2-47187, Jan. 2010, [Online]. Available : http://www.nrel.gov/.

[41] S. Eftekharnejad, V. Vittal, G. Heydt, B. Keel, and J. Loehr, "Small signal stability assessment of power systems with increased penetration of photovoltaic generation: A case study," *IEEE Trans. on Sustainable Energy*, vol. 28, no. 2, pp. 960–967, May 2013.

[42] B. Tamimi, C. Caizares, and K. Bhattacharya, "System stability impact of large-scale and distributed solar photovoltaic generation: The case of Ontario,

Canada," *IEEE Trans. on Sustainable Energy*, vol. 4, no. 3, pp. 680–687, Jul. 2013.

[43] "IEEE Standard for interconnecting distributed resources with electric power systems," *IEEE Std 1547-2003*, Aug. 2003.

[44] R. Tonkoski, L. Lopes, and T. EL-Fouly, "Coordinated active power curtailment of grid connected PV inverters for overvoltage prevention," *IEEE Trans. Sustainable Energy*, vol. 2, no. 99, pp. 139–147, Apr. 2011.

[45] T. Stetz, F. Marten, and M. Braun, "Improved low voltage grid-integration of photovoltaic systems in Germany," *IEEE Trans. Sustainable Energy*, vol. 4, no. 2, pp. 534–542, Apr. 2013.

[46] F. Katiraei and J. R. Aguero, "Solar PV integration challenges," *IEEE power and energy magazine*, vol. 9, no. 3, pp. 62–71, Jun. 2011.

[47] US Department Of Energy Sunshot Initiative. [Online]. Available: https://solarhighpen.energy.gov/

[48] R. A. Walling, R. Saint, R. C. Dugan, J. Burke, and L. A. Kojovic, "Summary of distributed resources impact on power delivery systems," *IEEE Trans. Power Delivery*, vol. 23, no. 3, pp. 1636–1644, Jul. 2008.

[49] T. Senjyu, Y. Miyazato, A. Yona, N. Urasaki, and T. Funabashi, "Optimal distribution voltage control and coordination with distributed generation," *IEEE Trans. Power Delivery*, vol. 23, no. 2, pp. 1236–1242, Apr. 2008.

[50] W. Glassley, and J. Kleissl, and H. Shiu , and J. Huang, and G. Braun , and R. Holland, "Final report on current state of the art in solar forecasting," California Renewable energy forecasting, Resource data and mapping, California renewable energy collaborative, [Online]. Available : http://uc-ciee.org/.

[51] B. M. Hodge, D. Lew, and M. Milligan, "NREL/CP550057340 short-term load forecasting error distributions and implications for renewable integration

studies," *IEEE Green Technologies Conference, Denver, USA*, pp. 1–8, Apr. 2013.

[52] "Engineering recommendation G83, Issue 2, Recommendations for the connection of type tested small-scale embedded generators(up to 16a per phase) in parallel with low voltage distribution systems," Energy Network Association, Technical Report, Dec. 2012, [Online]. Available : http://www.energynetworks.org/.

[53] B. Craciun, T. Kerekes, D. Sera, and R. Teodorescu, "Overview of recent grid codes for PV power integration," *13th International Conference on Optimization of Electrical and Electronic Equipment (OPTIM), 2012, Brasov*, May. 2012.

[54] "Engineering recommendation G59/2, Issue 2, Recommendations for the connection of generating plants to the distribution systems of licensed distribution network operators," Energy Network Association, Technical Report, Apr. 2011, [Online]. Available : http://www.energynetworks.org/.

[55] BDEW technical guideline for generating plants connected to the medium-voltage network. [Online]. Available: http://www.bdew.de

[56] F. Mango, A. Grtn, M. Liserre, and A. Aquila, "Overview of anti-islanding algorithms for PV systems. Part I: Passive methods," *12th International Power Electronics and Motion Control Conference, Portoroz, EPEPEMC-2006*, pp. 1878–1883, Aug. 2006.

[57] ——, "Overview of anti-islanding algorithms for PV systems. Part II: Active methods," *12th International Power Electronics and Motion Control Conference, Portoroz, EPEPEMC-2006*, pp. 1884–1889, Aug. 2006.

[58] Z. Ye, A. Kolwalkar, Y. Zhang, P. Du, and R. Walling, "Evaluation of anti-islanding schemes based on nondetection zone concept," *IEEE Trans. on Power Electronics*, vol. 19, no. 5, pp. 960–967, Sep. 2004.

[59] W. Bower and M. Ropp, "Evaluation of islanding detection methods for utility-interactive inverters in photovoltaic systems," Sandia National Laboratories, Technical Report SAND2002-3591, Nov. 2002, [Online]. Available : http://prod.sandia.gov/.

[60] I. Abdulhadi, X. Li, F. Coffele, P. Crolla, A. Dysko, C. Booth, G. Burt, and N. Schaefer, "International white book on der protection: Review and testing procedures," European Distributed Energy Resources Laboratories, DERlab Report No.R-004.0, 20011-12, [Online]. Available : http://der-lab.net/.

[61] J. Hernandeza, J. Cruzb, and B. Ogayara, "Electrical protection for the grid-interconnection of photovoltaic-distributed generation," *Electric Power Systems Research*, vol. 89, pp. 85–99, Aug. 2012.

[62] "The distribution code and the guide to the distribution code of licensed distributed network operators of Great Britain," Technical Report, Sep. 2013, issue 19 of the distribution code of licensed distribution operators of Great Britain [Online]. Available : http://www.dcode.org.uk/.

[63] "Application guide to the European standard EN50160 on voltage characteristics of electricity supplied by public distribution systems, Electricity product characteristics and electromagnetic compatibility," Union of the electricity industry urelectric, Technical Report, Jul. 1995.

[64] Y. Bae, T. Vu, and R. Kim, "Implemental control strategy for grid stabilization of grid-connected PV system based on German grid code in symmetrical low-to-medium voltage network," *IEEE Trans. on Energy Conversion*, vol. 28, no. 3, pp. 619–630, Sep. 2013.

[65] W. Bower and M. Ropp, "Recommendations for unified technical regulations for grid-connected PV systems," Sunrise project : 6th framework programme for research and technological development of the European commission, Technical Report, 2009, [Online]. Available : http://www.pvsunrise.eu/.

[66] E. Troester, "New Geman grid codes for connecting PV systems to the medium voltage power grid," *in 2nd International workshop on concentrating photovoltaic power plants : Optical design, Production, Grid connection, Darmstadt, Germany*, pp. 1–4, Mar. 2009.

[67] D. Geibel, G. Arnold, and D. Martini, "Confirmation of extended electrical properties of PV invereters according to German MV grid code - experience in the certification process," *Paper 1132 in 21st International Conference on Electricity Distribution (CIRED) , Frankfurt, Germany*, pp. 1–4, Jun. 2011.

[68] Thomas Stetz, "Monitoring of PV-systems, integration of PV plants in distribution grids, OTTI-seminar, Munich, Germany," Jun. 2011, [Online]. Available : http://www.iwes.fraunhofer.de/.

[69] P. Kotsampopoulos, N. Hatziargyriou, B. Bletterie, and G. Lauss, "Review, analysis and recommendations on recent guidelines for the provision of ancillary services by distributed generation," *in 2013 IEEE International workshop on intelligent energy systems (IWIES), Vienna, Austria*, pp. 185–190, Nov. 2013.

[70] E. Demirok, P. Gonzalez, K. Frederiksen, D. Sera, P. Rodriguez, and R. Teodorescu, "Local reactive power control methods for overvoltage prevention of distributed solar inverters in low-voltage grids," *IEEE Journal of Photovoltaics*, vol. 1, pp. 174–182, Dec. 2011.

[71] A. Ellis, R. Nelson, E. VonEngeln, R. Walling, J. MacDowell, L. Casey, E. Seymour, W. Peter, C. Barker, B. Kirby, and J. Williams, "Review of existing reactive power requirements for variable generation," *IEEE Power and Energy Society General Meeting, 2012, San Diego, USA*, pp. 1–7, Jul. 2012.

[72] S. Probert and S. Nutt, "Generator fault ride through (FRT) investigation stage 1 literature review," Transpower New Zealand Limited, Technical Report, Feb. 2009, [Online]. Available : http://www.nerc.com/.

[73] A. Chatterjee and A. Keyhani, "Thevenin's equivalent of photovoltaic source models for MPPT and power grid studies," *IEEE Power and Energy Society General Meeting 2011, Detroit, Michigan, USA*, pp. 1–7, Jul. 2011.

[74] C. Riordan and R. Hulstron, "What is an air mass 1.5 spectrum? solar cell performance calculations," *Conference record of the twenty first IEEE photovoltaic specialists conference, Kissimmee, Florida, USA*, pp. 1085–1088, May. 1990.

[75] C. Gueymard, D. Myers, and K. Emery, "Proposed reference irradiance spectra for solar energy systems testing," *Solar energy*, vol. 73, no. 6, pp. 443–467, Dec. 2002.

[76] Reference solar spectral irradiance: Air mass 1.5. [Online]. Available: http://rredc.nrel.gov/solar/spectra/am1.5/

[77] G. Holmes and T. Lipo, *Pulse width modulation for power converters: principles and practice.* John Wiley and Sons, 2003.

[78] A. Yazdani and R. Iravani, *Voltage-sourced converters in power systems.* John Wiley and Sons, 2010.

[79] R. Teodorescu, M. Liserre, and P. Rodriguez, *Grid converters for photovoltaic and wind power systems.* John Wiley and Sons, 2011.

[80] T. Esram and P. Chapman, "Comparison of photovoltaic array maximum power point tracking techniques," *IEEE Trans. on Energy Conversion*, vol. 22, no. 2, pp. 439–449, Jun. 2007.

[81] GEPVp-200-M 200W photovoltaic module for 600V application. [Online]. Available: http://www.ge-energy.com/

[82] B. Pal and B. Chaudhuri, *Robust control in power systems.* Springer, 2006.

[83] P. Kundur, *Power system stability and control.* McGraw-Hill New York, 1994.

[84] C. L. Masters, "Voltage rise: the big issue when connecting embedded generation to long 11 kV overhead lines," *Power Engineering Journal*, vol. 16, no. 1, pp. 5–12, Feb. 2002.

[85] A. G. Madureira and J. A. P. Lopes, "Coordinated voltage support in distribution networks with distributed generation and microgrids," *IET Renewable Power Generation*, vol. 3, no. 4, pp. 439–454, Dec. 2009.

[86] A. G. Madureira, J. A. P. Lopes, A. Carrapatoso, and N. Silva, "The new role of substations in distribution network management," *in 20th International conference and exhibition on electricity distribution - Part 2, CIRED2009, Prague, Czech Republic*, pp. 863–863, Jun. 2009.

[87] A. G. Madureira and J. A. P. Lopes, "Voltage and reactive power control in MV networks integrating microgrids," *in Proceedings International conference on Renewable energies and Power quality (ICREPQ 2007), Sevilla, Spain*, pp. 1–5, Mar. 2007.

[88] M. Coddington, B. Mather, B. Kroposki, K. Lynn, A.Razon, A.Ellis, R. Hill, T. Key, K. Nicole, and J. Smith, "Updating interconnection screens for PV system integration," National Renewable Energy Laboratory, Technical Report NREL/TP 5500-54063, Feb. 2012, [Online]. Available : http://www.osti.gov/bridge.

[89] L. M. Cipcigan and P. C. Taylor, "Investigation of the reverse power flow requirements of high penetrations of small-scale embedded generation," *IET Renewable Power Generation*, vol. 1, no. 3, pp. 160–166, Sep. 2007.

[90] R. H. Liang and C. K. Cheng, "Dispatch of main transformer ULTC and capacitors in a distribution system," *IEEE Trans. Power Delivery*, vol. 16, no. 4, pp. 625–630, Oct. 2001.

[91] R. W. Uluski, "VVC in the smart grid era," in *IEEE Power and Energy Society General Meeting 2010, Minneapolis, USA*, Jul. 2010, pp. 1–7.

[92] M. McGranaghan, T. Ortmeyer, D. Crudele, T. Key, J. Smith, and P. Barker, "Renewable systems interconnection study: Advanced grid planning and operations," *Technical Report : Sandia National Laboratories*, Feb. 2008.

[93] F. A. Viawan and D. Karlsson, "Combined local and remote voltage and reactive power control in the presence of induction machine distributed generation," *IEEE Trans. Power Systems*, vol. 22, no. 4, pp. 2003–2012, Nov. 2007.

[94] ——, "Voltage and reactive power control in systems with synchronous machine-based distributed generation," *IEEE Trans. Power Delivery*, vol. 23, no. 2, pp. 1079–1087, Apr. 2008.

[95] R. A. Walling and K. Clark, "Grid support functions implemented in utility-scale PV systems," in *2010 IEEE PES Transmission and Distribution Conference and Exposition, New Orleans, USA*, Apr. 2010, pp. 1–5.

[96] T. Gonen, *Electric Power Distribution System*. McGraw-Hill Book Company, 1986.

[97] Regulation features of digital tapchanger control Beckwith M-2001B. [Online]. Available: http://www.beckwithelectric.com/

[98] Regulation features of ICMI UVR-1 universal voltage regulator control specification. [Online]. Available: http://www.icmiinc.us/

[99] Mcgraw-Edison VR-32 Regulators and CL-5 series control. [Online]. Available: http://www.cooperindustries.com

[100] MJ-4A(TM) and MJ-4B(TM) Voltage regulator control panel. [Online]. Available: http://www.energy.siemens.com/

[101] P. A. N. Garcia, J. L. R. Pereira, S. Carneiro Jr, V. M. daCosta, and N. Martins, "Three-phase power flow calculations using the current injection method," *IEEE Trans. Power Systems*, vol. 15, no. 2, pp. 508–514, May. 2000.

[102] P. A. N. Garcia, J. L. R. Pereira, and S. Carneiro Jr, "Voltage control devices models for distribution power flow analysis," *IEEE Trans. Power Systems*, vol. 16, no. 4, pp. 586–594, Nov. 2001.

[103] R. Singh, B. C. Pal, and R. A. Jabr, "Distribution system state estimation through Gaussian mixture model of the load as pseudo-measurement," *IET Generation Transmission and Distribution*, vol. 4, no. 1, pp. 50–59, Jan. 2010.

[104] C. W. Brice, "Comparison of approximate and exact voltage drop calaculations for distribution lines," *IEEE Trans. on Power Apparatus and Systems*, vol. 101, no. 11, p. 4428, Nov. 1982.

[105] T. A. Short, *Electric Power Distribution Handbook*. CRC Press LLC, 2004.

[106] W. H. Kersting, *Distribution system modeling and analysis*. CRC Press LLC, 2002.

[107] M. Fan, V. Vittal, G. Heydt, and R. Ayyanar, "Probabilistic power flow studies for transmission systems with photovoltaic generation using cumulants," *IEEE Trans. Power Systems*, vol. 27, no. 4, pp. 1–12, Nov. 2012.

[108] ——, "Probabilistic power flow analysis with generation dispatch including photovoltaic resources," *IEEE Trans. Power Systems*, vol. 28, no. 3, pp. 1–9, May 2013.

[109] Y. Kim, S. Ahn, P. Hwang, G. Pyo, and S. Moon, "Coordinated control of a DG and voltage control devices using a dynamic programming algorithm," *IEEE Trans. Power Systems*, vol. 28, no. 1, pp. 42–51, Feb. 2013.

[110] T. Karakatsanis and N. Hatziargyriou, "Probabilistic constrained load flow based on sensitivity analysis," *IEEE Trans. on. Power Systems*, vol. 9, no. 4, pp. 1853–1860, Nov. 1994.

[111] N. Hatziargyriou, T. Karakatsanis, and M. Papadopoulos, "Probabilistic load flow in distribution systems containing dispersed wind power generation," *IEEE Trans. on. Power Systems*, vol. 8, no. 1, pp. 159–165, Feb. 1993.

[112] H. Zechun, W. Xifan, and G. Taylor, "Stochastic optimal reactive power dispatch: Formulation and solution method," *International Journal of Electrical Power & Energy Systems*, vol. 32, no. 6, pp. 615–621, Jul. 2010.

[113] G. Calafiore and M. Campi, "Uncertain convex programs: randomized solutions and confidence levels," *Mathematical Programming*, vol. 102, no. 1, pp. 25–46, Jan. 2005.

[114] I. Roytelman, B. Wee, and R. Lugtu, "Volt/Var control algorithm for modern distribution management system," *IEEE Trans. Power Systems*, vol. 10, no. 3, pp. 1454–1460, Aug. 1995.

[115] S. Sarykalin, G. Serraino, and S. Uryasev, "Value-at-risk vs. conditional value-at-risk in risk management and optimization," *Prsented at INFORMS annual meeting, Tutorials in Operations Research, Hanover, USA*, Oct. 2008.

[116] M. Fila, G. Taylor, J. Hiscock, M. Irving, and P. Lang, "Flexible voltage control to support distributed generation in distribution networks," in *43rd International Universities Power Engineering Conference, UPEC 2008, Padova*, Sep. 2008, pp. 1–5.

[117] R. A. Jabr, "Robust self-scheduling under price uncertainty using conditional value-at-risk," *IEEE Trans. Power Systems*, vol. 20, no. 4, pp. 1852–1858, Nov. 2005.

[118] K. Otani, J. Minowa, and K. Kurokawa, "Study on areal solar irradiance for analyzing areally-totalized PV systems," *Solar Energy Materials and Solar Cells*, vol. 47, no. 1, pp. 281–288, Oct.1997.

Appendix A

PV model parameters

Table A.1: PV simulation parameters

Parameter	**Value**
Number of cells in series in one module	54
Number of parallel connected modules	144
Open circuit voltage	$33V$
Open circuit voltage coefficient	$-0.12V/C$
Short circuit current of the module	$8.21A$
Short circuit current coefficient	$5.6mA/C$
Maximum power point current	$7.6A$
Maximum power point voltage	$27.2V$
Filter inductance	$100\mu H$
Filter capacitance	$369\mu F$

Appendix B

Multi machine system data

Table B.1: Transmission line data on 100 MVA base

From Bus	To Bus	Series Resistance pu	Series Reactance pu	Shunt susceptance pu
1	101	0.001	0.012	0.0
2	102	0.001	0.012	0.0
3	13	0.022	0.22	0.33
3	13	0.022	0.22	0.33
3	13	0.022	0.22	0.33
3	102	0.002	0.02	0.03
3	102	0.002	0.02	0.03
11	111	0.001	0.012	0.00
12	112	0.001	0.012	0.00
13	112	0.002	0.02	0.03
13	112	0.002	0.02	0.03
101	102	0.005	0.05	0.075
101	102	0.005	0.05	0.075
111	112	0.005	0.05	0.075
111	112	0.005	0.05	0.075

Table B.2: Load Flow Data

Bus	Voltage magnitude	Angle degree	P Gen [pu]	Q Gen [pu]	P load [pu]	Q load [pu]	Shunt susceptance [pu]
1	1.03	8.21	7.0	1.3386	0.0	0.0	0.0
2	1.01	-1.5040	7.0	1.5920	0.0	0.0	0.0
11	1.03	0.0	7.2172	1.4466	0.0	0.0	0.0
12	1.01	-10.2051	7.0	1.8083	0.0	0.0	0.0
101	1.0108	3.6615	0.0	0.0	0.0	0.0	0.0
102	0.9875	-6.2433	0.0	0.0	0.0	0.0	0.0
111	1.0095	-4.6977	0.0	0.0	0.0	0.0	0.0
112	0.9850	-14.9443	0.0	0.0	0.0	0.0	0.0
3	0.9761	-14.4194	0.0	0.0	11.59	2.12	3.0
13	0.9716	-23.2922	0.0	0.0	15.75	2.88	4.0

Appendix C

UKGDS 95-bus system data

Table C.1: UKGDS load data

Bus number	Active power(kW)	Reactive power(kVAr)
1	940	170
2	0	0
3	10	2
4	0	0
5	20	4
6	0	0
7	20	4
8	0	0

Continued on next page

Table C.1 – *Continued from previous page*

Bus number	**Active power(kW)**	**Reactive power(kVAr)**
9	0	0
10	0	0
11	0	0
12	0	0
13	0	0
14	20	10
15	0	0
16	10	3
17	0	0
18	0	50
19	930	310
20	10	1
21	0	0
22	20	6
23	20	6
24	40	10
25	0	0
26	50	10

Continued on next page

Table C.1 – *Continued from previous page*

Bus number	**Active power(kW)**	**Reactive power(kVAr)**
27	0	0
28	20	6
29	0	0
30	0	0
31	10	1
32	40	10
33	20	6
34	20	6
35	0	0
36	40	10
37	140	30
38	10	1
39	10	1
40	0	0
41	0	0
42	20	4
43	40	10
44	0	0

Continued on next page

Table C.1 – *Continued from previous page*

Bus number	**Active power(kW)**	**Reactive power(kVAr)**
45	0	0
46	0	0
47	10	3
48	0	0
49	10	2
50	0	0
51	20	6
52	40	10
53	0	0
54	20	6
55	0	0
56	0	0
57	10	3
58	10	1
59	0	0
60	10	3
61	10	3
62	20	4

Continued on next page

Table C.1 – *Continued from previous page*

Bus number	**Active power(kW)**	**Reactive power(kVAr)**
63	0	0
64	20	4
66	20	6
67	0	0
68	20	6
69	10	3
70	0	0
71	0	0
72	0	0
73	10	3
74	50	10
75	0	0
76	0	0
77	0	0
78	0	0
79	30	6
80	0	0
81	0	0

Continued on next page

Table C.1 – *Continued from previous page*

Bus number	**Active power(kW)**	**Reactive power(kVAr)**
82	40	10
83	0	0
84	650	130
85	0	0
86	0	0
87	80	20
88	0	0
89	70	10
90	40	10
91	0	0
92	120	20
93	0	0
94	40	10
95	0	0

Table C.2: UKGDS line data

From bus number	To bus number	Resistance(ohm)	Reactance(ohm)
1	2	0.0590359	0.0612018
1	85	0.0664169	0.0688490
2	4	0.1180355	0.4027364
3	4	0.2095962	0.0918269
4	6	0.2541000	0.2456300
5	6	0.2934371	0.1285504
6	8	0.3129060	0.2138433
7	8	0.4192045	0.1836538
8	10	0.1564530	0.1069156
9	10	0.3569500	0.1815000
9	28	0.2515227	0.1101947
9	29	0.4283400	0.2178000
10	11	0.3650449	0.2494778
11	13	0.2346795	0.1603855
12	13	0.2095962	0.0918269
13	15	0.2868305	0.1960200
14	15	0.2515227	0.1101947

Continued on next page

Table C.2 – *Continued from previous page*

From bus number	**To bus number**	**Resistance(ohm)**	**Reactance(ohm)**
15	17	0.3129060	0.2138433
16	17	0.1676818	0.0734591
17	25	0.1564530	0.1069156
18	19	0.1452000	0.1403600
19	21	0.4356000	0.4210800
20	21	0.1592481	0.0608993
21	22	0.1089000	0.1052700
22	23	0.3650449	0.2494778
23	24	0.2346795	0.1603855
24	25	0.2607550	0.1781967
25	27	0.2086040	0.1425622
26	27	0.1303775	0.0891044
29	30	0.3353636	0.1469182
29	31	0.2934371	0.1285504
30	32	0.3129060	0.2138433
30	34	0.1349029	0.0892496
32	33	0.3772780	0.1652860
34	35	0.4188052	0.2499013

Continued on next page

Table C.2 – *Continued from previous page*

From bus number	**To bus number**	**Resistance(ohm)**	**Reactance(ohm)**
35	36	0.1888568	0.1249446
35	39	0.4171959	0.2851244
36	37	0.2698058	0.1784992
37	38	0.2583350	0.1104246
39	40	0.1564530	0.1069156
40	41	0.1427800	0.0726000
40	53	0.2086040	0.1425622
41	42	0.2515227	0.1101947
41	43	0.2855600	0.1452000
43	44	0.2141700	0.1089000
44	45	0.1137521	0.0434995
45	46	0.2141700	0.1089000
46	47	0.2855600	0.1452000
46	48	0.4283400	0.2178000
48	49	0.4283400	0.2178000
48	50	0.3353636	0.1469182
50	51	0.2583350	0.1104246
50	52	0.6458254	0.2760736

Continued on next page

Table C.2 – *Continued from previous page*

From bus number	**To bus number**	**Resistance(ohm)**	**Reactance(ohm)**
53	54	0.3650449	0.2494778
53	55	0.2515227	0.1101947
54	59	0.4418557	0.1844524
54	75	0.3129060	0.2138433
55	56	0.3353636	0.1469182
55	57	0.5030454	0.2203773
57	58	0.3353636	0.1469182
59	60	0.2095962	0.0918269
59	62	0.1767447	0.0737858
60	61	0.3772780	0.1652860
62	63	0.3093002	0.1291191
63	64	0.2515227	0.1101947
63	65	0.2209218	0.0922262
65	66	0.3534773	0.1475595
66	67	0.3093002	0.1291191
67	68	0.1137521	0.0434995
67	69	0.5302220	0.2213453
69	70	0.2651110	0.1106666

Continued on next page

Table C.2 – *Continued from previous page*

From bus number	**To bus number**	**Resistance(ohm)**	**Reactance(ohm)**
70	71	0.0910041	0.0347996
71	72	0.1767447	0.0737858
72	73	0.3534773	0.1475595
72	74	0.4860328	0.2028928
75	76	0.1564530	0.1069156
76	77	0.2209218	0.0922262
76	80	0.2607550	0.1781967
77	78	0.3534773	0.1475595
78	79	0.5302220	0.2138433
80	83	0.1564530	0.1069156
80	86	0.2346795	0.1603855
81	82	0.3296524	0.0485452
81	94	0.1825285	0.1247389
82	95	0.5933719	0.0873862
84	85	0.0469601	0.1258400
86	87	0.3353636	0.1469182
86	90	0.3129060	0.2138433
87	88	0.5868742	0.2571129

Continued on next page

Table C.2 – *Continued from previous page*

From bus number	**To bus number**	**Resistance(ohm)**	**Reactance(ohm)**
88	89	0.2737141	0.0567006
90	91	0.0782265	0.0534578
91	92	0.3296524	0.0485452
92	93	0.1977866	0.0291247
93	94	0.1043020	0.0712811